ISTANBUL TECHNICAL UNIVERSITY ★ GRADUATE SCHOOL OF SCIENCE ENGINEERING AND TECHNOLOGY

SEDIMENTARY RECORDS OF ACTIVE FAULTING IN KUMBURGAZ BASIN, SEA OF MARMARA

M.Sc. THESIS

NURETTİN YAKUPOĞLU

Department of Geology Engineering

Geological Engineering

January/2017

ISTANBUL TECHNICAL UNIVERSITY ★ GRADUATE SCHOOL OF SCIENCE ENGINEERING AND TECHNOLOGY

SEDIMENTARY RECORDS OF ACTIVE FAULTING IN KUMBURGAZ BASIN, SEA OF MARMARA

M.Sc. THESIS

NURETTİN YAKUPOĞLU

(505141336)

Department of Geology Engineering

Geological Engineering

Thesis Advisor: Asst.Prof. Dr. Gülsen UÇARKUŞ

January/2017

ISTANBUL TEKNİK ÜNİVERSİTESİ ★ FEN BİLİMLERİ ENSTİTÜSÜ

AKTİF FAYLANMANIN KUMBURGAZ HAVZASINDAKİ SEDİMANTER KAYITLARI, MARMARA DENİZİ

YÜKSEK LİSANS TEZİ

NURETTİN YAKUPOĞLU

(505141336)

Jeoloji Mühendisliği Bölümü

Jeoloji Mühendisliği

Tez Danışmanı: Yrd.Doç.Dr Gülsen UÇARKUŞ

Ocak/2017

Nurettin YAKUPOĞLU, a M.Sc. student of İTU Graduate School of Science Engineering and Technology student ID 505141336, successfully defended the thesis entitled "SEDIMENTARY RECORDS OF ACTIVE FAULTING IN KUMBURGAZ BASIN, SEA OF MARMARA", which he prepared after fulfilling the requirements specified in the associated legislations, before the jury whose signatures are below.

Thesis Advisor:	**Asst.Prof. Dr. Gülsen UÇARKUŞ**	.....
	Istanbul Technical University	
Jury Members:	**Assoc.Prof. Dr. K.Kadir ERİŞ**	.....
	Istanbul Technical University	
	Prof. Dr. Erol SARI	.....
	Istanbul University	

Date of Submission : 20.01.2017

Date of Defense : 23.01.2017

FOREWORD

"Sedimentary Records of Active Faulting in Kumburgaz Basin, Sea of Marmara" titled graduate thesis is taken place in Istanbul Technical University, Graduate School of Science Engineering and Technology Institute, Geological Engineering between 2015-2016.

This thesis is supported by MARsite (2014) Project. Majority of experiments and measurements are executed in East Mediterranean Centre for Oceanography and Limnology Laboratories.

For this thesis, I'd like to thanks to my beloved advisor Asst. Prof. Dr. Gülsen Uçarkuş who helped me about how to be a scientist, a professional. She shared her experiences and knowledge about any topic that I struggled with. She gave me chances to prove myself and encouraged me to take responsibility.

Both Prof.Dr M.Namık Çağatay and Assoc. Prof. Dr. K.Kadir Eriş who accepted me as a member in EMCOL among others, were like my co-advisors who showed me the way how to work with a team and how to do good science. Their endless knowledge about the marine sciences was a great favor to me and to fellow young scientists. It was a privilege to be a member of such an extraordinary facility.

I'd like to thank my colleagues in EMCOL, they were really supportive and helpful during the whole two years of working side by side. They taught me again the very meaning of friendship and being a team.

My special thanks to Prof. Dr. Pierre Henry and his associates to help me by giving insights and thoughts to my study. Thus, providing opportunity to execute Radiocarbon analyses in CEREGE Radiocarbon Laboratory.

I'd like to thanks to captains and all crew members of pourquoi pas? who attended the MARsite cruise in 2014. They have recovered the sediment core and CHIRP profiles so that, this thesis had a data set to work with.

Last but not least, I'd like to thank Prof. Dr. Ziyadin Çakır and Prof. Dr. Elif Sertel for supporting me financially during my education. They trusted me thus, supported me. I hope, I have been proven myself to their trust and support.

This faculty is like my home since 2008, the time I have started my education. During 7 years, most of the scientists were accepted and acknowledged me not only as a student but as a colleague. My special thanks to Prof. Dr. Boris Natalin, Dr. Cengiz Zabcı, Asst. Prof. Dr. Nazlı Olgun, Prof. Dr. Mehmet Sakınç, Prof. Dr. Emin Özsoy, Ass. Prof. Dr. Oğuz Göğüş.

Ocak 2017

Nurettin Yakupoğlu
Geology Engineer

TABLE OF CONTENTS

Page

ABBREVIATIONS

µ-XRF : Micro-X-Ray Fluorescence
AD : Anno Domino
AMS : Accelerator Mass Spectrometry
BP : Before Present
cmbsf : centimeter below sea floor
cps : count per second
EMCOL : Eastern Mediterranean Centre of Oceanography and Limnology
GPS : Global Positioning System
km : kilometer
mm/yr : millimeter per year
MSCL : Multi Sensor Core Logger
myr : million year
NAF : North Anatolian Fault
NNAF : Northern Branch of North Anatolian Fault
SoM : Sea of Marmara

LIST OF TABLES

Page

LIST OF FIGURES

Page

SEDIMENTARY RECORDS OF ACTIVE FAULTING IN KUMBURGAZ BASIN, SEA OF MARMARA

SUMMARY

Sea of Marmara (SoM) is located at the west part of the ~1600 km long North Anatolian Fault (NAF) being a conduit between Black Sea and Aegean Sea. SoM contains five sedimentary basins at the northern border due to active tectonic regime of NAF. 2500 years long historical earthquake history is recorded which has destroyed cities and caused human loss within ~150 major earthquakes. Most active branch of the NAF in SoM is the Northern Branch playing the fundamental role in forming the tectonically active sedimentary basins which had become a perfect archive to preserve and a spectacular laboratory to examine the earthquake-triggered depositions.

In subaqueous paleoseismology studies, sediment-gravity flow deposits are often used as a method to establish earthquake history of the related region. The term seismoturbidite is earthquake-triggered turbidites which have the particular stratigraphical, sedimentological and geochemical characteristics. However, the distinctive features could not very well be fully explained or described yet thus, this is the starting point of the thesis in which to ensure a proper description for distinctive features of term.

MARsite (2014) cruise is recovered sediments cores by “pour quoi pas?” to establish a multi-disciplinary study in SoM in order to investigate tectonic, oceanographic history. Thesis contains one piston core and several seismic reflection profiles from the MARsite project. Experiments and observations are executed in the East Mediterranean Centre for Oceanography and Limnology (EMCOL) laboratories. Radiocarbon analysis is executed by CEREGE radiocarbon laboratory.

One of the locations which is chosen for coring is Kumburgaz Basin where Central segment of NNAF passes, especially interested because the complicated seismicity of the segment. Holocene history of the Kumburgaz basin is not fully revealed both seismically and oceanographically therefore, a multi-parameter study has executed on seismoturbidite layers by using physical, geochemical, textural and paleontological methods to find out; (1) unravel 7000 years long tectonic history of the region, (2) determine concept of seismoturbidite by accentuating distinctive features, (3) find the answer the ambiguous behavior of the Central Segment whether it is creeping of locked.

Recovered piston core CS-01 contains 28 seismoturbidites layers. By using MSCL, XRF, grain-size and smear slides we obtained sedimentological aspects of the depositions. Inverse graded turbidites are identified and their deposition dynamics are explained by presence of bathymetric barrier in Kumburgaz Basin. Amalgamated turbidites (stacked turbidites) are detected by using elemental proxies which is also precursor for the determination of the time interval for sediment-gravity flow deposits. Most important feature for seismoturbidite which is seiche effect, has been identified almost all turbidite units in the CS-01. Water oscillations are mainly caused by

earthquakes which affect the sedimentary structures in the successions so that, most of the subunits of turbidites are missing because of constant seiche controlled laminations. Smear slide study showed species whose being habitants in infralittoral and upper circalittoral sections of the submarine environment, are identified proving that sediment-gravity flow deposits initiated entrainment from the upper slope region (circalittoral and further up) in SoM. Lastly, 8 out of 14 ages which have been obtained, is used for age model by using Bayesian statistics method. Core however contains sediments loss from the top ~830 years, model includes the date between BP 830 to BP 7170 years. Therefore 6000 years of sedimentary records is obtained and first 10 seismoturbidites are correlated with historical records.

AKTİF FAYLANMANIN KUMBURGAZ HAVZASINDAKİ SEDİMANTER KAYITLARI, MARMARA DENİZİ

ÖZET

~1600 km uzunluğundaki Kuzey Anadolu Fayı'nın batı kısmında bulunan Marmara Denizi, Ege Denizi ve Karadeniz arasında bir geçiş bölgesi görevindedir. Marmara Denizi kuzey kısmında Kuzey Anadolu Fayı'nın aktif teknotik rejimi dolayısıyla beş büyük sedimanter havzaya sahiptir. İnsan hayatına mal olan ve şehirleri yokeden ~150 deprem ile 2500 yıllık uzun deprem geçmişi kayıtlar altındadır. Kuzey Anadolu Fayı'nın Marmara Denizi'ndeki en aktif kolu olan Kuzey kol, depremle tetiklenen çökeller için korunaklı muhteşem bir arşiv ve dikkat çekici bir laboratuvar olan sedimanter havzaları şekillendiren biçimlendiren bir role sahiptir.

Deniz altı paleosismoloji çalışmalarında, sediman-gravite akıntı çökelleri deprem tarihi çalışılacak alanda kullanılan genel bir metottur. Sismotürbidit terimi, kendine özgü stratigrafik, sedimantolojik ve jeokimyasal karakteristiklere sahip depremle tetiklenen türbiditlerdir. Fakat ayırt edici özellikleri henüz tam olarak açıklanamamış veya tanımlanamamıştır ki, tezin başlangıç noktası da terimin ayırt edici özelliklerini belirleyen, uygun bir tanımlama yapmaktır.

Bu tür su altı paleosismoloji çalışmalarında, çoklu-parametre yöntemler kullanılarak daha keskin sonuçlara ulaşılır. Bu nedenle yapılan bu çalışmada çok sensörlü karot alıcısı (MSCL) ile yoğunluk ve manyetik duyarlılık ölçümü yapıldı. X-ray Floresans aleti ile kalsiyum, potasyum, demir, mangan, stronsiyum element ölçümleri yapılarak fiziksel parametreler ile korelasyon sağladık. Tane boyu analizlerini MasterSizer (Malvern) kullanarak gerçekleştirildi.

Marmara Denizi'nde ojinografik ve tektonik geçmişi incelemek üzere, "pourquoi pas?" gemisi ile multi disiplin bir çalışma için karotlar alınması amacıyla MARsite (2014) seferi düzenlenmiştir. Bu tez, MARsite projesine ait uzun bir piston karot ve beraberinde birkaç sismik yansıma profillerini kapsamaktadır. Tüm deneyler ve gözlemler Doğu Akdeniz Oşinografi ve Limnoloji Merkezi (EMCOL) laboratuvarlarında yapılmıştır. Radyokarbon analizi ise CEREGE radyokarbon laboratuvarında gerçekleştirilmiştir.

Emcol kapsamında XRF, MSCL, Mastersizer, loglama ve smear-slide çalışmaları yapılmıştır. Yaklaşık 10 yıllık bu tür konularda çalışmalar yürüten ve projeler üreten bir kurumdur. Emcol laboratuvarlarında gerçekleştirilen deneyler sonucunda elde edilen türbidit seviyeleri Radyokarbon analizi için Cerege (Fransa)'ya yollanmış gelen sonuçlar ile yorumlamalara geçilmiştir.

Karot alımı için seçilen bölgelerden biri olan, Kuzey Anadolu Fayı'nın Kuzey kolundaki Orta Segmentin geçtiği Kumburgaz Havzası segmentin anlaşılamayan davranışı nedeniyle özellikle ilgilenilmiştir. Hem tektonik olarak hem de oşinografik olarak havzanın Holosen boyunca tarihi tam olarak bilinmemektedir ki bu nedenle, sismotürbidit birimleri üzerinde fiziksel, jeokimyasal, dokusal ve paleontolojik metotlar ile (1) 7000 yıllık havzanın teknonik geçmişi, (2) ayırt edici özellikleri

belirleyerek ve önemini göstererek sismotürbidit konseptini belirlemek, (3) asismik kayan veya kilitli olan Orta segmentin belirsiz davranışına bir cevap bulmak amacı ile çoklu-parametre çalışması uygulanmıştır.

Çıkarılan piston karotu CS-01 28 sismotürbidit birimi içermektedir. MSCL, XRF, taneboyu, smearslide çalışmaları kullanılarak çökellerin sedimantolojik özelliklerini belirlenmiştir.Ters boylanmış türbiditler belirlendi, Kumburgaz Havzası'nda bulunan batimetrik bariyerin varlığı ile bu çökelmenin dinamiği açıklandı. Normal şartlarda yukarı doğru azalan bir tane boyu değişimi gösteren türbiditler, sismik profil ve batimetri haritasıyla varlığı kanıtlanan bariyer nedeni ile terslenerek çökelmiştir. Bu çökelme dinamiği "hidrolik atlama" prensibi ile açıklanmaktadır. Aynı yapı kurak bölgelerdeki "dune" yapılarında görülen çapraz tabakalı laminasyonlardaki ters derecelenme örneği ile aynıdır.

Amalgama türbiditler, aynı zamanda sediman-gravite akıntı çökellerinin zaman aralıklarını belirleyen elemental değişimler ile tespit edildi. Amalgama yapısı bir veya birden fazla peşpeşe gelişen olaylar sonucunda oluşan çökel istifine verilen isimdir. Bu yapının varlığının kanıtlanması Kumburgaz'daki türbiditlerin birden fazla çökel içerdiğini bu da diğer göstergeler göze alındığı zaman deprem ile oluşabileceğini desteklemektedir. Amalgama yapının kaç ayrı zamanda oluştuğunu mangan anomalisi ile yakalanmaktadır. Tezde örneği verilen amalgama yapıların bir kısmını tabanda temsil eden bir mangan anomalisi ile temsil edilmektedir. Bu yapı birden çok türbiditin peşpeşe aynı olay nedeni ile çökeldiğini göstermektedir.

Buna karşın, birden fazla mangan anomalisi ile belirlenen amalgama türbiditler de mevcuttur. Bunların varlığı amalgama türbiditin belli bir zaman aralığında belirli sayıdaki olay neden ile çökeldiklerini göstermektedir. CS-01 karotunda iki mangan anomalisine sahip türbiditlere rastlanmıştır.

Çoklu mangan anomalisi redox ufkunun göçünün birden daha fazla gerçekleştiğini buda birden daha fazla ani sedimantasyona maruz kaldığını gösterir ki, depremle geldiği tespit edilen bu yapılarda bulunan amalgama yapılar bir depremi ve peşisıra gelen bir arkçının varlığını göstermektedir.

Sismotürbiditler için en önemli ayırt edici özellik olan "su kolunu salınım etkisi" neredeyse CS-01 de ki tüm türbidit seviyelerinde belirlendi. Bu salınım hareketi normalde kabul edilen türbiditlerin dışında ara seviyelerin daha karmaşık ve yer yer eksik olduklarını göstermektedir. Salınım olması gereken sedimantasyon dinamiğini değiştirmekte ve çökelme mekanizmasını bozmaktadır ki, CS-01 karotundaki türbiditlerde salınım etkisi ile oluşan laminasyonlu yapı türbiditlerin yaklaşık %70 ini oluşturmaktadır.

Salınımın bir önemli göstergesi ise, çökel boyunca sedimanter yapıları etkileyen su salınımları genelde deprem ile meydana gelir ki devamlı su kolonu salınımına bağlı oluşan laminasyonlar nedeni ile karottaki türbiditlerin altbirimlerinin çoğu eksik görülmüştür.

Smearslide çalışması infralitoriyal ve üst sikloritorial bölgeye ait canlıların karottaki varlığını göstermiştir ki sediman-gravite akıntı çökellerinin sediman kaldırıp taşımaya başladığı seviyenin Marmara Denizi'nde yamaç üstü (siklolitoral ve üstü) bölgelerden olduğunu kanıtlamaktadır. Son olarak, elde edilen 14 yaştan sadece 8 tanesi kullanılarak "Bayesian" istatistik metoduna dayanan bir yaş modeli oluşturulmuştur. Karot hernekadar ~830 yıllık sediman kaybına uğramış olsa da, model GÖ 830 dan

GÖ 7170 yıllık kayıt içermektedir. Böylece 6000 yıllık sedimanter kayıt elde edilmiş olup ilk on sismotürbidit seviyesi tarihsel deprem kayıtları ile eşleştirilmiştir.

Sonuç olarak bu çalışmada, sismotürbiditlerin tanımlanması, dünyada kullanımı ve belirlenmesinde bakılan yöntem ve "proxy"ler detaylıca işlenmiştir. Kumburgaz Havzası'nın morfotektonik yapısı açıkça ortaya konulmuştur. CS-01 sediman karotunda incelenen türbiditlerin bu sayede kaynakları ve çökelme mekanikleri belirlenebilmiştir. Marmara bölgesinde son yaklaşık 6000 yıllık sedimanter kayıt incelenmiş ve bölgenin depremselliği üzerine bilgi sağlamıştır.

1. INTRODUCTION

1.1. Scope and Aim of the Study

Sea of Marmara (SoM) which is located as a conduit between Aegean Sea and Black Sea, is bordered by two submarine branches (northern and middle) of North Anatolian Fault (NAF) (McKenzie 1972, Seeber et al 2004) (figure 1.1). NAF is a dextral continental transform fault (dextral kinematics) (Ketin 1948; Armijo et al., 2002; Şengör et al., 2005) which has generated more than 55 (Ms>6.8) earthquakes in the last two millennia (Ambraseys and Finkel, 1991, 1995; Guidoboni et al., 1994; Ambraseys and Jackson, 2000; Ambraseys, 2002). Dense tectonic activity causes slope instability along the northern shelf area. Because of this, co-seismic sedimentation sequences are deposited, being a unique laboratory for subaqueous paleoseismology studies.

Particularly after 1999 earthquakes, many international projects focused on understanding the submarine branched of the NAF in SoM. Now we have considerable amount of knowledge about geometry and kinematics of all basins in SoM, except from Kumburgaz Basin. The tectonic and earthquake history of this relatively small and shallow basin remains not well-understood. This thesis focusses on the study of the stratigraphy, Holocene earthquake history and tectonic character of the Kumburgaz Basin based on the analysis of the sediment cores, seismic reflection profiles and submarine morphology.

This study focuses on Kumburgaz Basin, which is relatively shallow, and smaller basin comparing, is located between Central basin and Çınarcık basin of Northern SoM. 21-meter-long Piston core which is the deepest studied so far, has been recovered at the depocenter of the basin where sequences warping to the main strand of the NNAF.

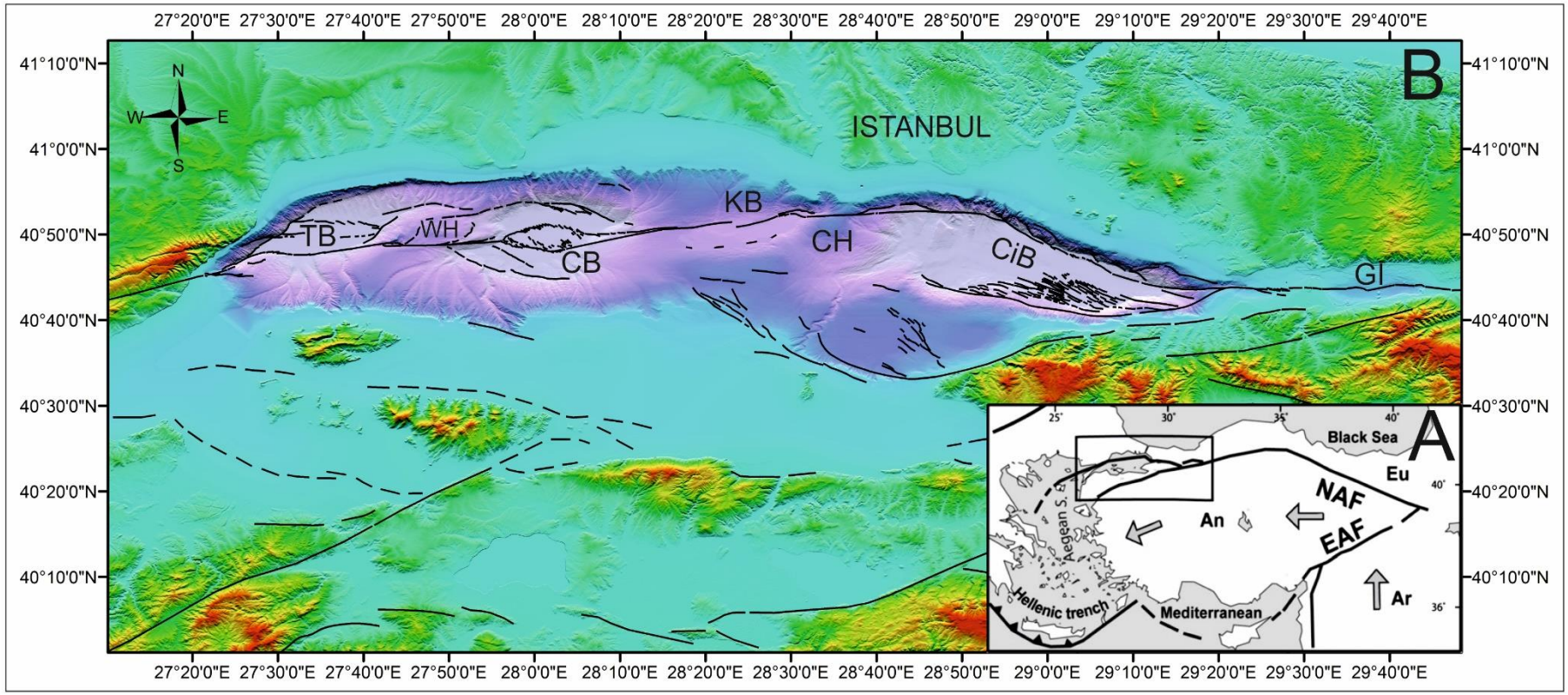

Figure 1.1: Location of the Study and Tectonic Setting a) General tectonic setting of Turkey, inset map represents current tectonic setting of Turkey and surroundings. Movement of Arabia (Ar) and Anatolia (An) is marked with arrows relative to Eurasia (Eu). b) High Resolution Multi-Beam Bathymetry Map of Sea of Marmara, morphological aspects are named with abbreviations (CB, CiB, CH, GI, KB, TB, WH are Central Basin, Cinarcik Basin, Central High, Gulf of Izmit, Kumburgaz Basin, Tekirdag Basin, Western High respectively.) and faults are displayed with black lines after Uçarkuş, (2010).

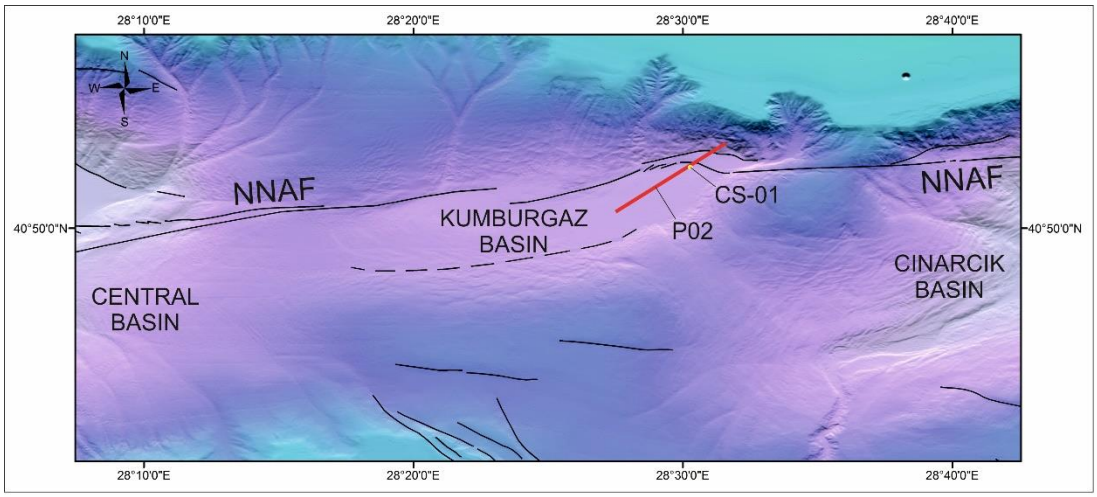

Figure 1.2: Bathymetry map of Kumburgaz Basin and surroundings. Faults are indicated with black lines. Core CS-01 and corresponding seismic line is marked.

In the Core CS-01, 28 turbidite layers have been identified based on their sedimentological, geochemical, textural properties of the core sediment (see figure.7). Such wide multi-parameter analyses provide us to recognize the depositional processes due to different hydrodynamic and paleoclimatic conditions prevailed during the Holocene in the Kumburgaz Basin.

Thesis combines proxies, which have been used since, and presents distinctive aspects of seismoturbidites with depositional models for each dynamic condition. Furthermore, morphological effects are processed and explained by displaying different grading trends and overlaying successions. Moreover, subsequent depositions are identified which indicates subsequent earthquakes. By aging seismoturbidites, last 7000 years of paleo-earthquake history is quite explained thus, implications for creeping versus locked debate of Central Segment is given by examining previous earthquake intervals which have been identified on the sediment core.

1.2. Hydrological Properties of Sea of Marmara

Different salinity characteristics of Mediterranean and Black Sea causes bidirectional flow through the Dardanelles and Bosporus. Therefore, SoM has two layered water column, which constrains motion of bottom currents. As Mediterranean originated bottom column (38.5‰ salinity) flows through Black Sea, top column that is originated from Black Sea (18‰ salinity) flows to Aegean Sea (Ünlüata et al 1990).

Through mixing and diffusion between Mediterranean and Black Sea, salinities ranges to 36‰ and 22‰ respectively so that, the halocline level is estimated at -25 m depth.

Surface water circulation of SoM is related with anticyclonic loop due to the difference of water level between Aegean and Black seas (Beşiktepe et al 1994). Especially during late autumn and summer, water flowing through Bosporus, which is originated from Black Sea, causes the top water circulation in SoM. Southern oriented flowing upper layer, which have 60-75 cm/sec velocity, turns firstly to westward motion then direction changes to northwestward orientation due to presence of Armutlu Peninsula. Lastly, it is directed to Dardanelles by moving through all Bay of Tekirdağ. This anticyclonic behavior effects Çınarcık Basin, Central High, and Central Basin respectively. Furthermore, on Prince Islands, Armutlu Peninsula and the region between Surface water flow velocities changes locally and seasonally between 20-50 cm/sec. Regeneration time for top water column lasts 4-5 month due to meteorological conditions (Ünlüata et al 1990, Beşiktepe et al 1994). Salinity of surface water may fluctuate (25-26‰) due to mixing causing from intensity of winter and autumn weather conditions (Beşiktepe et al 1994).

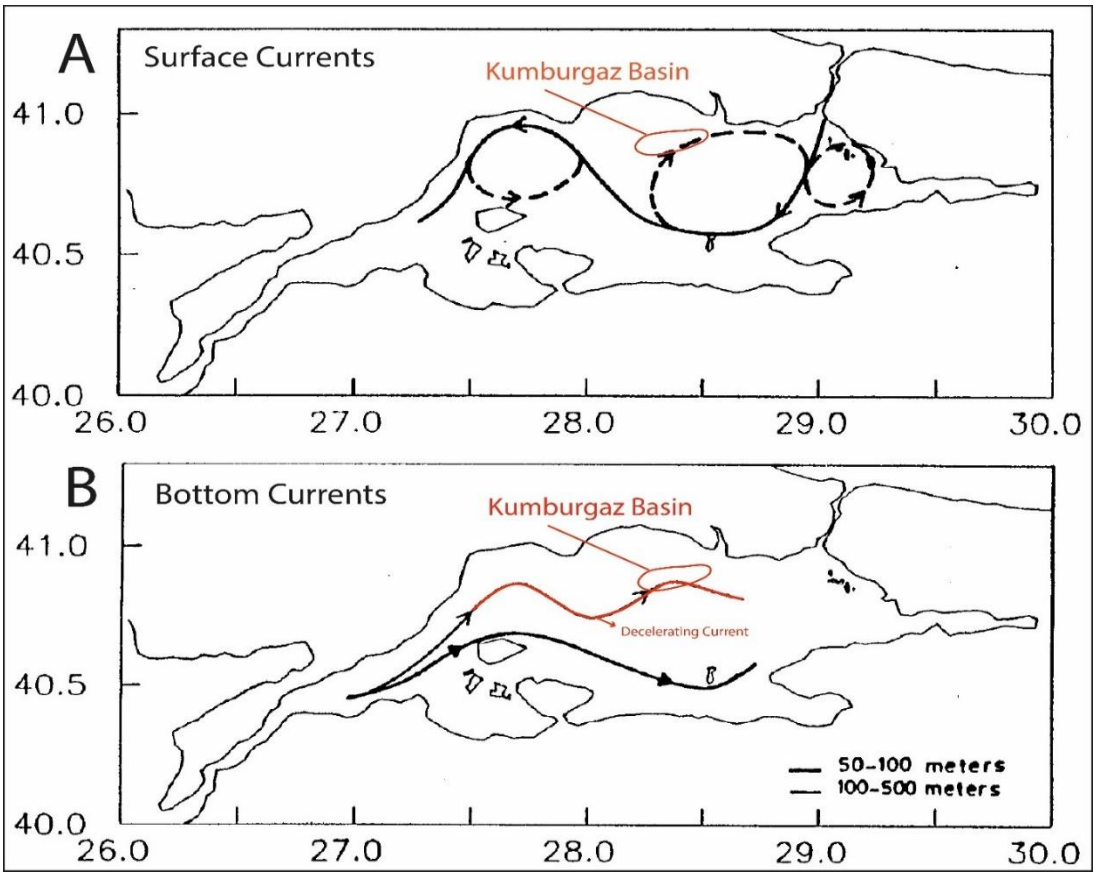

Figure 1.3: Two layered water columns of Sea of Marmara. A) Surface currents, which are originated from input of Black Sea. Continuous lines represent permanent currents in summer seasons. Dashed lines represent repetitive temporal currents. Currents are circulating over Kumburgaz Basin; however, halocline is around -25 m depth. B) Bottom currents that are originated from Mediterranean. Currents are spreading into the depths (between -100 to -500). Loosening causes deceleration of flow velocity. Note that, bottom currents reaching Kumburgaz from west in a sluggish manner thus, currents are not able to reach Çınarcık Basin and further basins in Gulf of Izmit. (Modified from Beşiktepe et al 1994)

Bottom current initiates its motion from Dardanelles, spreads to the depths of SoM which forms a west-east directed slackly motion and lasts at the Bosporus. Regeneration time for bottom column lasts 6-7 years. With the seasonal changes, bottom current is clearly seen on Tekirdağ Basin. In winter, current subside and decelerate in Tekirdağ basin and Western and Central high prevents the eastward-decelerated motion. Therefore, Basins relatively eastern to the Tekirdağ Basin are rather invulnerable to the effects of the bottom currents. Furthermore, eastern basins become broadly poor on oxygen content (Ünlüata et al 1990)

2. PREVIOUS STUDIES AND METHODOLOGY

2.1. Previous Studies

It is aimed to summarize what have been studied before in terms of Subaqueous Paleoseismology which, is divided into parts to accentuate how studies can differ basin to basin on various hydrodynamic conditions. Note that, only the related aspects between thesis and previous studies were mentioned in the text. Because the aim of the study is to identify the distinctive features of seismoturbidites so that, description of studies may not contain all the data and interpretations which have found and explained in the related studies.

Sea of Marmara is focused, which four basins located on Northern part. Basins in SoM have exclusive nurturing systems, diverse depths therefore, unequal dynamics. we stress on the lakes, much more conservative areas, relatively shallower regions than the basins in SoM. Some of the distinctive features of sediment-gravity flows are more apparent than any other places and it will be briefed about broad seas and ocean margins, which is the kinematics may differ in described studied.

2.1.1. Sea of Marmara

Sarı & Cağatay (2006) is an exclusive study in case of proxies, taking place in Sea of Marmara about sediment-gravity flow units. Study is located in Çınarcık Basin, which is investigated by two gravity cores. Foraminifera assemblages are classified and shallow level habitant species are identified. It is important to make such an exception because presence of infralittoral and upper circalittoral species suggests that disruption at upper valley is severe which is pointed out as a proxy to prove the sediment-gravity flows are generated by earthquakes. They improved their ideas by displaying the presence of detrital material and grainsize distributions in the related layers. Most important aspect is the elimination of other triggers by investigation of morphological, ecological and climatological aspects of the basin and surroundings. Therefore, they concluded the investigated units are triggered by earthquakes thus, any other trigger mechanism is unlikely to be a reason for slope failure in Gulf of Izmit. Dynamics of

the region is crucial to be contained in the equation to evaluate the sediment-gravity flows origin.

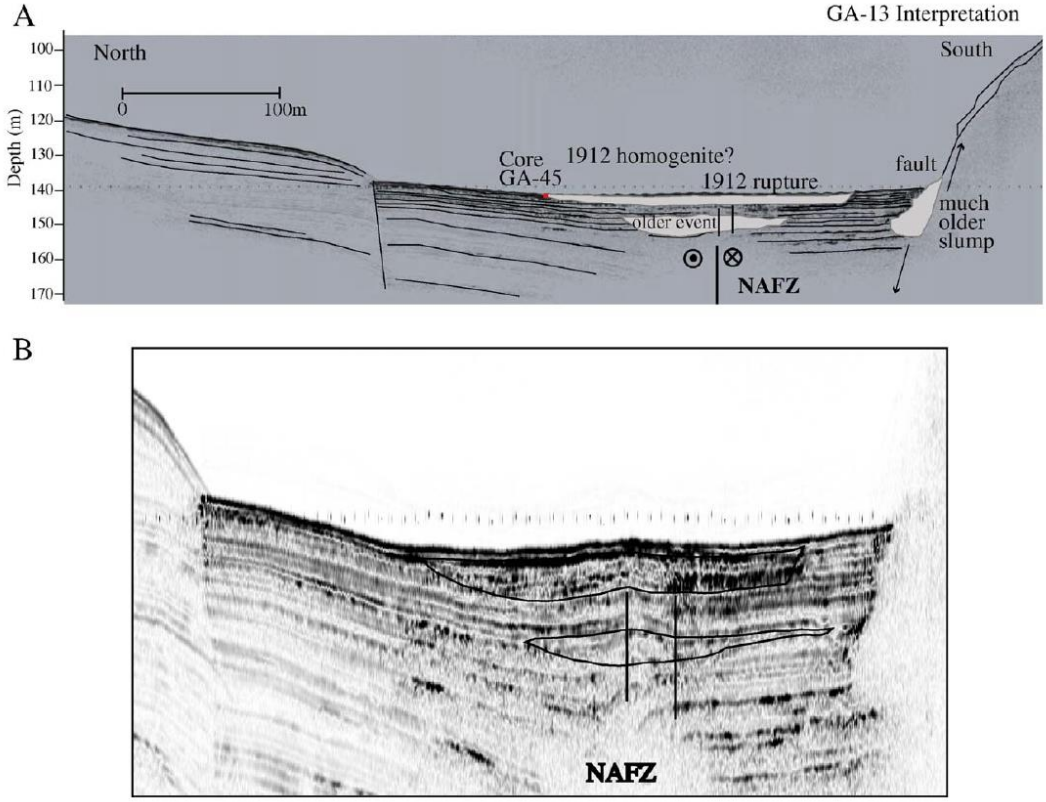

Figure 2.1: Seismic reflection profile located on Tekirdağ basin. Authors focusses on the presence of acoustically transparent layers interpreted as homogenite sequences. McHugh et al (2006) It also identifies the 1912 Mürefte earthquake's homogenite.

McHugh et al (2006) contains dataset both Tekirdağ and Izmit Basins. They use multi-parameter proxies to establish the earthquake-triggered sedimentary units for 2000 years of history. With the high-resolution seismic reflections (figure 2.1), they were able to identify homogenite of 1912 Ganos earthquake. They also correlate seismic reflections with the core study. They suggest that depocenter which have flat topography due to seiche currents are the most secure regions for the traces of co-seismic sedimentation (figure 2.2). Due to sediment-gravity flows slope, particles are entrained thus, eroded. They suggest the absence of units on seismic profiles are caused by erosion. Mentioning seiche related disturbance is the way of showing the proof for earthquake-triggered sedimentation.

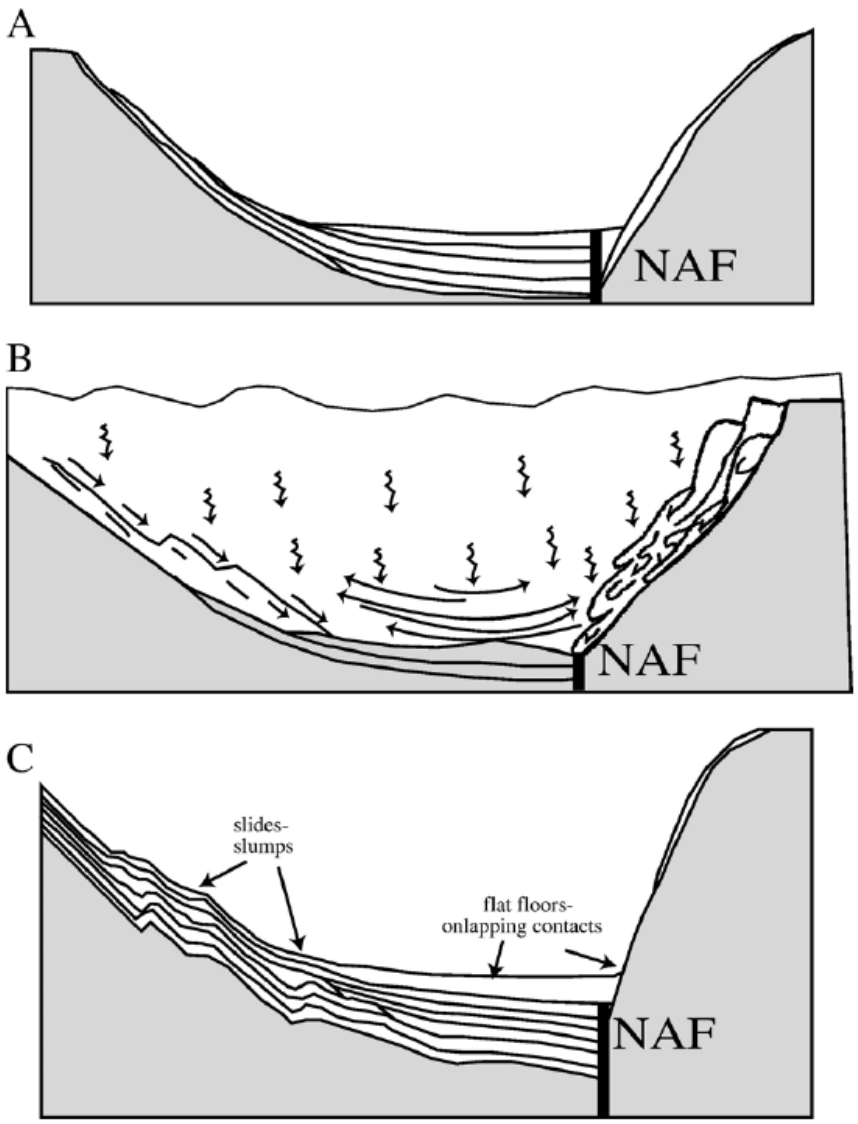

Figure 2.2: McHugh et al (2006) explains the depositional processes from constant hemipelagic sedimentation to earthquake-triggered sedimentation.

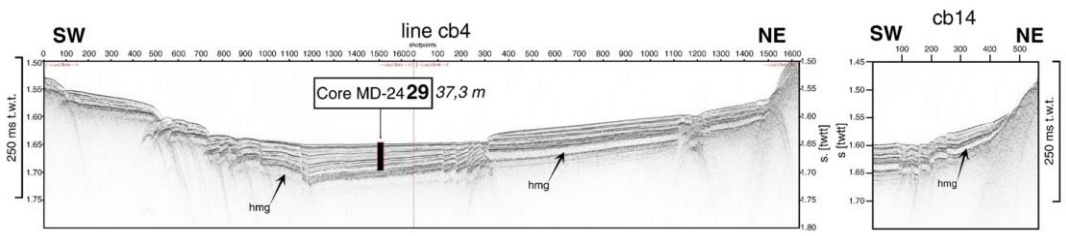

Figure 2.3: Beck et al., (2007) is detected the presence of acoustically transparent layer in Central basin. It is interpreted as homogenite sequence.

Beck et al., (2007) contains northern basins of SoM. After 2002 MARMARASCARPS cruise, at least last 20 kyr history of Marmara basins are studied thus, stated sedimentary fill mostly dominated by turbidites. However, study especially focuses on Central basin with core data and seismic reflection profiles therefore, a unique almost 8 m long homogenite sequence is detected (figure 2.3). In Eriş et al., (2012) (see subsequent paragraph), same homogenite unit is also traced in Çınarcık Basin. Seismic reflection profiles are failed to show coarse grained section of turbidites because of their limited thickness. However, meters long homogenous mud shows an acoustically transparent layer which is detectable. They suggest in one of the depositional models, presence of reflected turbidites. One of the major precursor of this study is showing the existence of seiche effect on sediments which have been mentioned as a cause for segregation. Truly, seiche can be differentiated basin to basin. However, according to basin's topography seiche can alter the suspension (figure 2.4). Moreover, presence of sedimentary structures such as ball and pillow, flaser bedding, erosional base and traces of soft sediment deformation supports their idea of earthquake-triggered depositions.

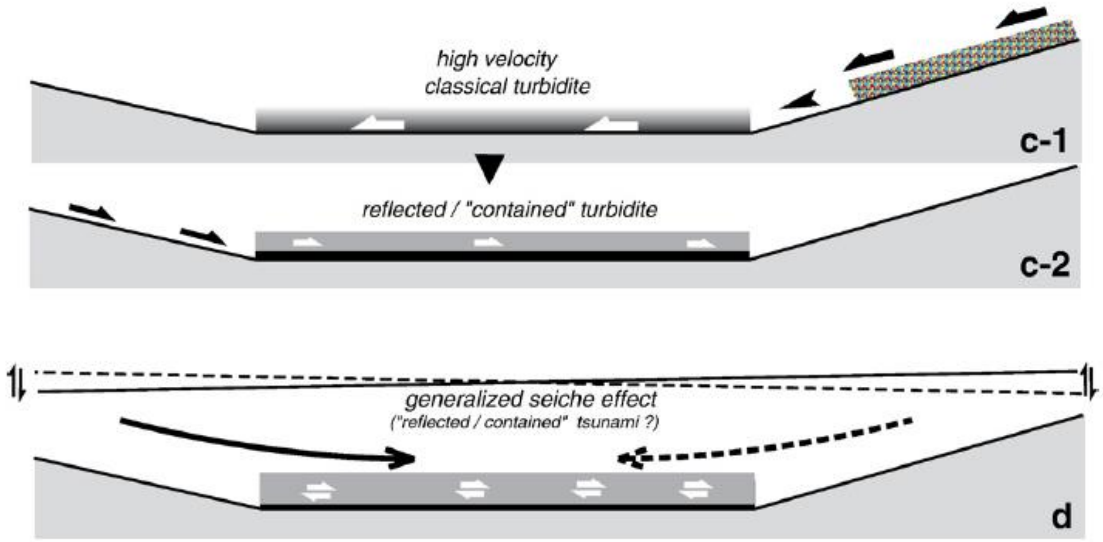

Figure 2.4: It is estimated if the morphology is sufficient sediment-gravity flow can experience a reversed motion onto recently deposited sequence (Pickering & Hiscott 1985). Depositional model in Beck et al (2007) shows the possibility of reflected/contained turbidite deposits due to morphology and water oscillations.

Eris et al., (2012) is a critical study to show how different dynamics affect even co-seismic sedimentation. Study is located at Çınarcık Basin, the widest and deepest basin in SoM. In the studied core, they have identified various turbidites within different

textural aspects. They used C-M graphs to show the different transportation mechanisms to vindicate the changes of hydrodynamics. Clearly, C-M graph indicates there is a strong sharp transition between sublayers of turbidite succession. Furthermore, a mega-turbidite (figure 2.5) is located around 1 m long in the lacustrine part of the core which is also visible on seismic reflection profiles. They correlate the mega turbidite which contains erosional base coarse grained layers at basal part and homogenous mud dominant cap, with the similar unit (figure 2.6) described as acoustically transparent layer, homogenite in Beck et al., (2007).

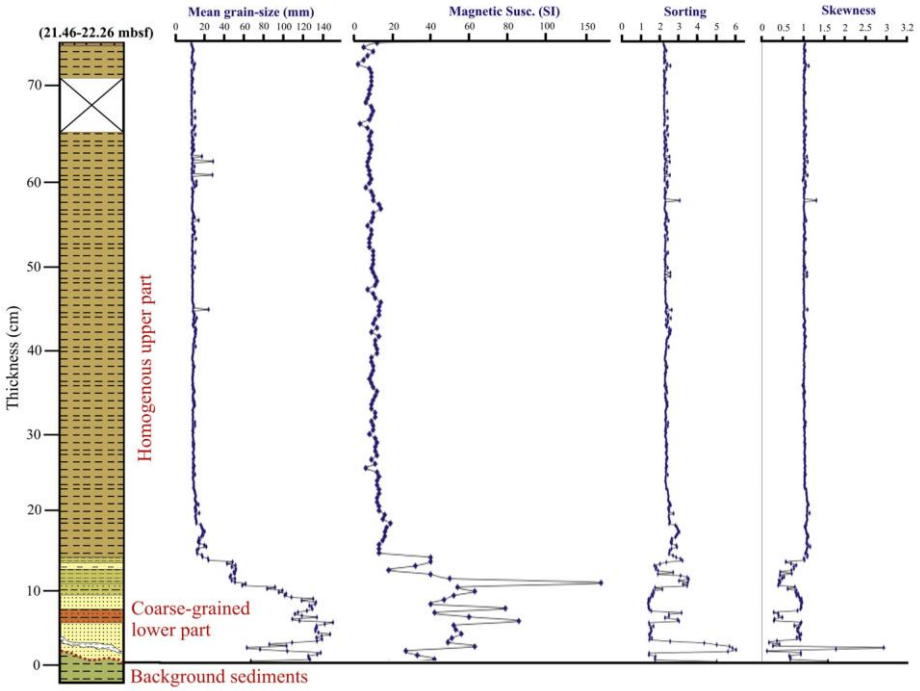

Figure 2.5: Eriş et al (2012) is identified the presence of a mega-turbidite unit between 21-22 mbsf. Magnetic susceptibility and grain-size parameters indicate the boundary between turbidite and homogenite precisely.

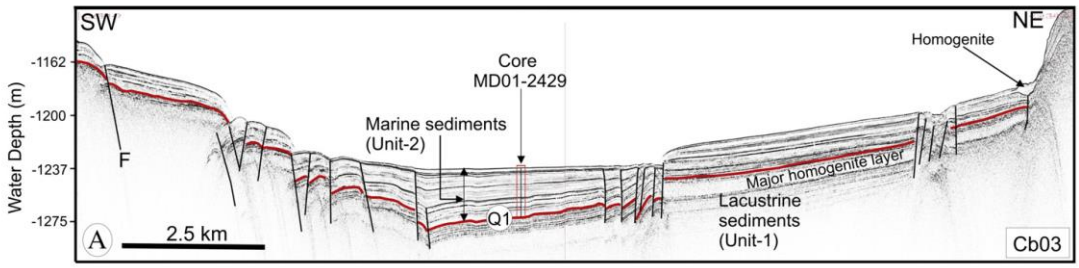

Figure 2.6: Seismic reflection profile on Eriş et al (2012). Authors assert the major homogenite layer is similar to the layer which is identified in Beck et al (2007).

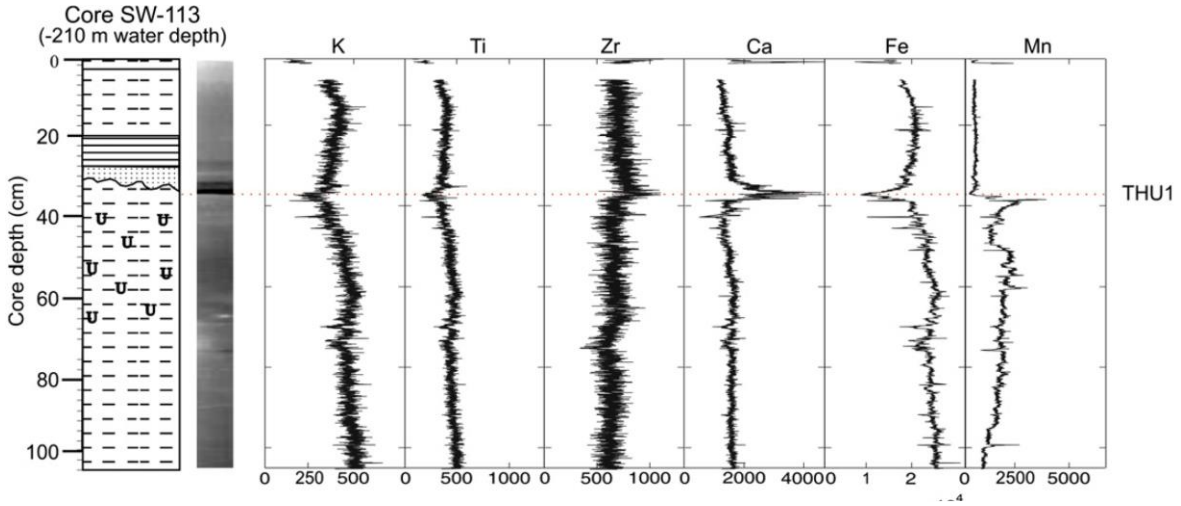

Figure 2.7: Cağatay et al (2012) shows the elemental proxies on the THU1. Mn pulse at the basal part of the succession. Detrital input is shown by Fe, K, Zr. Organic material content is displayed by Ca decrease through the succession.

Cağatay et al (2012) studied Izmit Gulf by being recovered two short cores in Karamursel Basin. Study determines the THUs (Turbidite-Homogenite Units) by using physical properties (density, magnetic susceptibility, grain size, radiography) and geochemical (elemental analyses) aspects (figure 2.7). Especially, study uses Mn as a proxy to determine the redox fronts so that, it is being connected with co-seismic sedimentation by explaining that sediment-gravity flows supply sediments which is ended up generation of new redox fronts. They also used C-M graphs (figure 2.8) to show the different dynamics within a succession. Furthermore, the composition is classified with elemental proxies by displaying the ratio of organic and detrital materials. They encountered normal graded sequences and subdivided the layers with corresponding elemental composition which is suggested to see enrichment of detrital material at the basal part of the succession and with a gradual manner, proxies switch back to the state where background sedimentation has.

Drab et al 2012 studied Tekirdağ and Central basins of SoM. They detected synchronous triggering for turbidites in both basins. They used grain-size parameters to distinguish sublayers and different dynamics of corresponding turbidites thus, they constrain the successions by using Mn pulses. As a result, they find seismoturbidites relating with 1912 Mürefte earthquake. They distinguished turbidites in lateral extent, proximal and distal manner to correlate with seismic trigger.

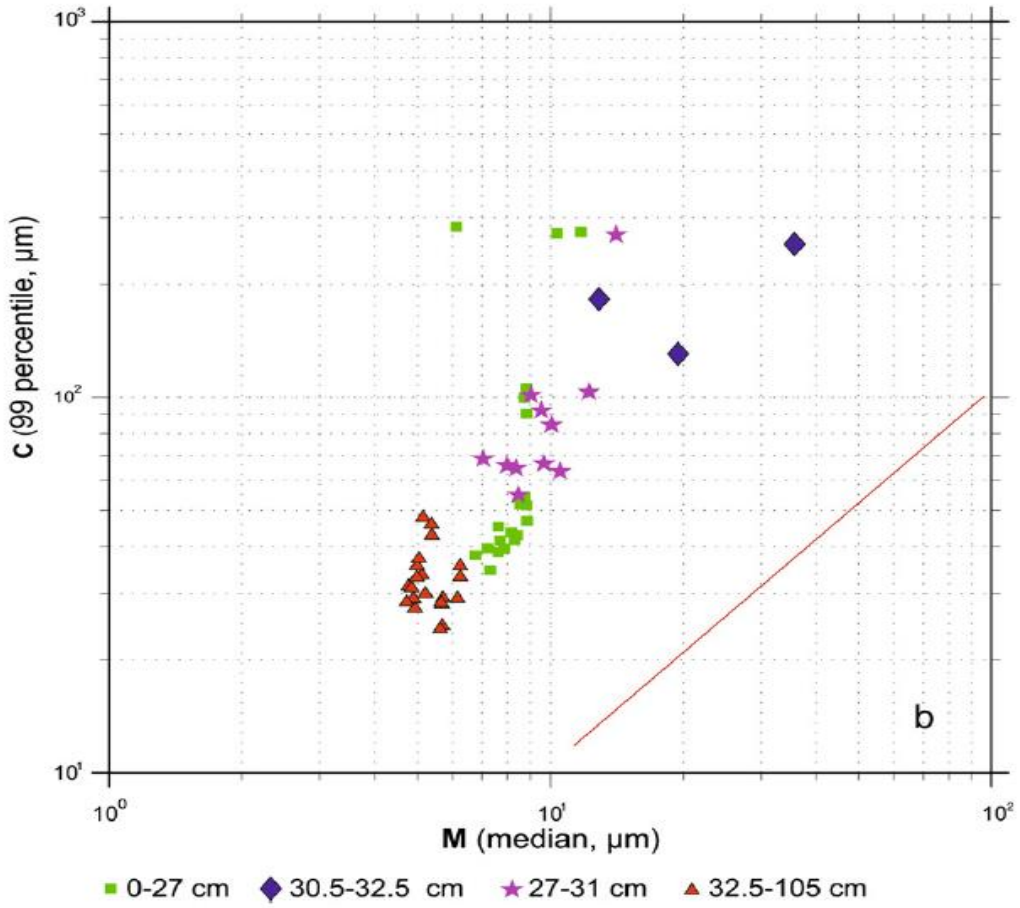

Figure 2.8: C-M graph of THU units in Cağatay et al 2012. C-M graphs displays the different sedimentary transportation sequences. Blue dots are basal coarse part, pink stars are laminated silty layers, green squares are homogenous silty mud (homogenite) and red triangles represents the hemi pelagic sediments.

Drab et al (2015) contains two piston cores from Çınarcık Basin and one from Western High to correlate the earthquake horizons in co-seismic sedimentation. Purpose of the study is to obtain submarine earthquake history of the Çınarcık Basin by correlating the results with the core recovered from Western High. To identify the turbidites, physical elemental and textural properties are exercised (figure 2.9). Multiple locations of the sediment cores are provided the existence of synchronous triggering which is the proof of the origin is earthquake. Especially in SoM, sedimentary basins are conservative in itself. Same aged turbidites are very likely to be triggered from earthquake shaking. Even a rupture can trigger turbidites in adjacent basins.

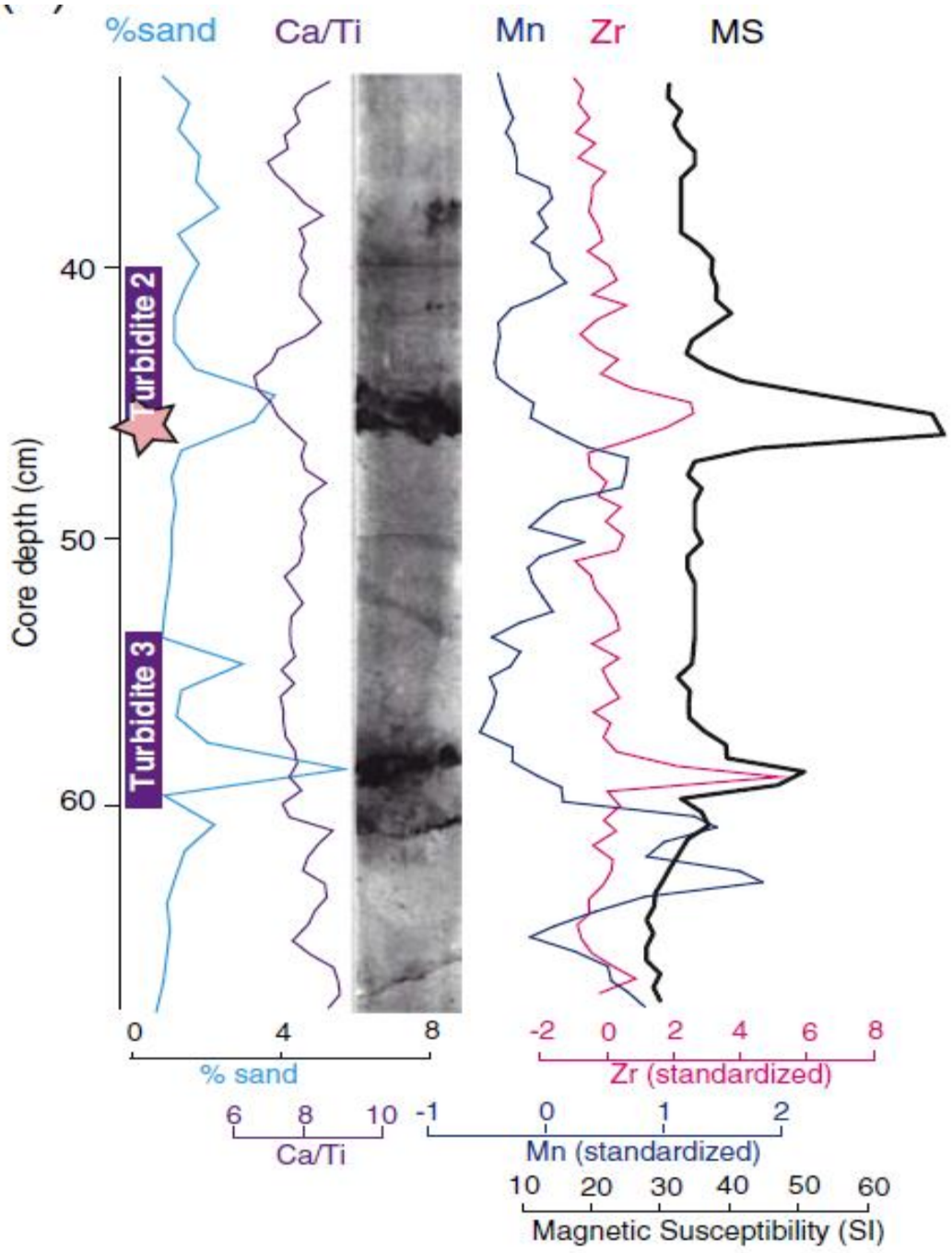

Figure 2.9: Drab et al (2015) displays a seismoturbidite units by showing elemental, physical proxies. Note that, Mn pulse for each turbidite is located at the basal parts. Magnetic susceptibility shows the presence of detrital material.

McHugh et al (2014) focuses on Central Basin in SoM. They used grain-size and elemental analyses to discover earthquake-triggered units. Three, ten-meter-long core is used for this study therefore lateral extent of units are detected. They used radiocarbon ages to find the correlation between turbidites and historical earthquakes moreover, they suggest there may be a connection between turbidites and determination of segmentation. In this case, they found earthquakes that happened on

Central Basins thus, they found earthquakes that related with adjacent segments which again correlated with turbidites in Central basin. Furthermore, they suggest that absence of turbidite which have been generated by 1912 earthquake indicates rupture of 1912 had not reached to Central Basin.

2.1.2. Lakes

Beck et al 1996 contains core study at Lake Annecy in Alpine region. 50 event have been detected on cores especially concentrated on deglaciation period. They firstly, eliminated the morphological aspects to diminish trigger possibilities. Lake Annecy has minimum floor slope which neglect to generation of spontaneous failure due to overloading. Furthermore, coring site has enough distance to river mouths so that, effects of flooding and fore set setting are eliminated. They display stratification of sediment-gravity flow deposits by normal grading sequences interpreted as grain flow debris flow and turbidite deposits containing micro-fractures and ball & pillow structures.

Beck et al 2009 studies sedimentary fill of Lake Le Bourget and Lake Annecy in Alpine region. They have recovered several cores for each lake. They have used both seismic profiles and grain-size distributions in order to identify sediment-gravity flow deposits. They especially detected traces of 1822 earthquake which displays normal grading Turbidite-Homogenite units. Additionally, they showed sedimentary structures and soft sediment deformations along the successions.

Their hypothesis on seiche is interesting because of behavior of water oscillations are just alter the suspension deposition. According to ages of each sediment-gravity flow deposits, they assert the concept of slump versus flood turbidite comparison. They distinguished those types by using grain-size distribution. Skewness-Sorting graphs showed the differences of slump and flood turbidites mechanisms. Therefore, flood turbidites are explained by delta fore set failures after major flood event by-passing a delta.

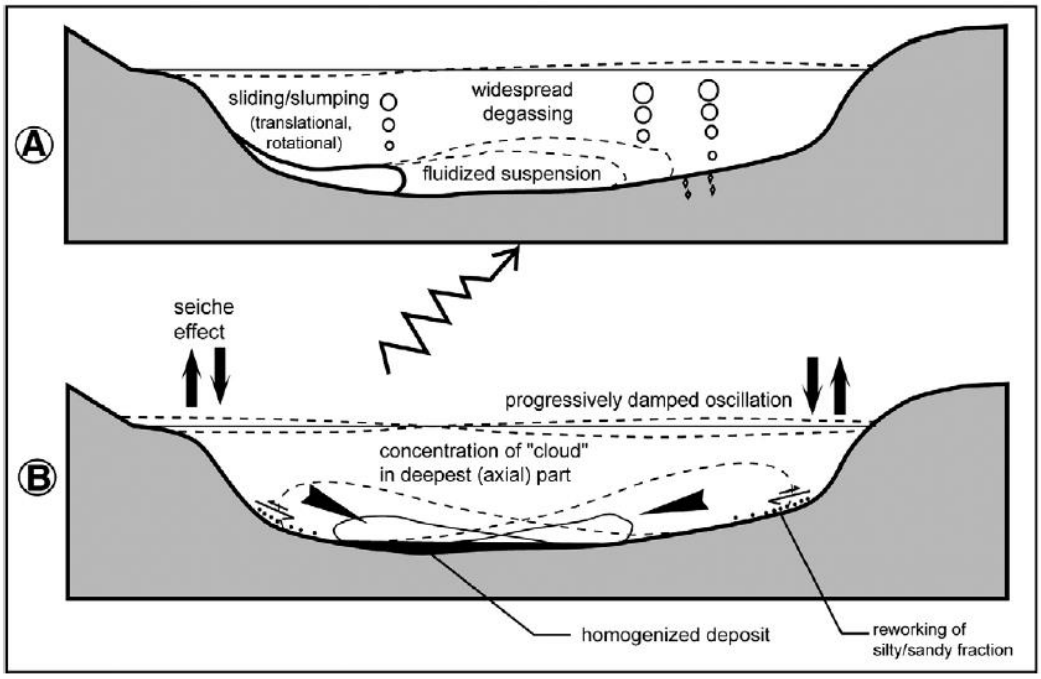

Figure 2.10: Segregation due to water oscillation in Lake Annecy. Due to seismic event, waters oscillations continuously disturb the instantaneous sedimentation. In Lake Annecy, it only delays the deposition of homogenous mud (Beck 2009).

Avşar et al (2015) contains historical records of Boraboy Lake which is located along NAF. They used multiple coring to determine sedimentary records origin. They used physical, especially geochemical proxies and aged the core by using ^{137}Cs and excess ^{210}Pb measurements and AMS radiocarbon measurements from plant fragments. Therefore, they obtained flood-storm related depositions due to heavy rains. Moreover, they distinguished 4 event which has been triggered by earthquakes. Distinction between triggers are well explained by using elemental proxies and organic carbon fractions (figure 2.11). They used elemental proxies by measuring standard deviation so that, only abrupt values show pulses. Therefore, even the most minor changes are visible on XRF graphs. Finally, they suggest trends for each seismically-triggered event. It is clear that their tendency is more alike which can be a classification for earthquake-triggered depositions.

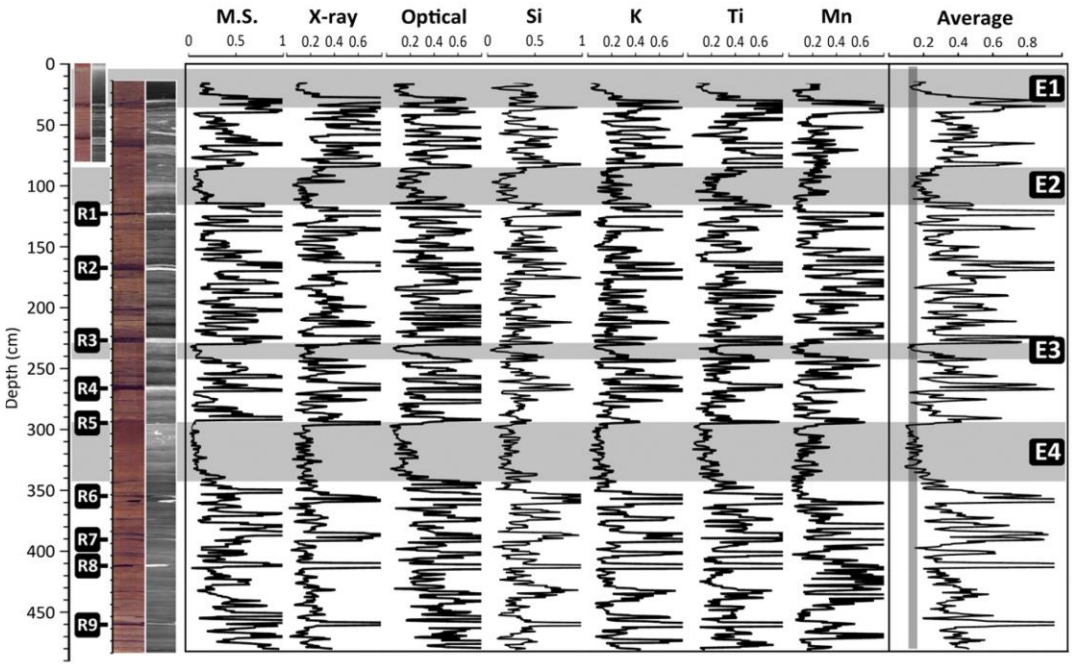

Figure 2.11: XRF results of Avşar et al., (2015). Note that, they used average and standard deviation of elemental proxies so that, only the anomalies would reach in XRF tables.

Hubert-Ferrari et al., (2012) is a paleo seismological study on a sag pond along NAF. Study focused on specific earthquake that has occurred in last millennia. 2-meter-long coring contained 4 sediment-gravity flow deposits which 3 out 4 are correlated with major earthquakes in surrounding area. They used physical, sedimentological, and geochemical proxies to establish the sequences are sediment-gravity flow deposits. Sag pond is named Asacitepecik Lake it is near Gölova and Suşehri between Sivas and Erzincan. Therefore, their aim was the detect 1939 earthquake which still have had the traces of offset displayed by seismic profiles so that they were able to identify 1939, 1668, 1254 earthquakes by strongly correlate with sedimentary sequences. They also eliminated climatological changes which can quite mislead the correlation. However, they showed another sequence which would have been a trace of an historical earthquake, records are not mentioning a major earthquake with related age interval. It shows sequences related with relatively minor earthquake which still can trigger a failure.

Inouchi et al 1996 is a seismoturbidite study that contains 20 units in 3-meter-long sequence in Lake Biwa, Japan. Study contains multiple cores from shallow areas to depocenter of the lake, which provide to determine the down current change of current.

By doing so, it proves the energy drop of the currents, which is supported by thinning and fining through deepening. Furthermore, they correlated each deposition on different cores with a corresponding turbidite by using gradual change of grain size and thicknesses. It is also provided that to determine the flow direction of the current (figure 2.12). They identified turbidites by erosional base with sandy layers, parallel lamination that is visible on radiographic images. Density change is calculated by dry-weights of samples. As correlation between turbidites and earthquakes it is important to point out Lake Biwa did not contain turbidities corresponding minor earthquakes.

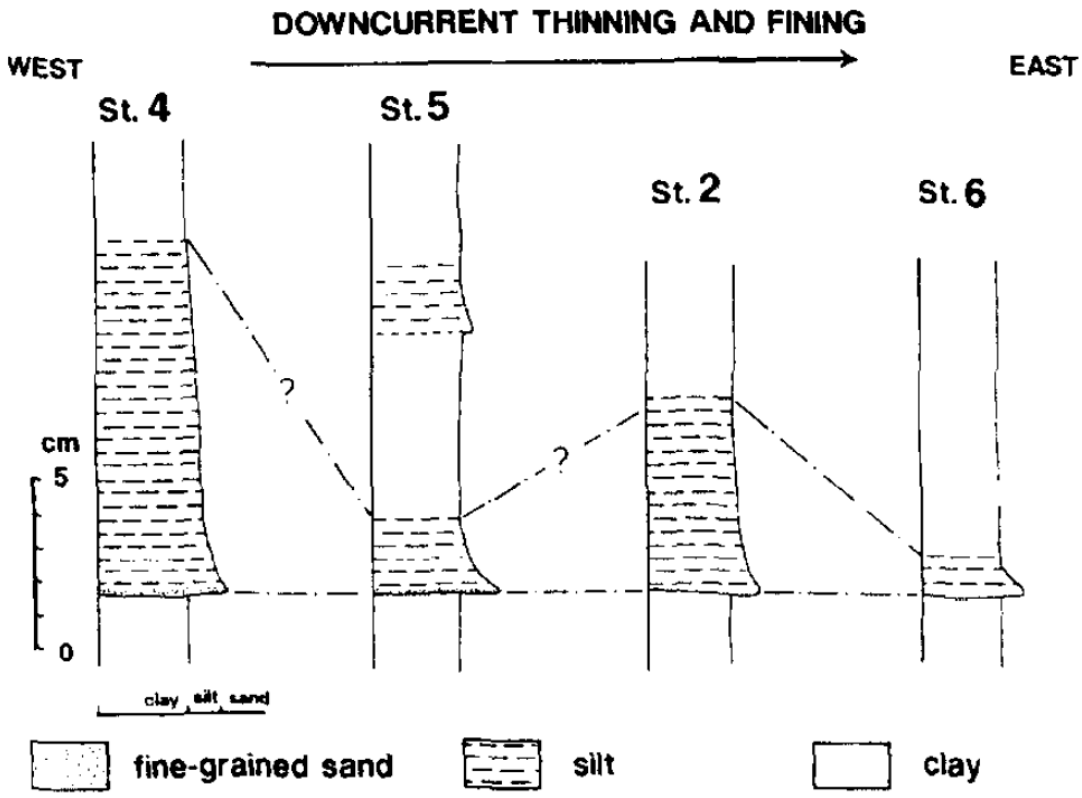

Figure 2.12: Four stratigraphic section from four cores in Lake Biwa. Inouchi et al 1996 shows the lateral extension of a specific event. It is clear to see gradual decrease in grain-size and thickness through east direction.

Shiki et al 2000 is one of the fundamental studies on seismoturbidites. They focused on the distinctive features on units in Lake Biwa, Japan. Abrupt changes in grain size are shown on specified subunits (lower sandy layer and upper silt bearing layer). Textural differences in which have explained as “fluctuation of the silt mode” is one of the important aspect. They started to classify turbidites by proving that whole

succession of Bouma Sequence is not observed in any succession. As for grain size distribution they strongly accentuate even though grading is traceable, it has not a gradual trend. Therefore, constant fluctuation is interpreted because of the generation of several fine-grained (muddy) turbidites, which suggest multiple or subsequent failure therefore seismic origin. Multiple coring provides the range of spreading for each horizon so that, they were able to identify lateral stratigraphic changes which helps to identify proximal and distal depositions. Furthermore, they came up with a depositional model that explains why there are major subunits present. In the model, they suggest bottom current (slump-originated, high-density flow) contains sand size material and upper current (interpreted as suspension cloud, which contains relict sands and mostly silt-clay size material). Authors very well are aware of that, to distinguish seismoturbidites from other triggers, there must be further studies to correlate with the current developments.

2.1.3. Broad seas and ocean margins

Polonia et al 2013 is studied the seismoturbidites in Ionian Sea. They used grain size, x-ray images, geochemistry, mineralogy and micropaleontology to distinguish the units. Study contains two cores that can be correlated with each other. General propose of micropaleontology is to restrict taxons with corresponding environments. By doing so, they have found out where seismoturbidites are generated from. By recognition of taxons in turbidites, they were able to unravel the travel path of currents. They have also encountered increment on Fe, Mn, and Ba and related with seismically triggered redox fronts.

Polonia et al 2016 contains cores and seismic profiles to identify earthquake-triggered depositions. After Polonia et al 2013, this study focuses on depositional model of seismoturbidites in Ionian Sea. They used textural, paleontological, geochemical and mineralogical proxies to provide data in order to establish seismoturbidite precursors. They subdivided each succession into STa to STd part to enlighten more accurate and more precise description for related succession regarding its depositional processes.

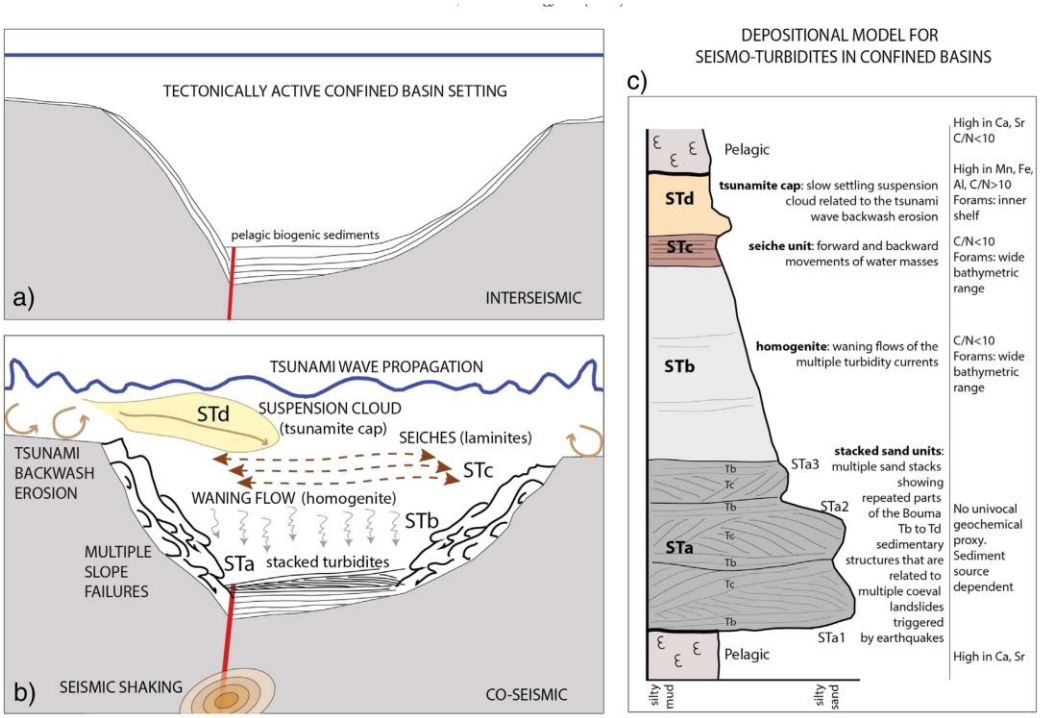

Figure 2.13: Depositional model from Polonia et al 2016. They procreate a stratigraphic column which displays seiche controlled sedimentation deposited after the homogenous mud suspension.

Stratification of an earthquake-triggered deposition is quite unique due to previous studies. Because they suggest the seiche controlled sedimentation deposited after the homogenite succession (figure 2.13). This is an abrupt situation regarding why seiche controlled sediments are delayed that long so that, there is enough time interval to homogenite deposition. When we compare various basins and lakes, it can be implied that seiche effect can alter basin to basin regarding its vastness and depth (see Discussion, seiche controlled sedimentation).

Nakajima & Kanai 2000 studies seismoturbidites in order to find the differences with Bouma Sequence. This is one of the few studies that tried to characterize the term Seismoturbidite. According to study, Seismoturbidites can show amalgamation which is caused by multiple failure at the slopes. Eliminated the other triggers. In discussion, they characterize the seismoturbidites with distinctive features in a figure (figure 2.14), which accentuates the differences with "Normal" turbidites, which is described by Bouma (1962).

Kastens & Cita 1981 is the first study identified homogenite layers (figure 2.15). Study contains seismic profile of Mediterranean ridge and Calabrian Ridge which shows acoustically transparent flat-lying sequences occurred by single event.

	"Normal" turbidites	"Seismoturbidites"
Sedimentary structures	Single bed, Bouma sequence	Amalgamated beds, irregular or incomplete sequence
Grain size variation	Normal grading	Normal grading, inverse grading, grain size break, fluctuation
Compositional variation	Uniform composition between beds, continuous change within bed	Variable composition between beds ± abrupt change within bed
Source	Single source	Multiple or line sources
Inferred depositional process	Deposition from single waning turbidity current	Deposition from a series of surge-type or sustained turbidity currents from the same or different sources

Figure 2.14: Difference of Normal turbidites versus Seismoturbidites in Nakajima & Kanai 2000.

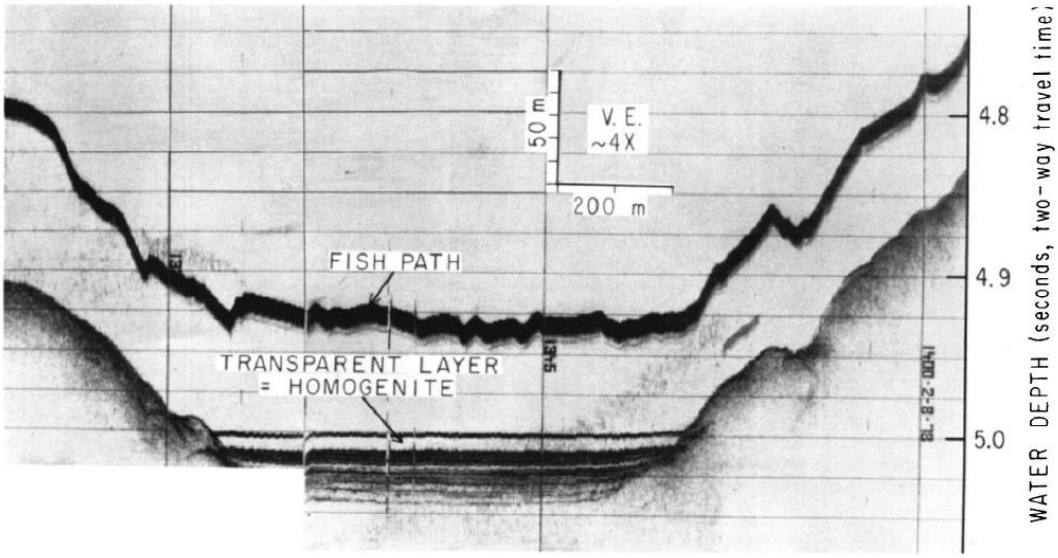

Figure 2.15: Acoustically transparent layers interpreted as homogenite on Kastens & Cita 1981 at Mediterranean Sea.

They found the source of the event as collapse of Santorini caldera which was quite powerful so that, it triggered a tsunami wave affected most of the Mediterranean region. Estimated tsunami is recorded both archeologically and geologically. Multiple locations they have investigated displays tsunami has moved to westward direction. Rugged southern regions were absent in homogenite layers.

Goldfinger et al (2008) is a combined study that includes Northern San Andreas Fault & Cascadia margin dataset recovering from sediment cores. It has been pointed out that synchronous trigger is the proxy to assert the turbidites are earthquake origin. It is a useful method where the coring is available on broad areas. If the aging is consistent with turbidites which is found in different core sites, it is clear to imply synchronous triggering had taken place. The region where synchronous trigger is wide enough to make the assumption of earthquake is the origin of these successions so that, technique provides the elimination of other triggers, which is unlikely to happen on broad, and

multiple submarine canyons having regions. In the study, they have used magnetic susceptibility and gamma density to display the anomalies and correlate with grain-size fluctuations on the turbidite layers.

2.2. Methods

In 2014, piston core CS-01 has recovered from Kumburgaz Basin (-833 mbsf) at latitude 40.54284 and longitude 28.30217 by "pour quoi pas?" Calypso coring provides very long coring by preventing the effects of friction between material and the cover (figure 2.16). Vacuum which is made by a piston, acts like an inverted syringe. However, force that is used on during coring somehow causes sediment loss from the top of the cover. It is measurable by correlating penetration length with sediments in cover.

Figure 2.16: Core recovery during MARsite cruise

EMCOL (East Mediterranean Centre for Oceanography and Limnology) is one of the finest facilities in the area of marine sciences. Facility initiated in 2005 at Istanbul Technical University with funds from the EC 6th Framework Programme. EMCOL contains core analyses laboratory, sedimentology and geochemistry laboratories and

core storage units. EMCOL which has been partner in many international projects, is specialized in geohazards in marine & lake basins and paleoclimate & paleo environmental reconstructions.

Besides from core recovery and radiocarbon analysis, rest of the measurements are executed by equipment in EMCOL laboratories. 80 mm diameter core have cut into 1 meter pieces at cruise and stored at EMCOL storage room at exactly 4-degree for further study. During the thesis study, core has divided into two pieces (one for study, other for achieves).

At EMCOL facility laboratories, lithological features are described by logging (figure 2.17). Textural properties are identified; color for each different lithology is described by using Muncell color scheme. Features that occurred through recovering the core are identified and precautions are taken. Sedimentary structures are identified and relative grain-size changes are determined as in interest of study.

Figure 2.17: Core logging in EMCOL's Sedimentology Laboratory. Lithological aspects are described. Sampling for grain-size or radiocarbon analysis are executed.

After division, achieve core is covered with protection and stored at 4-degree condition. Working part of the core is cleaned thus, sediment surface made smoother for further measurements. Pitted surface can affect the results by creating abrupt pulses even on homogenous layers. Physical properties (density, magnetic susceptibility) are

measured on working core by using Geotek MSCL (Multi-Sensor Core Logger) (Figure 2.18) device at one cm measurement interval. Density which measures an area of requested level on millimeter scale, is a tool to show porosity in which decreases from coarse to fine sediments.

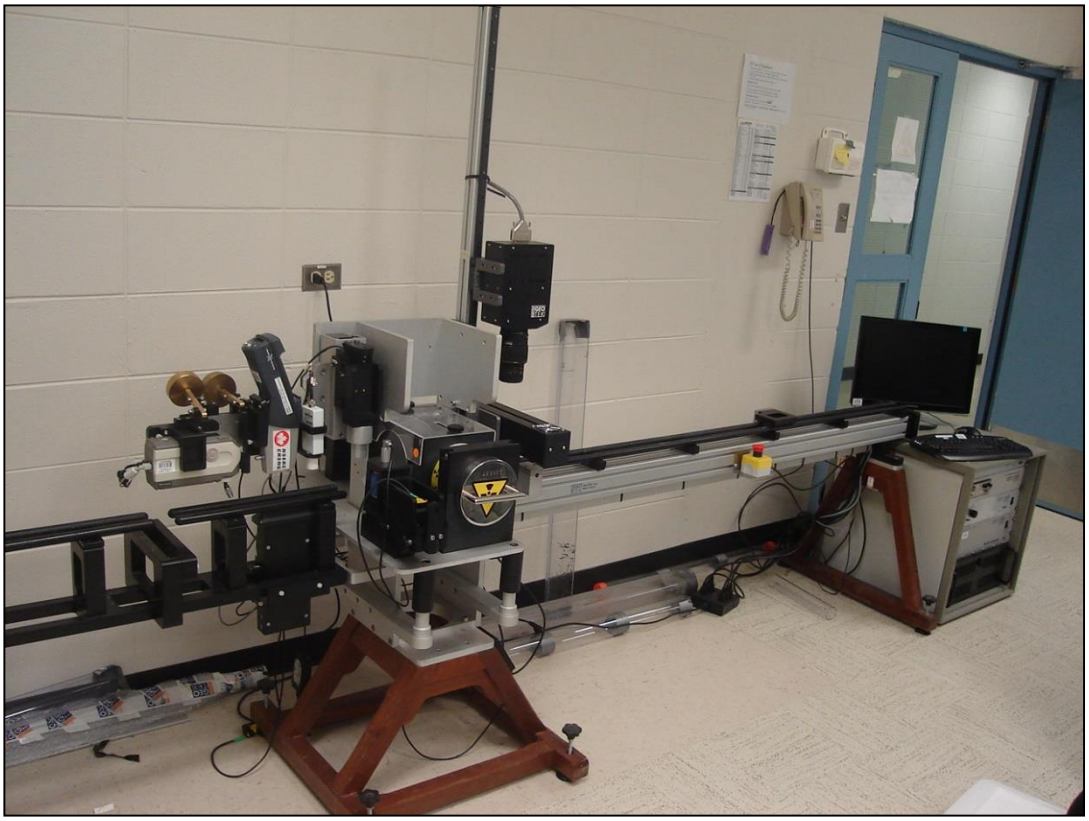

Figure 2.18: GEOTEK Multi sensor core logger (MSCL) provides measurements of physical properties of the sediments cores. Magnetic susceptibility, Gamma density is used for this study in 10 mm measurement interval.

Multi-elemental analyses are performed by Itrax XRF (X-ray fluorescence) (Figure 2.19) device at 1 mm measurement interval. Instrument has a 50 nm pixel resolution optical camera, a laser topographic surface sensor, an X-ray camera and XRF detector system. As pretreatments, before the experiment half core's surface is made smooth to prevent defects on each measurement. On mm scale measurement of a half core whose length is average 1 meter, tests last around 6-8 hours. During such long hours cause overheating which effects directly core's water content hence results will be effected. To prevent such an impact, it is established that film cover is used for preventing loss of water content. X-ray fluorescence analysis: Basically, instrument determinates elemental composition and concentrations on nm or mm scale by exposing the sediment surface to the X-ray beams.

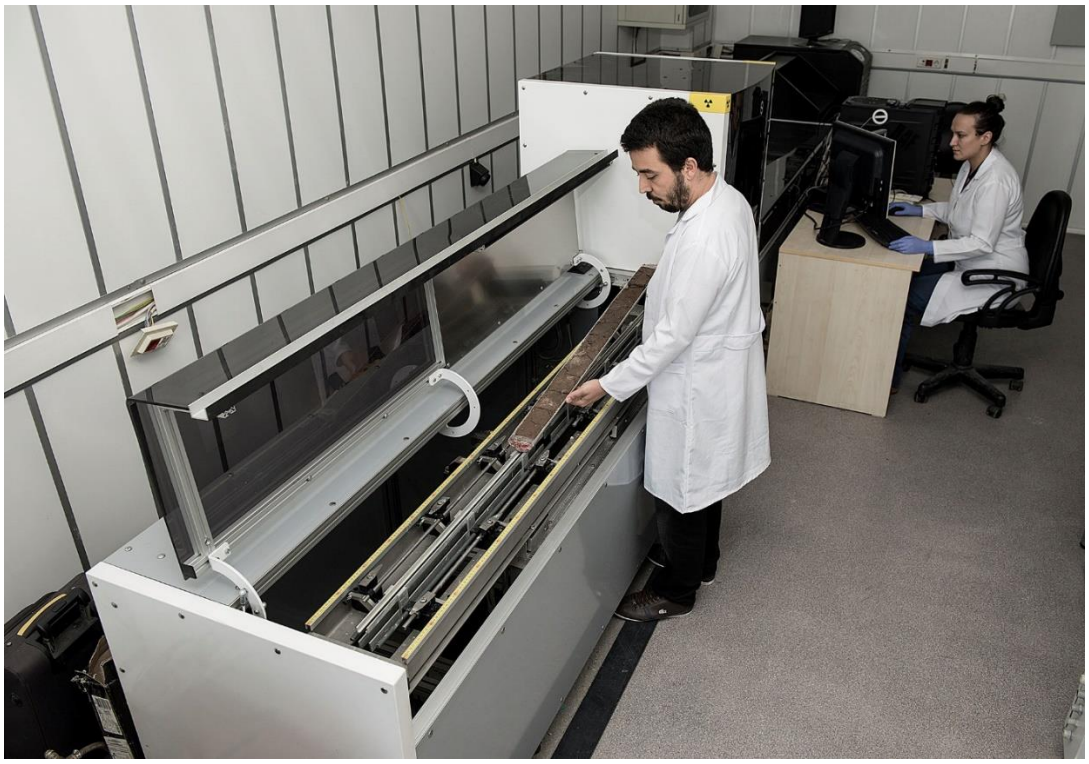

Figure 2.19: EMCOL's ITRAX XRF Core Scanner provides elemental analyses on sediments core with high resolution. Instrument also provides optical and radiographic images. Study contains elemental distributions, which is provided in 1 mm measurement interval.

Measurements of grain-size analysis are executed by Malvern Mastersizer Particle analyzer (figure 2.20) at 0.5 cm interval for per turbidite succession and 5 cm for background sedimentation. For the most natural results, no pretreatment has applied to samples. Organic materials are deducted from samples before each measurement. 10-15 percentage dissolution interval is monitored in each measurement. In stirrer tube, samples are waited to obtain fully mixture with distillated water. Ultrasound technique has performed by instrument to prevent clinging for clay size material. Each measurement performed twice, results are averaged and used for further study.

Figure 2.20: MALVERN Mastersizer Laser Particle Size Analyzer provides particle size measurements, which is used extensively on this study. Five mm sample interval provided high resolution grain size distributions on sediment core.

Smear-slides are prepared at 0.5 cm interval for each turbidite succession. As pretreatment, 63 nm size sieves used to deduct clay-size material. Each sample washed with distillated water. Slides are waited 40-degree oven for evaporation of water content. In slides, textural, petrological and paleontological aspects are examined in order to find differences in each interval.

Lastly, for C^{14} age analysis, at most two cm below for each turbidite succession, sample locations are chosen. Samples are washed with distillated water and through 63 nm size sieve used for extract the clay content. Rest is dried in 40-degree oven for collecting. Thus, planktonic foraminifera, epifaunal benthic foraminifera, whole-body shells, spicules are picked and stored in protective cover. 15 samples are prepared for analysis where executed by Cerege Radiocarbon laboratory.

3. MORPHOTECTONICS OF KUMBURGAZ BASIN

3.1. Tectonic Background

NAF extends west to east for nearly 1600 km (figure 1.1). Counter clockwise motion of Anatolian Block relative to Eurasia provides dextral kinematics (Barka & Kadinsky-Cade 1988, Şengör et al 1985, Armijo et al 2002, Le Pichon et al 2001, Le Pichon et al 2003, Yaltırak 2002, McKenzie 1972) with a right-lateral offset is around 50 to 85 km long (Armijo et al 1999) in estimated age of 10-13 myr (Armijo et al 2004, Reilinger 1997, McClusky et al 2000, Şengör 1979). Based on GPS current slip rate is estimated 24 mm/yr (Reilinger 1997, Straub et al 1997, McClusky et al 2000). Submerged Section of NAF in SoM is around 180 km long which is the Northern Branch of NAF containing the ~%80 of the total motion accommodation (McClusky et al 2000, Provost et al 2003, Armijo et al 2002, Reilinger et al 2006).

There are two different opinions about kinematics for the submerged section of the NAF. One of is pure strike slip motion along singular strand (Le Pichon et al 2001, 2003). Counter argument suggest that fault system contains normal component therefore pull-apart basins are formed due to oblique kinematics and the presence of slip partitioning (figure 3.2) (Cormier et al 2006, Armijo et al 2002, 2004, 2005, Seeber et al 2004).

Previous authors are intrigued by the current ambiguous behavior of the Central Segment of the NNAF, which passes through Kumburgaz Basin. After 1999 earthquakes (Barka et al 1999, Toksoz et al 1999, Reilinger et al 2000) and 1912 Mürefte earthquake (Rockwell et al 2001, Altunel et al 2004), seismic gap on Sea of Marmara is restricted from Prince Island's Segment to Central Segment of NNAF (figure 1.1, figure 3.1). Eventually, studies focused on upcoming rupture, which was estimated for causing devastating loss at especially Istanbul (Parsons et al 2000, 2004, Hubert-Ferrari et al 2000). Nevertheless, a hypothesis is asserted and supported by previous instrumental studies (Ergintav et al 2014, Sakic et al 2016) showing that there is a possibility that Central Segment may creep thus, cannot accumulate stress as expected. This is an extremely important issue to be solved, because Marmara Region

is the densest place in population and the center of the both industry and management in Turkey. Even now, government plans to reinforce the housing continues due to evaluated hazard possibilities. Therefore, it is obligatory to know the intensity of the earthquakes to display much more accurate scenarios for future catastrophes.

3.2. Morphology of Kumburgaz Basin

Kumburgaz basin is located along the NNAF on the Central High slightly NE-SW and has an elongated shape (figure 1.1, figure 3.1). It is the smallest basin both in depth (833 m) and size (21 km W-E, 6 km N-S) between Northern Basins of SoM. Northern margin of the basin where the submarine canyons are present (figure 3.3, figure 3.4), is the northern shelf (~-85 m) of SoM (over 9-12 degree steep slopes). Southern margin is more deep (-380 m) and more gentle (3-4 degree) than opposite margin in which the main strand of the NNAF passes through where depression concentrated on. Eastern margin is bounded by Central High which shows a clear total offset of NNAF (figure 3.2).

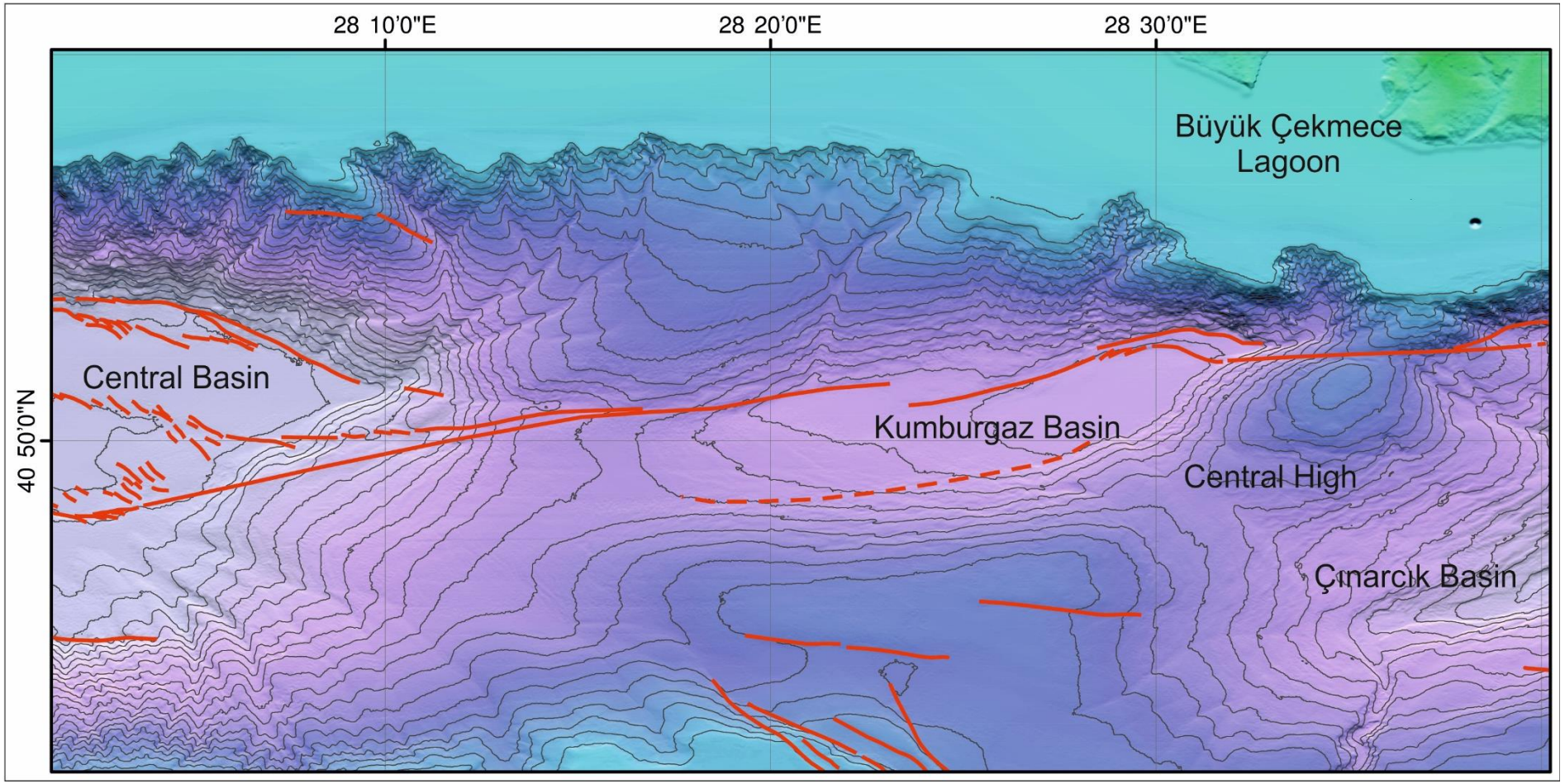

Figure 3.1: Bathymetry map of Kumburgaz Basin and surrounding region. Basin is bounded by NNAF from north, Central Basin from west, Central High from east margin. Kumburgaz Basin has 833 mbsl depth and contains 21 km west to east and 6 km north to south of area.

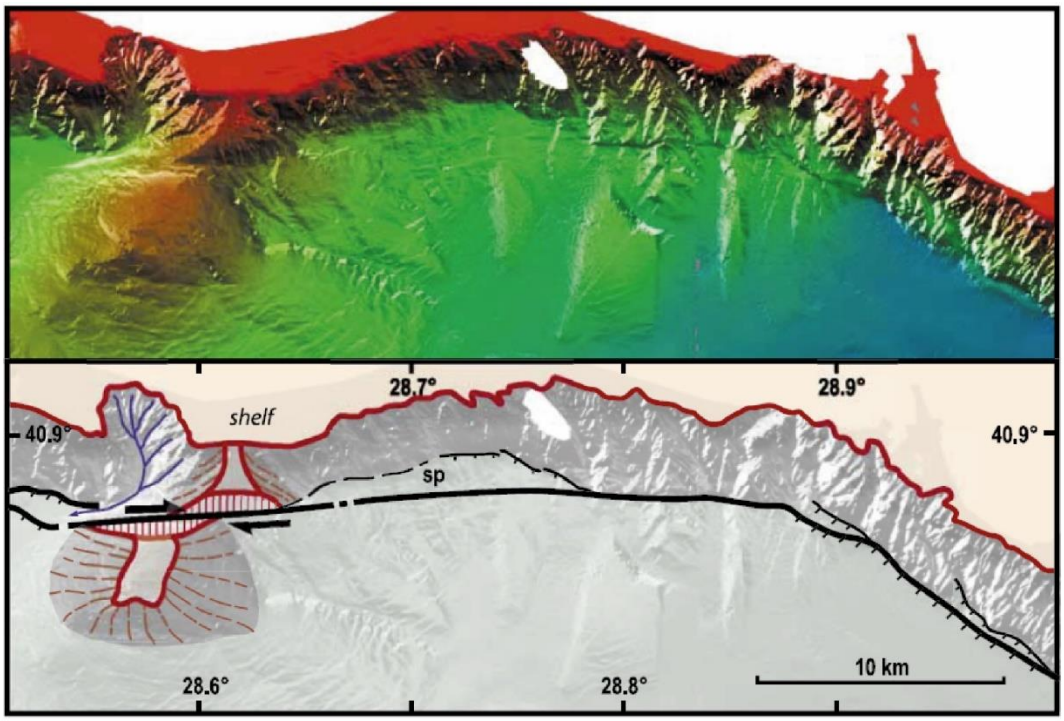

Figure 3.2: Bathymetry map and interpretations on western margin of Çınarcık Basin. Figure indicates ~3.5 km offset on Central High eastern margin of Kumburgaz Basin. Note that, at the very east margin of Çınarcık slip partitioning occurred (Armijo et al 2002).

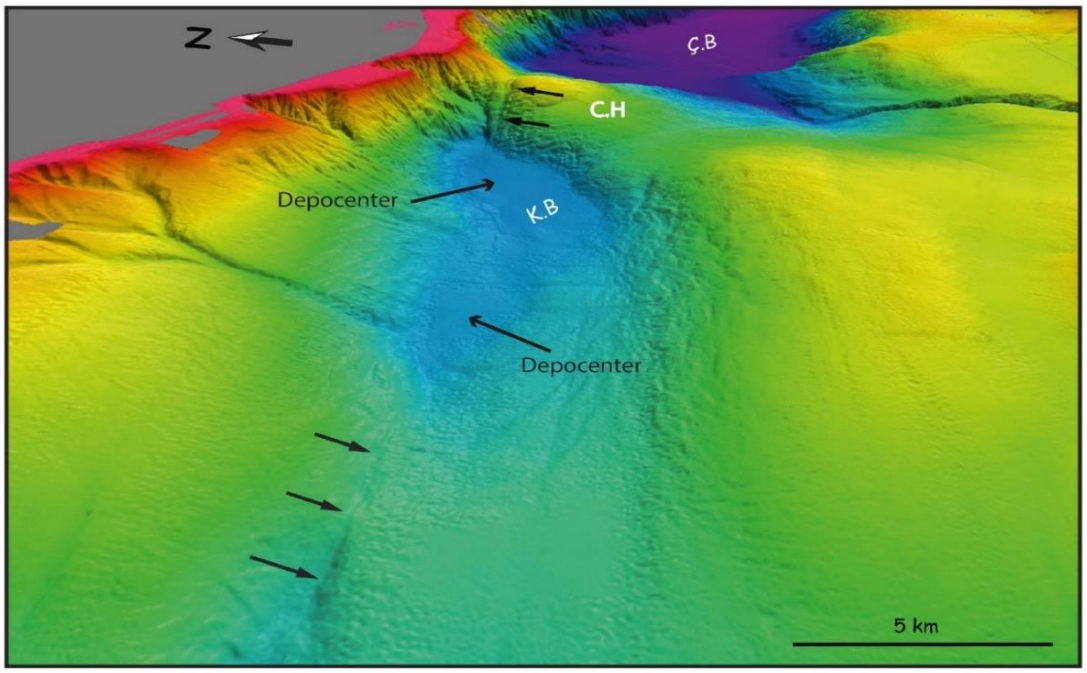

Figure 3.3: Morphologic and bathymetric view of Kumburgaz Basin Black arrows indicate the location of main strand of NNAF. Main depocenter is located towards eastern margin and there is smaller depocenter on the western side of the basin (see also figure 3.9). Abbreviations; Ç.B, C.H, K.B are Çınarcık Basin, Central High and Kumburgaz Basin respectively.

There are two submarine canyons that may supply sediments to the basin. NE canyon is located to the very east edge of the basin, having single narrow curving channel that reaches to the basin. On the contrary, Northern canyon is spreading almost all northern margin of the basin, which has several branches feeding the basin (figure 3.1, 3.3, 3.4). Mouth of the reaches to the shelf break. Büyükçekmece Lagoon, which extends into Çatalca Peninsula which mostly accumulates sediments to canyon mouths (Figure 3.1). As seen in the morphological view, there is a bathymetric barrier, which is located near NE of the canyon. Barrier is in 300 m length and around 75 m height (figure 3.4, 3.7). Presence of the barrier changes the dynamics of the currents accumulated from the NE canyon (see Inverse Grading Turbidites).

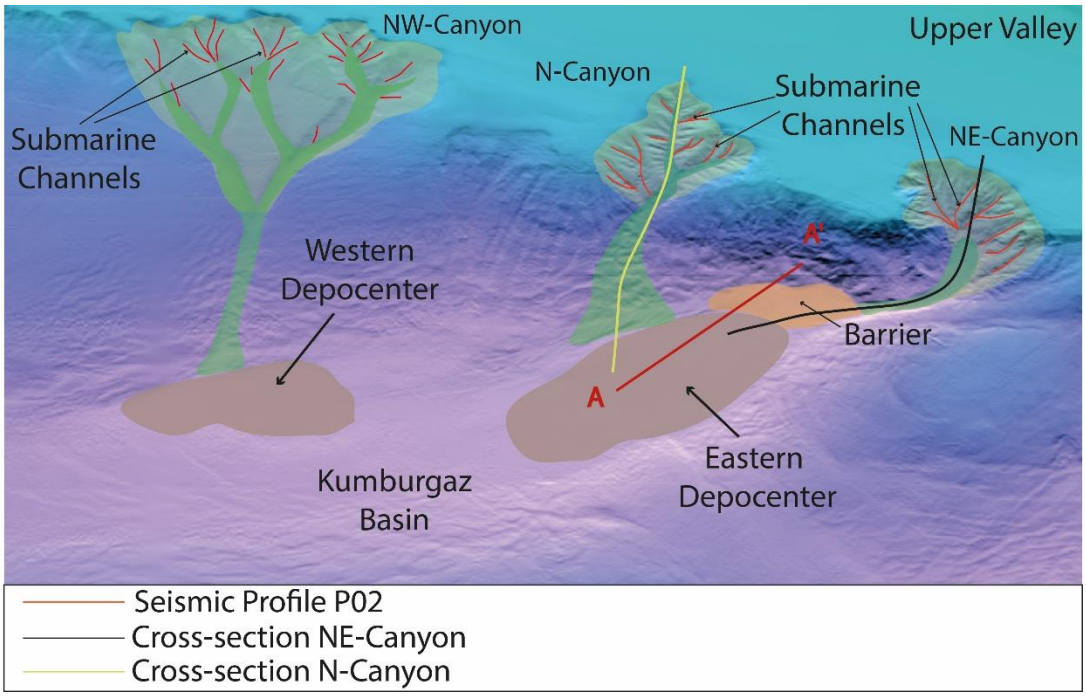

Figure 3.4: High Resolution Multi-Beam Bathymetry Map of Kumburgaz Basin; There are two major submarine channel systems supporting the basin (Northern and Northeastern Canyons). Canyons are created by the merging of submarine channels, which is represented by red lines. Although, Northeastern canyon is in a single braided structure, Northern Canyon has several braided submarine channels which merged into 2 main canyons where coincides at the ~- 400 m depth. Basin elements are highlighted by turquoise, green, light pink and light gray, represents upper valley, submarine channels, bathymetric barrier and basin floor respectively. Red line displays the orientation of Seismic Reflection Profile (P02). Yellow and black lines represent the hypothetic cross-section directions in Figure 4.4 Seismic Reflection Profile (P02) being located on Bathymetric Map; Profile reveals bathymetric barrier which has 300 m length and 75 m long height along the northeastern border of the basin, located around NNAF and Northern shelf scarp.

3.3. Tectonic and Sedimentary fill of Kumburgaz Basin

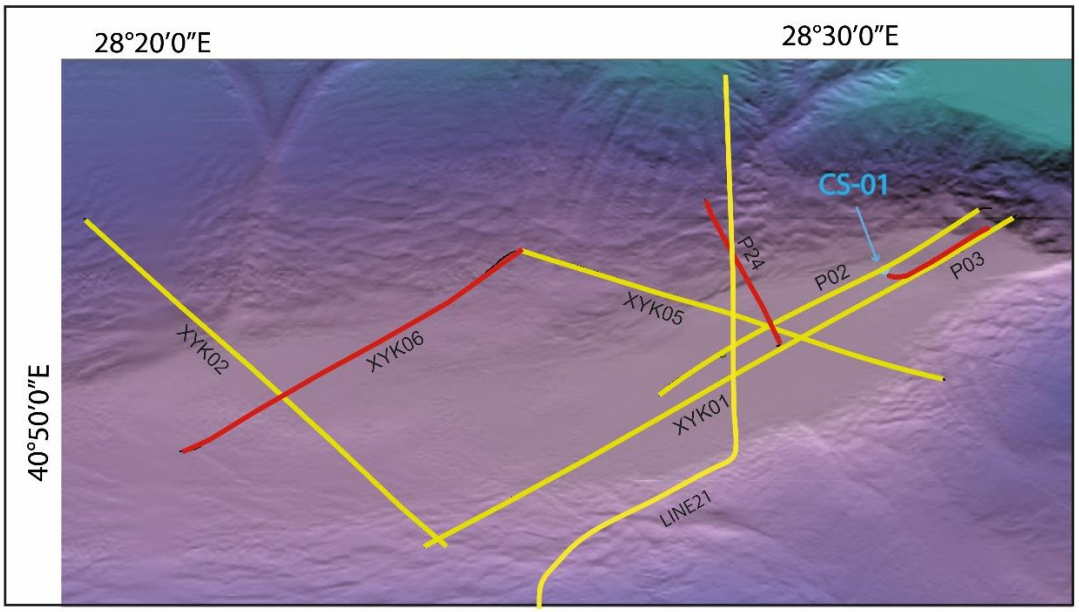

Figure 3.5: Seismic profiles on Kumburgaz Basin. Yellow lines represent seismic profiles displayed on thesis. Red lines show unused seismic reflection profiles. Core location is indicated.

Kumburgaz basin is bounded by NNAF to the north and by minor secondary faults to its southern margin (figure 3.8, 3.9). Chirp profiles show northward thickening sedimentary units towards the main fault indicating dip-slip component of the fault here (Figure 3.7, 3.8, 3.9, 3.10). At southern margin, sedimentary fill is less thicker compared to the northern margin. Secondary faults displace the sedimentary units with minor vertical offsets. Some faults exhibit typical strike-slip deformation reflection (figure 3.7, 3.8) as seen in the chirp profiles. Some secondary faults seem to be buried possibly due to high sedimentation rate and slow fault-slip rate in the center of the basin.

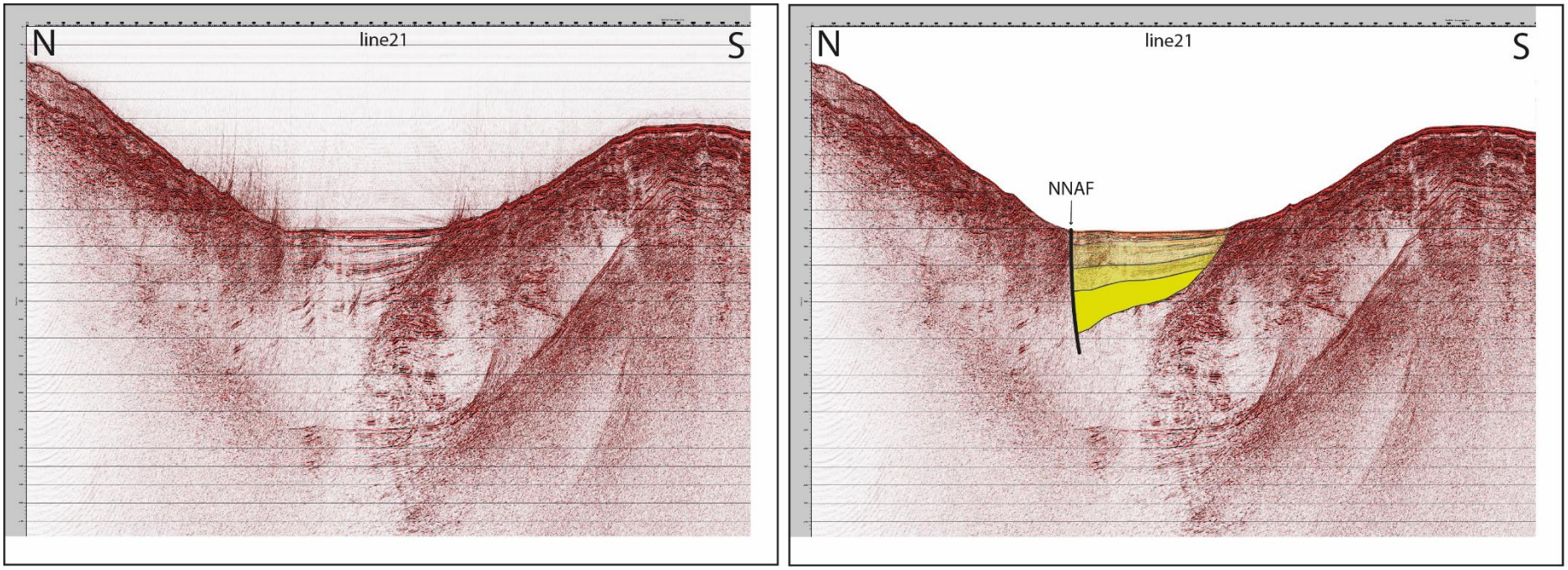

Figure 3.6: Multi-Channel Seismic Profile Line 21: Profile passes through N-S direction in Kumburgaz Basin (figure 3.5). Note that, only northern margin is bounded by a fault (NNAF). There is no major fault which extends to deeper strata. Significant reflections are marked with yellow lines shows the accommodation is also towards to northern margin where NNAF located.

In some profiles, it is clear to see gas escapes and related enhanced reflection through faults (figure 3.7, 3.8). CHIRP profiles provide a clear transition between marine and lacustrine units. Transition between marine lacustrine phases is located on -45 mbsf (figure 3.7). The piston core CS01 dates back to ~7000 years, which does not reach to the lacustrine fill. However, a previous study by Beck et al. 2007, already presents this transition based on the study on the 30-m long piston cores and chirp profiles (Armijo et al., 2005). Thus, we have correlated seismic reflection profiles by cross-cutting reflections. Since core CS01 is located on profile P02, marine-lacustrine transition is transported from P02 to other cross-cutting profiles (figure 3.8, 3.9, 3.10).

It is possible to see NNAF trace on seismic profiles however, secondary faults which bounds the basin at its southern margin is not traceable in every reflection profile. Furthermore, southern margin is not bounded any deep fault (figure 3.6). High resolution seismic reflection profiles show step-like structure at the southern margin which do not extend to depths. Therefore, Kumburgaz Basin seems to be a half-graben, where northern side of the basin is bounded by the main fault and southern part of the basin is deformed by a hanging-wall collapse due the transtension controlling the basin. Such fault configuration better explains the discontinues secondary faults.

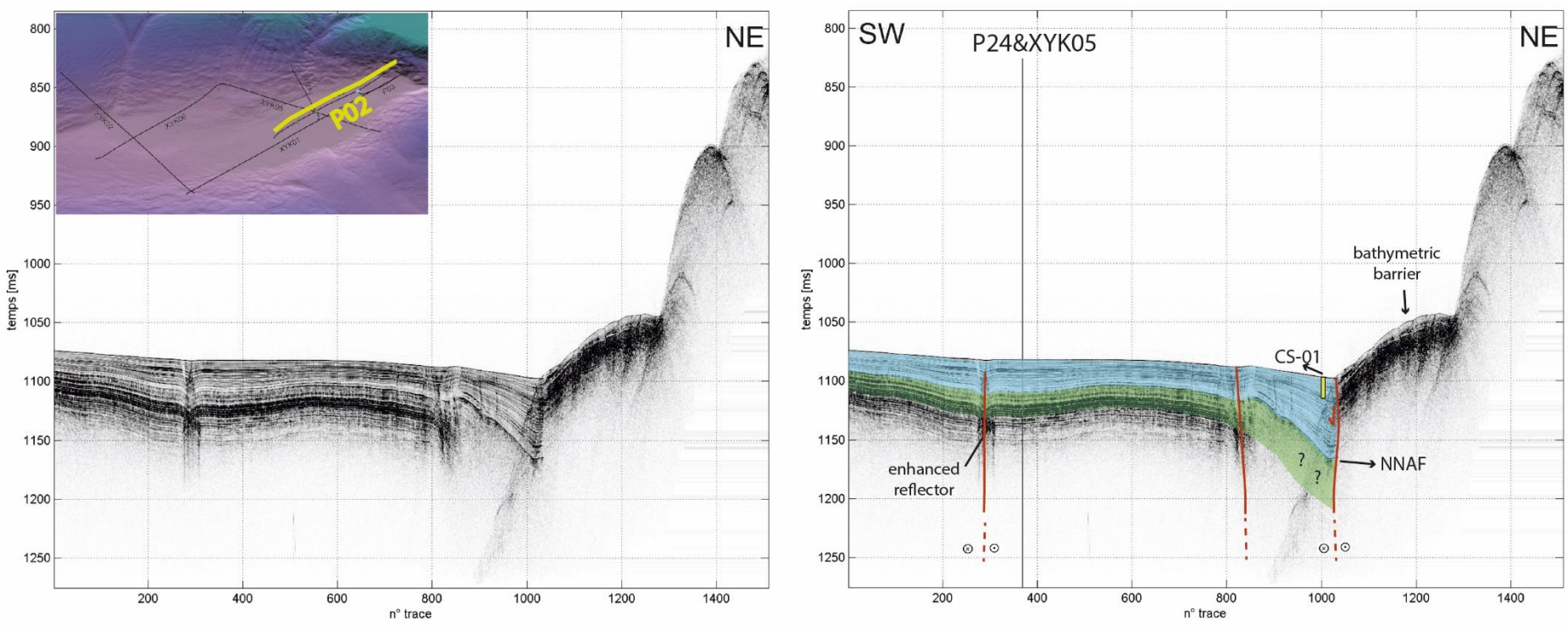

Figure 3.7: Seismic reflection profile P02 from MARsite (2014) main strand of NNAF is located on interpreted profile. Note that core does not penetrate lacustrine part, however, age of the core is correlated to establish a boundary of marine lacustrine units. Another aspect is the presence of secondary faults in which one of them seems to be a blind fault which is explained in the text (see Morphology of Kumburgaz Basin).

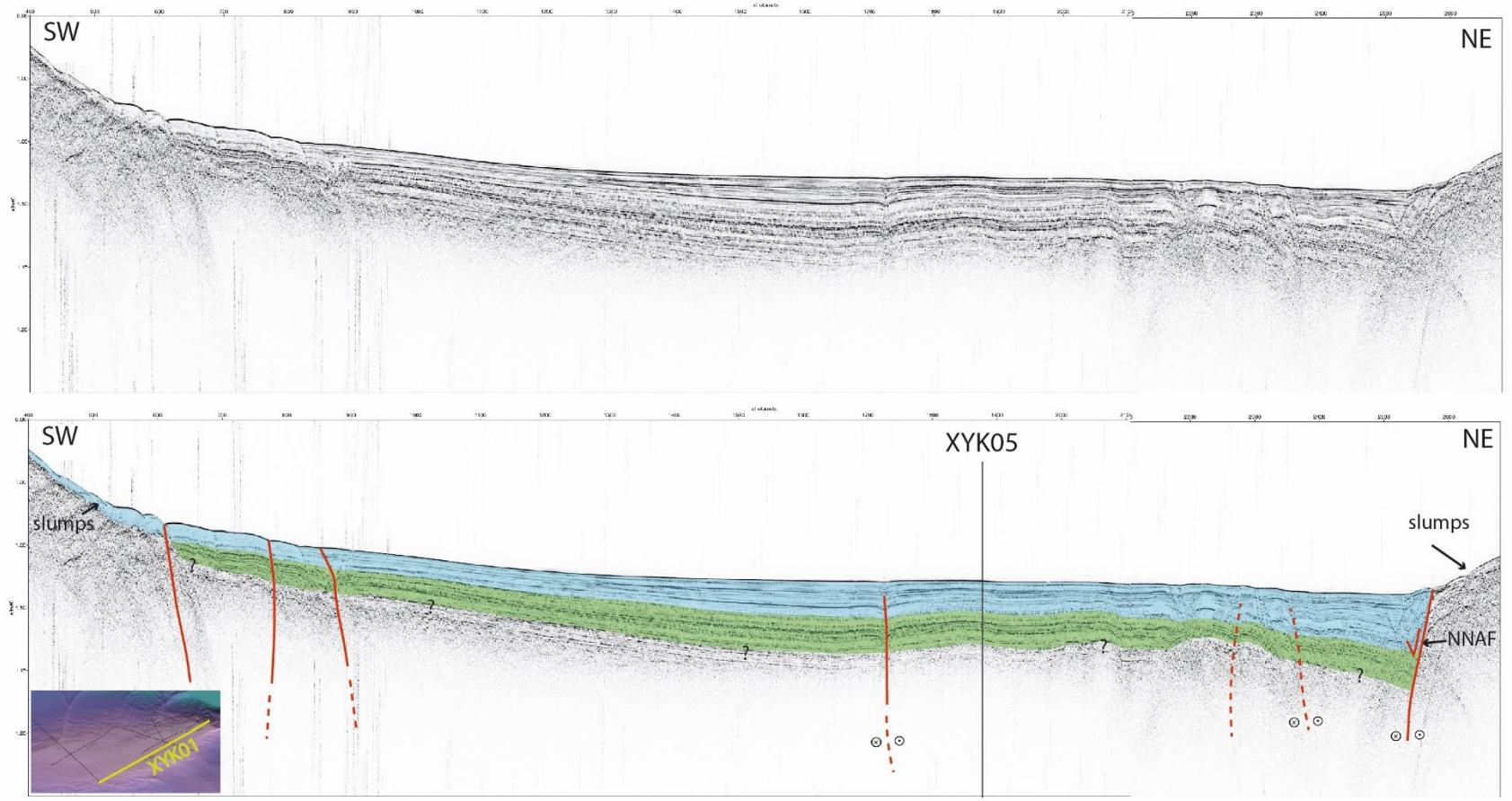

Figure 3.8: Seismic reflection profile XYK01 from MARMARASCARP (2005) Marine and lacustrine units through W-E orientation in Kumburgaz Basin. It is clear on profile to see northern and southern boundary faults. Note that relicts of recent submarine slumps are present at the margins of the basin shows that currents could not reach to basin floor due to lacking acceleration of plastic flow.

We have encountered in profile XYK02 (figure 3.9) there is a secondary depocenter located at the western margin of the basin. Secondary depocenter is fed only by the northwestern canyon (figure 3.4). Size of the secondary depocenter is 460 m to 480 m wide area which is almost the half of the basin's length. Boundaries of depocenter is NNAF by the northern margin and secondary fault by southern margin which is a ramp locating in the middle of basin.

We encountered in some profiles (figure 3.8, 3.9) traces of mass-wasting events. They are relicts of submarine slumps or failed debrites. If the sediment-gravity flows cannot excess the threshold for turbulent-laminar boundary, they generally are not able to reach the basin floor. Absence of debrites, slumps or other possible deposits and only the presence of turbidites support that these units are plastic flow deposits.

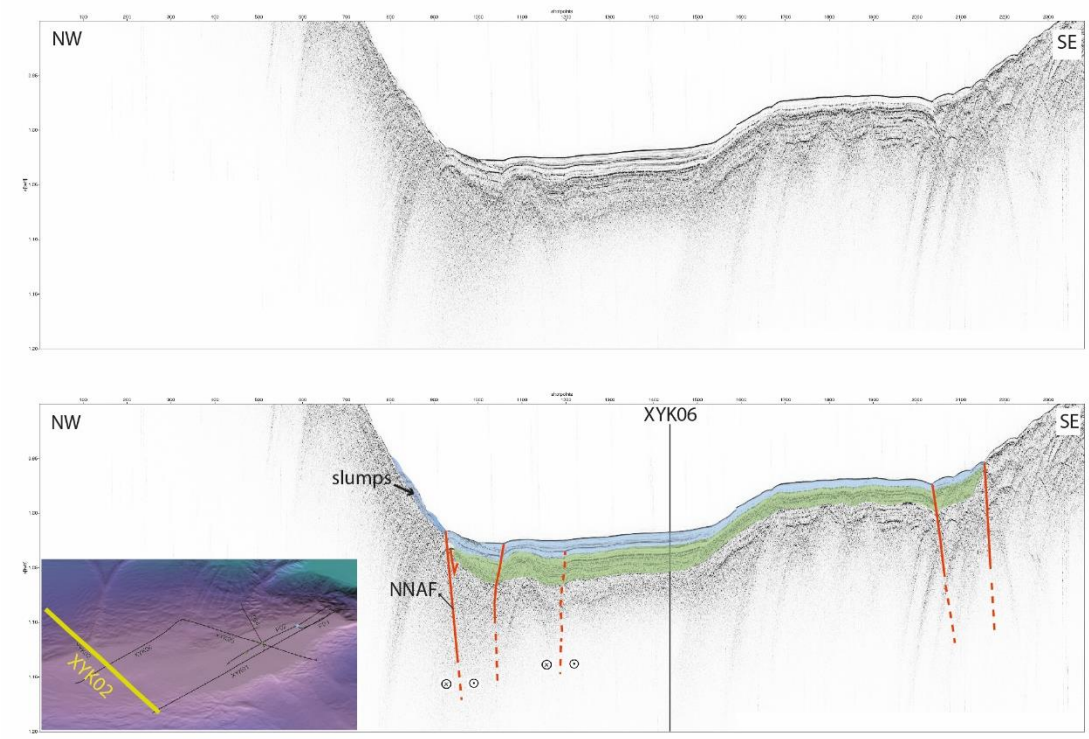

Figure 3.9: Seismic reflection profile XYK02 from MARMARASCARPS (2005). Conjugate fault twins are displayed on both margins. NNAF located on northern margin of the basin. Note that, presence of submarine slumps is concentrated on northern margin.

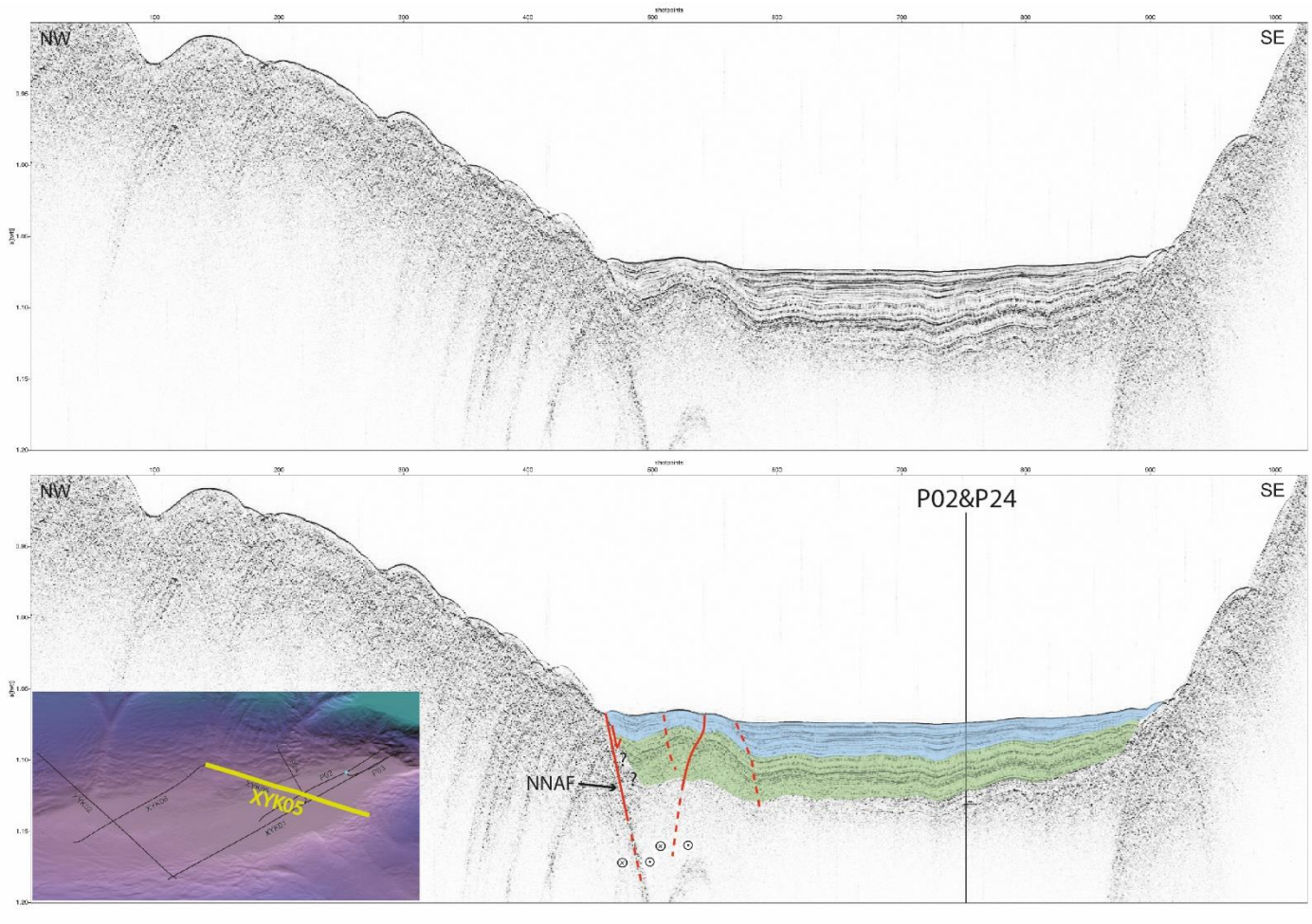

Figure 3.10: Seismic reflection profile XYK05 from MARMARASCARPS (2005). Profile reveals location of NNAF, adjacent possible conjugated fault twin. Basin is bounded by faults at both northern and southern margins

4. SEDIMENTARY RECORDS OF EARTHQUAKES: SEISMOTURBITIDES

4.1. Definition and Scope of Study of Seismoturbidites

Seismoturbidites are earthquake-triggered, mass-flow deposits that are mechanically produced from turbidity currents. Earthquakes can very well be a trigger mechanism to produce sediment-gravity flows. In most sedimentary basins, conservative lakes or ocean margins, accommodation of slumps, debrites, tsunamites and turbidites are common. Therefore, these instantaneous deposits can be used as archives for active tectonics where onshore trenching is not possible due to presence of submerged fault systems.

To use the term seismoturbidite there must be a distinctive description in which ways it is needed to be separated. Common remark on turbidites has been studied for decades (Sheldon., 1928, Signorini., 1936, Johnson., 1938, Kuenen and Migliorini., 1950, Shephard., 1951, Kuenen., 1957, 1958., Bouma 1962, Dott., 1963, Walton., 1967, Middleton and Hampton., 1973,, Piper., 1978, Stow., 1979, Lowe 1979, Mutti 1985, Shanmugam, 2000). The description has changed or altered by previous authors. However, seismoturbidites have additional properties which earns the distinction. Sedimentological differences such as, grain size fluctuations, abundancy of lamination, irregular grading trends, absence of Bouma sequences (Ta to Te), geochemical signatures and post-depositional water oscillations are used as exclusive features, which presents the difference of Seismoturbidites.

It is acceptable that earthquakes do not shake just a local region, which would have triggered a single current. On contrary, affected region is wide and disturbed material is not necessarily originated from just one submarine canyon. Moreover, not only ground is affected by an earthquake, but also water column is disturbed. Therefore, multiple-sourced depositions and/or effects of water oscillations are main distinctive aspects for seismoturbidites.

4.1.1. Brief History and Development of Co-Seismic Sedimentation

Usage of co-seismic sedimentation in paleoseismology has started with Heezen and Ewing (1952) which has been stated that earthquakes very well is a producing mechanism of a sediment-gravity flow. Especially within the last couple of decades, this idea has been applied and developed thriving so far, therefore the term Seismoturbidite (earthquake-triggered turbidite) (Mutti et al 1984) now provides the most promising approach for submarine paleoseismology for seismic hazard assessment. It has been solving various problems and questions related with submarine paleoseismology, such as; how far the segment has ruptured, where is the affected region also, clearing up the history of the region, precise calculation of the recurrence times and suggesting implications on segmentation.

These sequences are studied before with various proxies that describe Seismoturbidites at Northern San Andreas Fault (Adams 1990; Goldfinger et al., 2003b; Goldfinger et al., 2003b; Goldfinger et al., 2007; Goldfinger et al., 2011; Biasi et al., 2002;) which has almost the same kinematics as NAF, at Mediterranean Sea (Kastens, K., 1984: Kastens, K., Cita, M.B., 1981;Cita et al., 1982; Cita et al., 1984; Cita, M.B., Aloisi, G., 2000; Cita et al., 1996;), at Ionian Sea (Polonia et al., 2013, Polonia et al., 2016), at west coast of Iberian Peninsula (Goldfinger et al., 2010; Gracia et al., 2000; Masson et al., 2011), and at Japan Sea (Nakajima, T., Kanai, Y., 2000). Lakes are also extensively studied in a manner which provides earthquake records (Arnaud et al., 2002; Beck et al., 1996; Chapron et al., 1999; Inouchi et al., 1996; Nomade et al., 2005; Shiki et al., 2000; Beck 2009;). Especially, SoM was interested by scientist after 1999 earthquakes thus, studies contain Çınarcık (Sari, E., Cagatay, M.N., 2006, Eris et al 2012, Drab et al 2015), Tekirdağ (McHugh et al 2006, Drab et al 2012), Izmit (Cagatay et al 2012, Bertnard et al 2008), Central (Beck et al 2007, McHugh et al 2014, Drab et al 2012) basins of SoM where Seismoturbidite sequences found and aged and correlated with records of historical earthquakes.

Common remark on description is; Turbidites have erosional basement, proxies that indicate detrital input, parallel or cross laminations with alternation of silt and clay and homogenite part. Moreover, previous authors use various aging methods to determine the ages of the sediment-gravity flow deposits so that, they correspond the units with historical earthquakes. However, this thesis indicates that recognition of subunits of turbidites is rather haphazard due to both co-seismic and post-depositional effects

hence, sedimentary structures and texture are peculiar regardless to the imposed descriptions.

Although studies use the term Seismoturbidite or similar descriptions, there are few which care to develop the current description of seismoturbidite phenomena by using multi-parameter analyses or displaying depositional model exclusive only for earthquake-related sedimentation (Sarı & Cağatay 2006, Beck et al 2007, Cağatay 2012, Eriş et al 2012, Nakajima & Kanai 2000, and Polonia et al 2016). Because it is not fully differentiated from other trigger mechanisms which also produce turbidity currents. Furthermore, the term seismoturbidite is also not yet fully explained by textural differences and it is clear that current description of seismoturbidites have rather unaccustomed differences regarding to the Bouma Sequence.

4.2. Trigger Mechanisms of Turbidity Currents

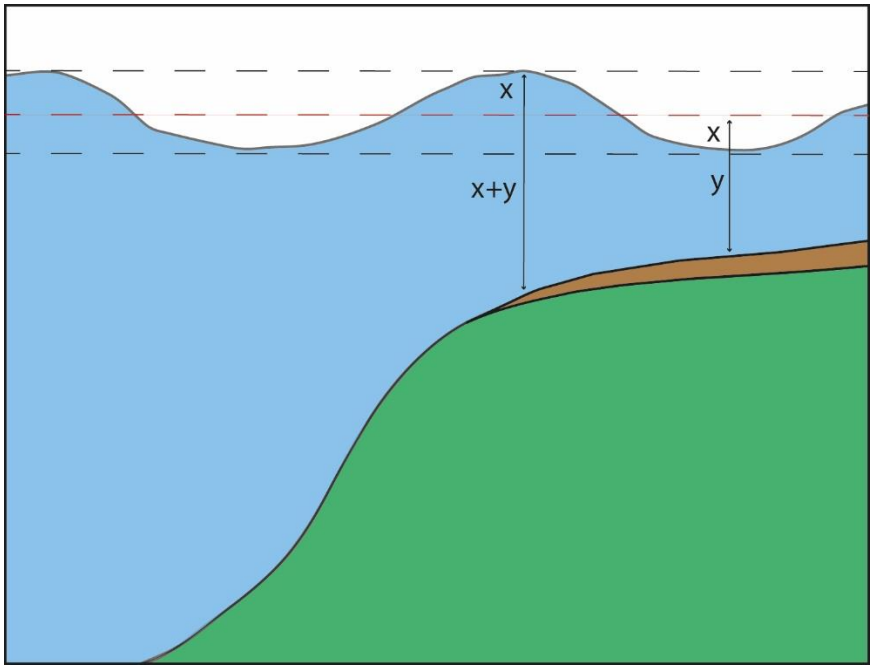

Figure 4.1: If the wave amplitude can reach the slope area, it can cause slope instability.

Storm waves may cause slope instability, which ends up triggering mass-wasting events. It is because of the distance between wave's lowest amplitude coincide to the supposedly unstable sediments. This kind of instability can occur where the height of the sea level should have been shallow enough to disturb the sediments below when

waves are generated. Additionally, the constant oscillation of the storm waves can produce significant pressure alternation on the sediments below. If material sustains repetitive shear stress changes, slope failure can occur. Note that, these previously mentioned situations are only possible where the sea level shallow enough to prevent the neglecting of wave's effect.

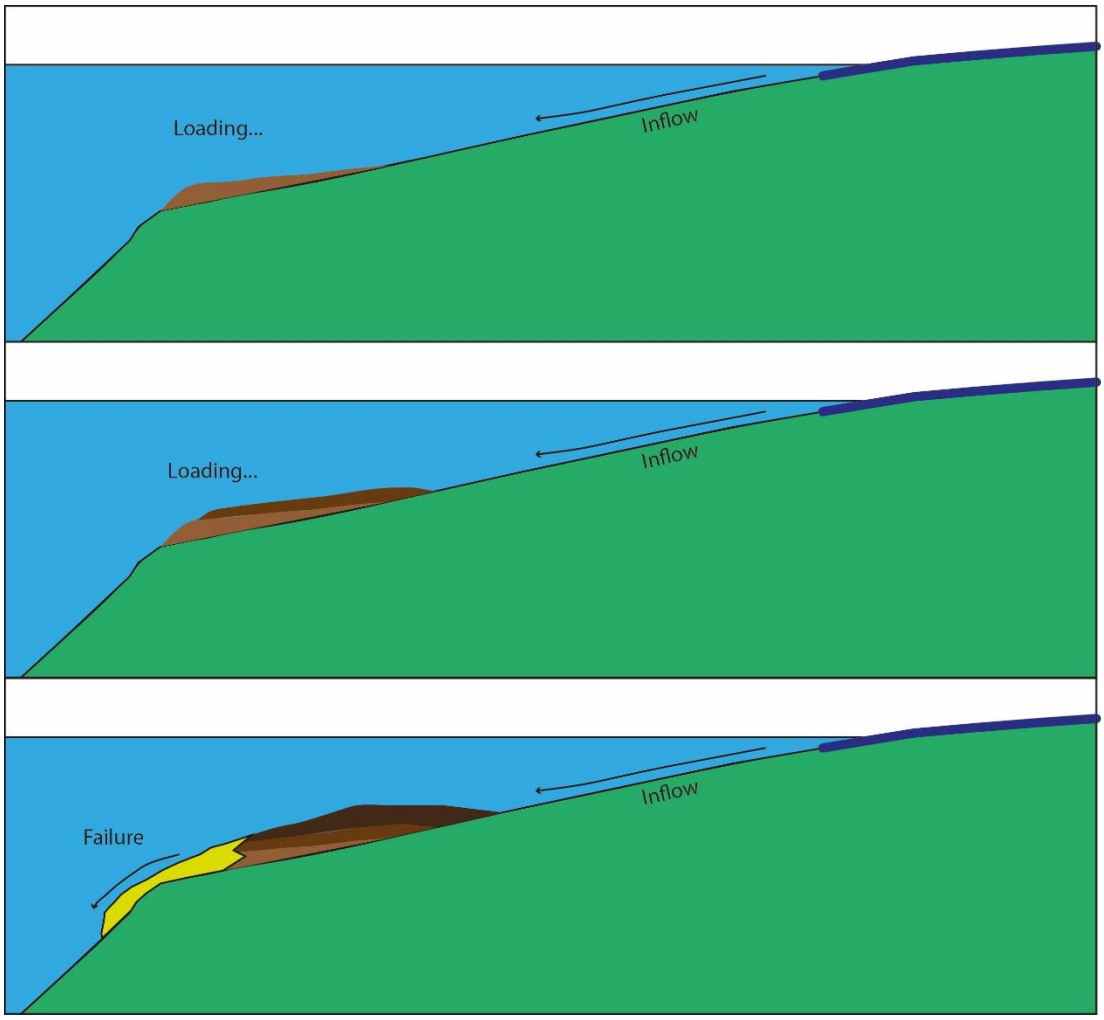

Figure 4.2: Progressive sediment load eventually causes slope instability If any other trigger wont initiated.

Similar to storm waves, tides may very well be a reason for slope failure. Downward motion of a tide can drag down the pressure on the slope if the slope is shallow and the tide range is wide. Furthermore, the upward motion of a tide may overload the pressure on the slope with the same logic. Generally, intensity of the tide is seen on range of supratidal at ocean margins. Therefore, conservative waters or shallow

elevated water masses are avoided to such an effect. If the slope is shallow and the tide range is wide, repeating pressure diversity is able to trigger the failure.

The regions, which have appropriate background for flooding events, can push the materials to subaqueous environments. If the dense material-rich muddy flow reaches to slope, may turn into turbidity current with the increasing steepness. It may contain detrital material as seismoturbidites have however, materials, which is carried in various grain-sizes. Interval between the coarsest to finest sediments is vast. Moreover, flood must have carried materials, which belong to offshore therefore; remains of terrestrial organic materials are abundant in the deposition. This kind of transportation needs close distance to slope, otherwise dense muddy flow piles up before reaching slope thus, will be detained until subsequent entrainment is triggered.

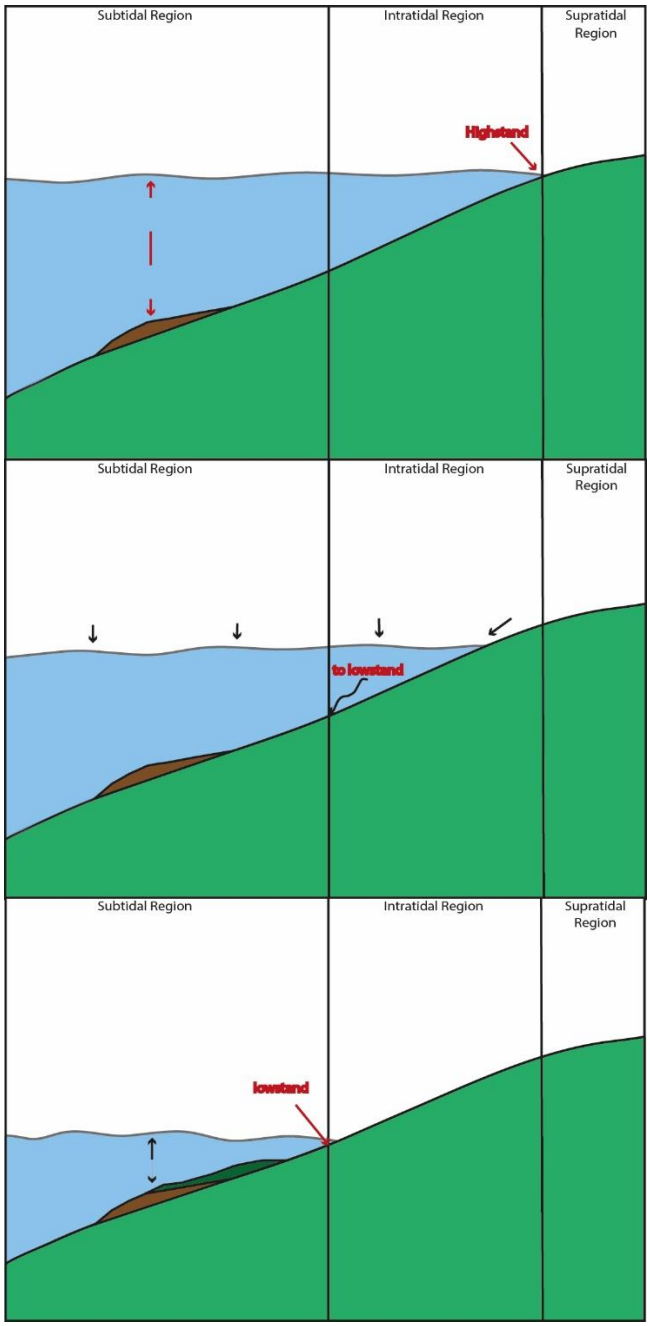

Figure 4.3: Strong repetitive tides can load sediment. Those sediments can be triggered by dynamic pressure change.

Overloading on slope may reduce the shear strength, which ends up with a failure. It needs inflow from terrestrial agents. Slope must be nurtured with high discharge rate of rivers (Mulder, T., and Alexander, J., 2001. Mulder, et al 2003 Mulder, T., and Syvitski, J.P.M., 1995.), which would have forcing sediments accumulate in alarming rates. Accumulated sediments lose stability in time, will surely fail or other triggers

may produce instability. In any case, mass wasting occurs thus, turbidity current may form.

4.3. How to identify Seismoturbidites?

Methods are widely covered in the chapter 2 thus, only the use of proxies will be covered in this chapter to comprehensively express the distinctive aspects of seismoturbidites. In subaqueous paleoseismology, seismic profiles are to map the spreading area of the mass-flow deposits. Mega-turbidites and Augias type turbidite/homogenite can be identified as well.

On sediment cores, there are series of experiments/measurements that is used to identify the mass-flow units (by Core logging). Following procedures are aimed to find the boundaries of units and physical (by MSCL), textural (by Grain-size distributions and Radiographic imaging) paleontological (by smear-slides) and geochemical (by XRF) properties. Finally, age of the units is calculated by radiocarbon analyses (by AMS and).

Recovered cores from marine surveys are examined in order to find exclusive proxies that relate the term Seismoturbidite. Textural, sedimentological, physical, geochemical and paleontological experiments/measurements are executed to display distinctive features by using them in together or separately.

4.3.1. Irregular Grading

Generally, turbidites are normal-graded sequences. Turbidity currents are indeed gravity flows. When the current reaches to basin floor, a gradual energy drop occurs, therefore sediments form normal grading sequences (Bouma, 1964). For exceptional cases, inverse graded turbidites may form due to different morphologies and hydrodynamics conditions.

In case of Seismoturbidites, it is possible to see such alignments on deposited sequences. However, successions show fluctuations due to water oscillations, during or after the deposition. Irregular pattern on grain-size distribution is a distinctive feature of Seismoturbidites.

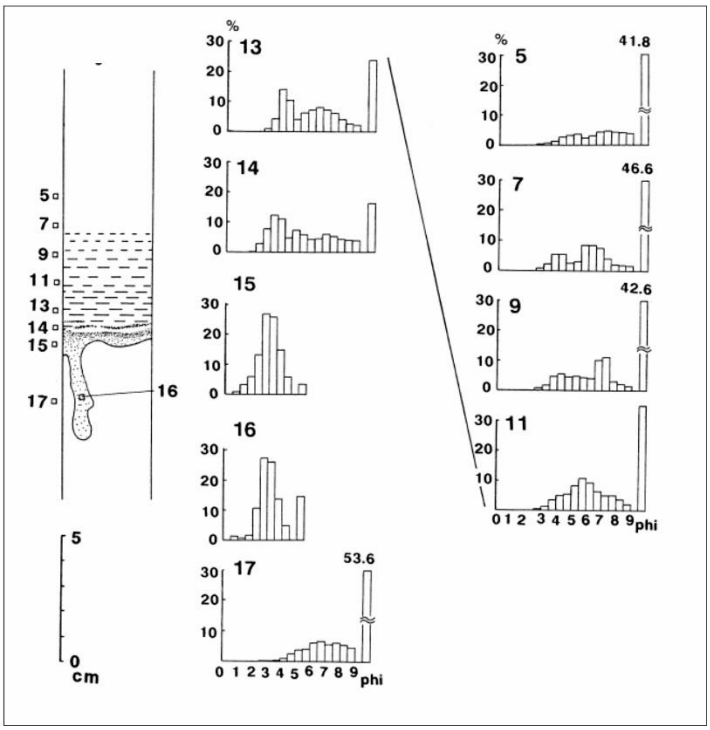

Figure 4.4: Grain size fluctuation through a seismoturbidite unit. Grain scale unit is phi, note that, irregular change in silt-clay size material so that there is no gradual trend appeared (Shiki et al 2000).

In some cases, Seismoturbidites contain more than one succession, in such case they are called amalgamated turbidites. When an earthquake shakes a significantly broad region, it triggers simultaneous currents. If those currents provide depositions, amalgamation occurs thus, multiple overlaying turbidites form which show constantly cut, partially graded depositions.

4.3.2. Variable Sources for Seismoturbites

Turbidity flow is a kind of erosive current thus; composition of eroded material can tell in what depth the current has generated. Theory suggests that shaking due to earthquakes is the most excessive trigger. Material from shallow parts of slope, must be dragged into the subsequently generated current. That is why determination of foraminifera that correspond to related depths can help to determine the depth of the sources.

Another aspect for composition is to determine the existence of detrital input in Seismoturbidite successions. Ca, Sr, K (calcite, aragonite, mica-bearing materials

respectively) is used for determination of tendency for detrital input. Fe is also used for both reasons; it is also counted for detrital input besides it is used as a correlation for magnetic susceptibility. For Seismoturbidites, detrital material must have been dragged from upper valley to the basin. To be able to move extensive amount of detrital material down to slope is one of the distinctive aspects of Seismoturbidites.

In some cases, composition abruptly changes in a Seismoturbidite succession. This drastic change is interpreted as amalgamation. Textural and geochemical aspects also support amalgamated structure. From separate canyons, turbidity currents wake and in alternating manner, deposition occurs on basin floor.

4.3.3. Sedimentary Structures

In Turbidites, commonly seen sedimentary structures are erosional or sharp basal contact with a flute cast or scour marks, parallel and cross lamination, ripples in different sublayers. In subaqueous paleoseismology, sediment cores are used for identification of turbidite layers. However, cores are not capable of preserving horizontal structures. It is hard to find a complete ripple or gentle cross lamination on a sediment core. Logging, grainsize measurements and radiographic images reveals the subunits of a turbidite layers and unravel sedimentary structures if there is any.

In some cases, soft sediment deformations are visible even on sediment cores. Such as, micro fractures, liquefaction, ball and pillow structures, vein structures, traces of bioturbation, boudinage from lateral spreading are seen on mass-flow deposits (Beck 2009).

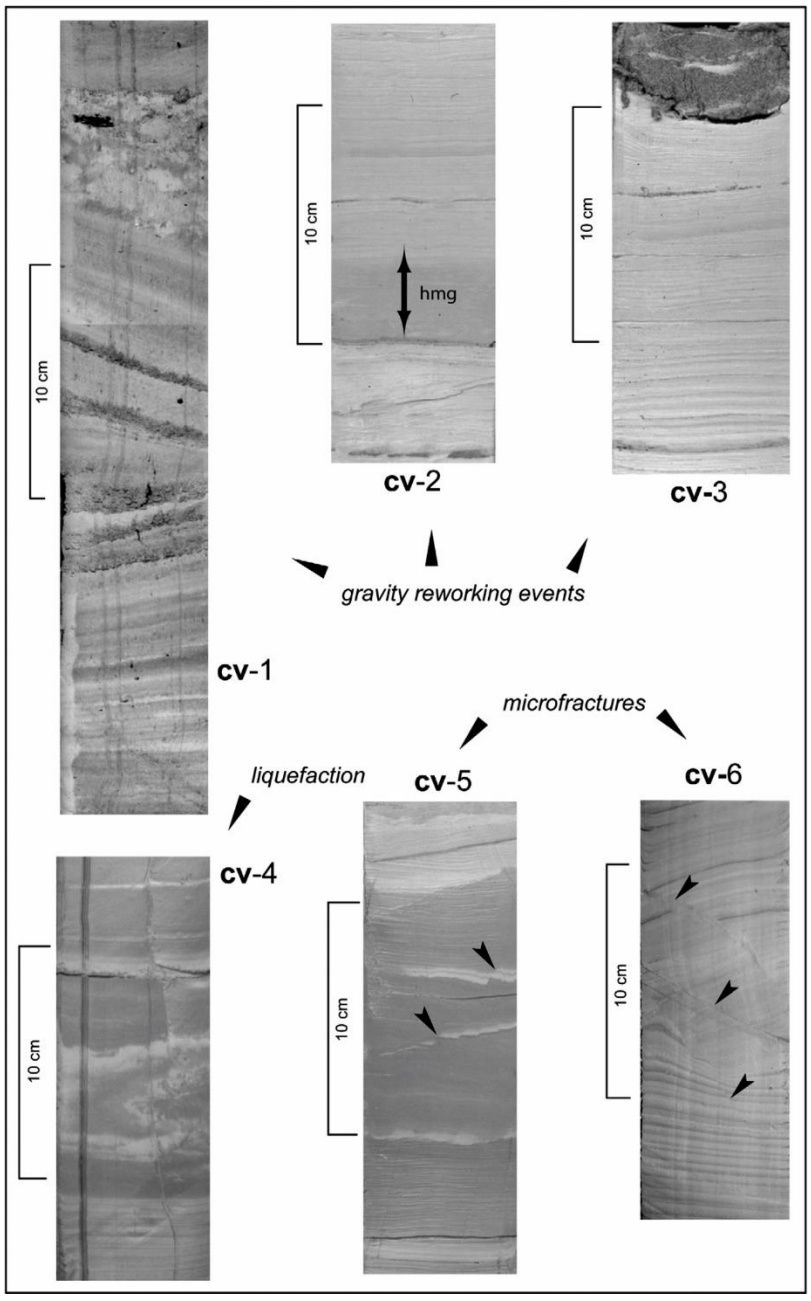

Figure 4.5: Soft sediment deformations are shown by Beck (2009) in Alpine Lakes. Note that, beside from constant laminated structure, liquefaction, microfractures can be originated from other triggers as well.

In Seismoturbidite studies, recognition of subunits is rather hit-or-miss based on literature description. It is stated that only Tb and Td units of a turbidite is formed by laminated structure (Bouma 1962). However, in most Seismoturbidites, alternated silt-clay or sand-silt laminations are composed of the whole succession. But that does not mean seismoturbidites only have Tb and Td subunits, it is because of water oscillations. Seiche-controlled sedimentation is generally seen by oscillation water

column, which strongly suggest that succession may have deposited from an earthquake-triggered turbidity current.

Oscillating water column causes laminated structures to form. While each seiche section occurs, a couplet of lamination will form. As seiche goes by, laminations pile up and form the turbidite. Eventually, oscillation will stop and suspension will become the dominant mechanism. That is why, presence of constant laminated structure is the most important feature that characterize Seismoturbidites. Laminations being formed by oscillation are generally in millimeter scale with identical composition. Therefore, it is almost impossible to see variation on logging. However, laminations are visible on radiographic images, which is sensitive to intensity of material.

4.3.4. Migration of redox front

Redox sensitive elements (Mn, Fe, Ni, Co, Cr, U and As) generally reacts when oxic-anoxic boundary disturbed. It is safe to imply that, instantaneous sedimentation is one of the reasons forcing the oxic-anoxic boundary to move up so that, earthquake-triggered sedimentation terminates in a very limited time right after the earthquake. Therefore, oxic-anoxic boundary migration or formation of new redox front is connected with the turbidite deposition.

Mn is used for this particular situation. Through constant suspension, sediments are piled up, subsequently pull oxic-anoxic boundary up gradually where penetration of oxygen is possible. Therefore, Mn enrichment occurs in a stable trend which is caused by the sedimentation rate is not excessing the vertical diffusion velocity of Mn+2 flux (Cağatay et al 2004).

If there is an abrupt accumulation adding additional sediments up to the oxic-anoxic boundary, it is forced to move up and is formed in a new horizon. When the boundary is carried upward abruptly, excessive amount of Mn+2 starts to vertical motion afterwards, until the new formed horizon where is traceable as a pulse of Mn enrichment on XRF measurement results.

New formed horizon is also counted for a redox front where redox sensitive elements migrated. Therefore, just below the initiation of a seismoturbidite succession there must be a Mn pulse correlating the new redox front has been formed. This proxy is used for the identification of the sediment-gravity flow deposits whether they are short-

lived instantaneous events (Cağatay et al 2012). Furthermore, Mn anomaly's location is used for the determining the exact horizon of the basal part of the Seismoturbidite.

Mn remobilization around the redox front is a process that takes time and it does not just happen during the deposition (Cağatay et al 2004). If there are multiple currents that overlaying each other in a succession (amalgamated turbidite), whole succession is corresponded with a single Mn pulse even though, there are multiple depositions.

If there are aftershocks or subsequent failures, which must be strong enough to create turbidity current, several seismoturbidites may form a package of multiple depositions that can be confused with a single event. In this case, Mn is the proxy that can distinguish the events with the corresponding pulses. Each event if not erode the entire previous deposition, is identified with Mn enrichments at the basal parts of each seismoturbidites.

4.3.5. Acoustically transparent layers on seismic reflections

High Resolution Seismic Reflection profiles are used for the identification of mass-flow deposits. With the combination of coring, these profiles offer extensive spatial stratigraphy. Moreover, with enough gridded profiling, it is possible to reveal the spreading and thicknesses of the units.

Single rupture of a segment regarding with the intensity of the earthquake, can trigger turbidity currents in multiple canyons spreading extensively into large areas. With sediment coring, obtaining seismic reflections are quite enough to reveal the existence of the co-seismic sedimentation.

In high-resolution seismic reflection data, layers which have negative reflection coefficient values, are interpreted as homogenite subunits of seismoturbidites. Again, regarding the intensity of the shaking and amount of sediment supply, these homogenite units reaching up to more than meter-long sequences, become traceable on seismic reflections. However, coarse-grained sequences are rather thin relatively to homogenites to be encountered on high-resolution seismic reflections.

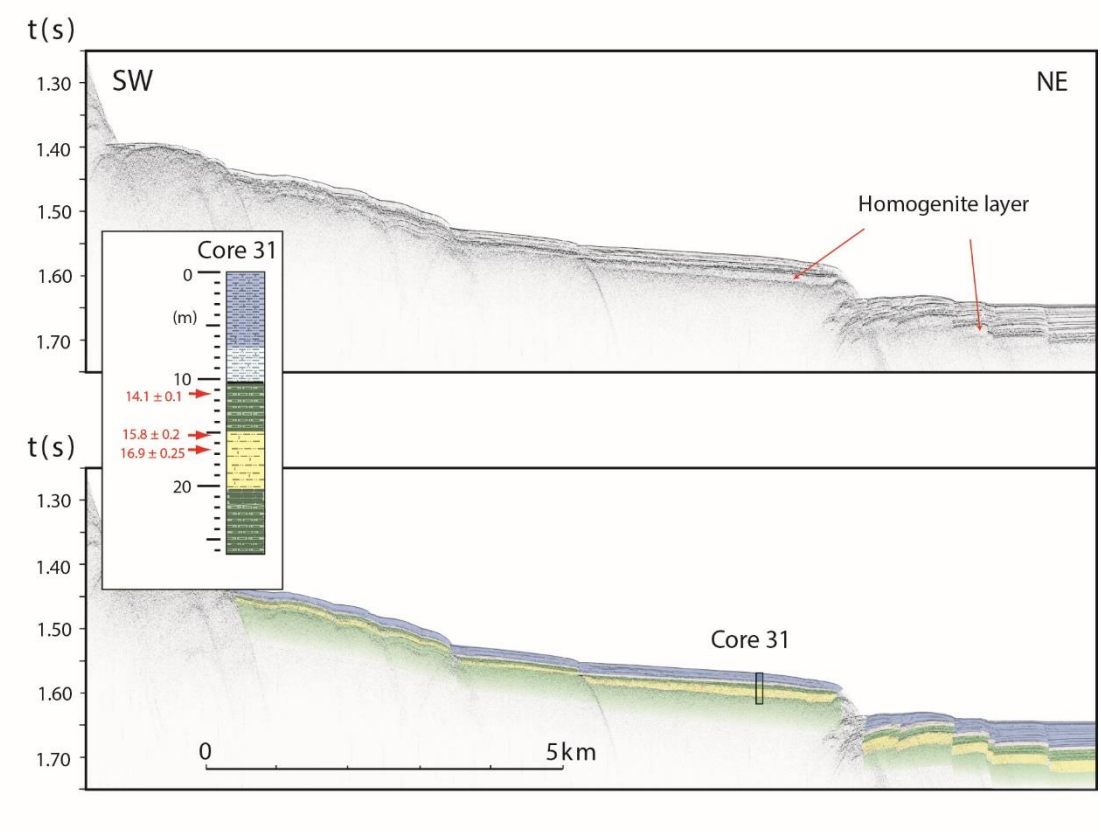

Figure 4.6: Major homogenite layer is detected in sedimentary fill of Central Basin by Beck et al (2007). They identified layer and correlated with core studies, therefore they managed to age the acoustically transparent layer. Blue color indicates marine unit, green color indicates lacustrine unit and yellow shows major homogenite layer.

Leading studies of these units are investigated various places at Mediterranean Sea (Kastens, K., Cita, M.B., 1981; Cita et al., 1984; Cita, M.B., Aloisi, G., 2000; Cita et al., 1996, Polonia et al., 2013, Polonia et al., 2016). Even in much more conservative waters (such as, Sea of Marmara), these units are identified on different basins and correlated with core studies (Beck et al 2007, Eriş et al 2012, McHugh et al 2006).

This part for seismoturbidites is dedicated to classify the distinctive features of earthquake-triggered turbidites. It is also informative about the trigger mechanisms generating sediment-gravity flow events. Even though, seismoturbidites originally are generation of turbidity currents, distinctive properties such as, grading, composition, sedimentary structures and geochemical traces also, depositional differences caused by amalgamation and water oscillations (see Discussion) vindicate the uniqueness of seismoturbidites among other sediment-gravity flow deposits.

Other trigger mechanisms, which can cause slope instability, must be eliminated by examining the region's hydrodynamic conditions, morphology, climatologic aspects. Seismic profiles and core studies provide spatial stratigraphy of the units. Combining

relevant parameters is the most convenient way to provide information about co-seismic sedimentation.

4.4. Turbidite Units of Sediment Core CS-01

4.4.1. Multi-parameter proxies

21 m long piston core, which is retrieved from Kumburgaz Basin, is analyzed for this study. According to lithology and core location on seismic profile P02 (Figure.2.), only most recent marine sedimentary sequence of SoM is identified. Because of the core location is depocenter, younger sequences of marine unit and abundant of sediment-gravity flow deposits are found.

Lithology of CS-01 consists of clay to sand size sediments. For background sedimentation clay and occasionally fine-silt size sediments are deposited. From first two meters, brownish (due to oxidation) to olive gray color is gradually seen, as to bottom, color turns into gray then dark gray between third and fifteen meter. The rest and the deepest part of the core is dark greenish gray color. In some sequences, FeS nodules and patches are found which makes the color more brownish (due to oxidation). Aside from the color, textural properties are subtle on pelagic sedimentation, which is formed by continuous suspension.

For the sediment-gravity flow units, color and virtual grain size is constantly changes. Turbidites are consisting of silt to fine-sand size material, most of them without an erosional basement due to inverse grading. Parallel lamination is the most visible sedimentary structure that identifies the sediment-gravity flow units. Laminations consist of fine sand and silt size alternations. Thicknesses are diversified from one to eight cm with counting homogenite part of the succession. Although the thicknesses are small in range, high-resolution multi-proxy analyses provided clear view of subunits if they exist (Figure 4.3, 5.2, 5.3).

As for physical aspects, magnetic susceptibility and density proxies are measured radiographic imaging has performed. In case of sediment-gravity flow units, most of them are with occasional pulses on magnetic susceptibility also, there is no general pattern to classify or interpret them. Tendency of proxies such density and x-ray radiography has combined, have the bounds of succession from basal part to top of the homogenite with sharp accuracy. Transition between homogenite and overlaying

hemi-pelagic sediments is labile due to only radiographic images. However, according to grading density whether increment or decrease, represents T unit (T-H, turbidite-homogenite) also, homogenite unit represented by stable or gently trending of density value due to clay size material with homogenous texture. In the core CS-01, some of the sediment-gravity flow units do not comprise homogenite sequence due to hydrodynamic conditions or post-erosional effects.

Grain size distribution (see Appendices) shows the coarsest material as fine sand on TH units which explains why the erosional basal parts are absent on the most of the turbidites in Kumburgaz Basin. Most of the sediment-gravity flow units show inverse grading per se, fluctuations on grain size causes irregularities. Increment of the gap between Dx50&Dx90 indicates the rise for standard deviation being interpreted as sorting which shows how sorted layers distributed on sediment-gravity flow units. Poor sorting is common on seismoturbidite sequences, especially where coarse grains are abundant. Moreover, irregularities on grain size also affects sorting which procreates multiple sequences of alternating moderately to poorly sorted even in cm long sediment-gravity flow unit.

For elemental proxies, Fe, K, Mn, Ca and Sr cps measurements are carried out to determine various horizons within the succession of T-H units. Mn reaches up to 2000-6000 cps at the very beginning of the T-H units then fade away through the succession. In some units, multiple pulses of Mn are identified. Moreover, Mn shows 3-8 cm long sequence of increment just below the Turbidite units. Very few examples do not have a prominent pulse, which would have been corresponded with a related T-H unit.

In a T-H unit, Fe values starts decreasing from 20-25k to 8-10k just before homogenite. K values which is lighter than Fe, shows fluctuation even in background sedimentation. For some units, K (originated from feldspar mica bearing material) forms similar trend with Fe showing gradual decrease up to the homogenite.

Ca (calcite bearing material) and Sr (aragonite bearing material) are combined to determine organic material fraction on each layer. Ca & Sr shows a sharp increase at top of the turbidite. Normally Ca and Sr values are around 2k and 600 respectively. Turbidite units on CS-01 carries organic material as detrital content thus, values on T-H units for Ca&Sr reach up to 6.5k and 1.3k respectively.

Microscopic observation for each T-H unit reveals textural properties of grains. 0.5 cm sampling interval shows gradual change on surface deformation of particles. Mostly, initial deposited particles have pitted surfaces. On contrary, particles in laminated layers have relatively smooth surfaces which is inferred how energy level loosened throughout a unit.

Each studied section reveals high fossil fraction containing bivalves, mollusks, spike fragments and benthic foraminifera assemblages. Identified species are ammodiscus, textularia, spiroloculina, quinqueloculina, binoculina, triloculina, dentalina, amphicoryna, legena, bolivina, brizalina, bulimina, uvigerina, chilostomella, ammonia. It is also found that species especially belong infralittoral and upper circalittoral sections of the submarine environment. Especially, ammonia, bulimina and elphidium are used in Çınarcık (Sarı & Cağatay 2006) as characterizing material, which comes from shelf and upper slope areas.

4.4.2. Extended core stratigraphy

Section 1 (appendix 1) is 1-meter-long sequence contains the most recent depositions in CS-01. First 50 cm has brownish color due to oxidation. Rest of the section has olive gray color. Last 20 cm of the section 1 is the part of first turbidity flow deposit. Unit is not detected during the logging because there is no evidence of textural or structural traces. However, multi-parameter analyses identified the existence of the sequence. Turbidite is bounded by Mn pulse reaching up to 3000 cps. Radiographic images display the constant lamination through succession. Fe and K gradually increasing in turbidite part up to 16000 cps and 400 cps respectively and has sharp decrease in homogenite. It is possible to see the anomaly on magnetic susceptibility near basal part of turbidite so that values are reaching to 45 u.S.I which contain 20-25 u.S.I normal trend. First encountered turbidite extends to section 2 (appendix 2) which has olive gray color. Second section has complete sequence of other 2 turbidite units. These turbidites are rather thinner turbidites regarding to other encountered units in CS-01. Due to their thin nature, magnetic susceptibility and density could not detect sharp changes. However, grain-size and radiographic images shows physical changes. Laminations are abundant on these turbidite units. Grain size parameters shows irregular pattern nevertheless sequences show inverse grading. Second turbidite shows Mn pulse at basal part reaching to ~2000 cps. Moreover, between turbidite units in the

section 2, there is another anomaly which is interpreted as FeS^- patches. These structures are generally identified by Mn pulse, magnetic susceptibility and Fe proxies. In section 2 we have initiated 2 radiocarbon analyses sampled below first and second turbidite units.

In Section 3 (appendix 3), hemipelagic sediments have gray color, no structures or textural aspects are identified except from 2 turbidite units. First turbidite shows very characteristic trend on description regarding responses of proxies (see distinctive features of seismoturbidites). ~2700 cps reaching Mn pulse bounds turbidite from basal level. Fe (10000 cps drop) and K (300 cps drop) decreases gradually through homogenite part. Ca and Sr increases and bounds the transition between turbidite and homogenite unit. Because first turbidite is ~5 cm long sequence there is no response on magnetic susceptibility. Inverse grading is visible on grain-size parameters. Second turbidite on section 3 shows similar tendencies however constant laminated structure due to water oscillation blurs grain-size trend. There are several FeS^- patches on section 3 which is represented by Fe anomalies.

In section 4 (appendix 4), background sediments show gray to olive gray color. Even though lithology is absent on textural aspects, radiographic images shows FeS^- patches at the bottom part of the section. There is also a turbidite unit which is bounded by 2 Mn pulses subsequently. Grain-size parameters support the repetitive structure. Density change is around 1.5 to 2 gr/cm^3 showing the whole sequence of turbidite unit. Ca and Sr increments are cut at the top of the turbidite.

Another turbidite unit is located on section 5 (appendix 5) which shows several FeS^- patches at the top of the section. Section is in gray color and there are no other structural aspects seen. Turbidite on section 5 is rather thicker compared to the average thickness of turbidite units in CS-01. ~14 cm long turbidite unit is bounded by single Mn pulse (reaching up to 7000 cps) and 10 cm long sandy-silty alternated laminations present. There is no clear grading trend on unit however, tendency seems to point out inverse origin. Thick turbidite part enables magnetic susceptibility to responds therefore it is visible that magnetic susceptibility values doubled (20 to 40 u.S.I) at the ~10 cm long turbidite part of ST7.

Section 6 (appendix 6) contains episodic climate change horizons which is also visible on radiographic images. Even though these horizons do not show any grain-size

differentiation generally Fe and K give responses on these horizons. The only traceable structure is the turbidite which is 8 cm long. This unit is bounded by couplet of Mn anomalies at basal part showing there is a time interval between whole depositions (see redox front migration). Ca and Sr are reaching up to 3500 cps and 1000 cps respectively at the top of the turbidite unit. Grain-size parameters again responses as a couplet of sand fractions.

Section 7 (appendix 7) shows 2 elemental horizons which is identified by decrease in Fe, Ca and Sr. Color is gray on whole section except a turbidite unit and several reduction zones which are represented by lighter colored layers and FeS^{-} nodules. Turbidite unit is bounded by several Mn pulses at the basal part (reaching up to 2500, 3000, ~4000 cps respectively.). There is no grain-size trend on turbidite unit. Organic material content is continuously cut by repetitive pulses (up to 4000 cps). Lamination is abundantly seen on turbidite unit. Bottom part of the section contain sand fraction besides from turbidite succession.

Section 8 (appendix 8) has gray color on hemipelagic sediments. Through section there is a turbidite unit which is bounded by Mn pulse (~3000 cps) at basal part and capped with Ca and Sr increment reaching up to 3000 and 1000 cps respectively. Turbidite unit is 10 cm long, 4 cm is covered with homogenous mud. There is no grading trend on turbidite unit however sand fraction reaches up to %30. There are FeS^{-} patches at bottom part of the section represented by Fe pulses.

Section 9 (appendix 9) contains sand fraction up to %20 on hemi pelagic sediments. There are 2 turbidite units present. First turbidite unit is bounded by Mn pulse reaching up to 1500 cps. Turbidite is capped by Ca and Sr increment (5000 and 1000 cps respectively) also there are 2 sand bearing layers showing 2 pulses up to %30 sand fractions. 4 cm long turbidite does not respond to magnetic susceptibility. Radiographic images reveal second turbidite on section 9. There is no Mn pulse at the basal part of turbidite. However, density shows a characteristic trend for a sediment-gravity flow deposit. Grain-size parameters show fluctuation on second turbidite. Moreover, Ca and Sr shows increment (2000 and 750 cps respectively) which is the transition of turbidite homogenite boundary.

Section 10 (appendix 10) displays hemi pelagic sediments with a turbidite succession. Section has gray color in general however, turbidite sand layers contain brownish

color. There are abundant FeS^{-} patches represented by Fe anomalies concentrated on top of the section. Around 30 cm there is a reduction zone detected by Mn increment. Turbidite in section 10 shows normal grading. Sand fraction of turbidite is reaching to %40 also brownish colored layers which are seemed to be detrital input, reacts with magnetic susceptibility values. Turbidite is bounded by 10 cm long Mn (reaching up 400-500 cps) sequence at basal part and capped with Ca and Sr increment (5000 cps and 1300 cps) at top. Detrital input (Fe and K) responses on sandy layers, values are decreasing (down to 10000 cps and 300 cps respectively) through succession.

Section 11 (appendix 11) is displayed at appendix 11 showing hemi pelagic sediments and 2 turbidite units. There is no textural aspects or structures except from turbidite units. First turbidite is 10 cm thick, normal grading sequence. Density is bounding top of the homogenite, there is no Mn response at basal part of the turbidite. Before homogenite, Ca and Sr increment (4000 and 700 cps respectively) are present at the top of the turbidite unit. 7 cm long second turbidite is bounded by Mn pulse at basal part and capped with Ca and Sr increment. Furthermore, detrital input (Fe and K are down to 4000 cps and 500 cps respectively) is depleted at the transition between turbidite and homogenite units.

In section 12 (appendix 12), radiographic images reveal repetitive laminated structures, most of them are contained in interpreted turbidite units. First turbidite is bounded by Mn pulse at basal part with 20 cm long sequence reaching up to 1500 cps. Turbidite unit contains multiple sand fractions which corresponds with dark laminations on radiographic images. First turbidite is capped with Ca and Sr pulses reaching up to 9000 cps and 1000 cps respectively. Sand fractions on turbidite are reaching up to %30-35 and they show good correlation with Fe and K drop (5000 cps and ~400 cps decrease). Second turbidite on section 12 is located on bottom part. Textural aspects show silty-sandy alternating laminated structure which can be correlated with radiographic images. Sand content is also detected with %relative grain size parameter reaching up to %35. 8 cm long turbidite is responding on magnetic susceptibility, values ranges 10-20 through succession. Beside from turbidites, there is no specific textural aspects on section 12, general color is gray dominated with muddy hemi pelagic sediments.

Section 13 (appendix 13) has dark gray color. Section is dominated by muddy texture however; sand content is reaching up to %5-10 in some levels. Deeper sections show

portion of cracks due to loss of water content. There is a turbidite present at the middle part of the section bounded by 20 cm long Mn anomaly from basal part. Sand content in turbidite is changing between %30 and %45. Homogenite part of the turbidite is dominated by large bivalve fragments and wood particles. Ca and Sr values reaching up to 10000 cps and 1200 cps respectively on top of the homogenite. Fe and K instant drop is detected at the contact between turbidite and homogenite. There is no significant response at magnetic susceptibility. Using density and visual identification turbidite is measured 8 cm long laminated structure 6 cm long homogenite covered with high organic content.

Section 14 (appendix 14) is showing dark gray color with muddy texture due to hemi pelagic sediments. A turbidite is identified on section 14 bounded by 10 cm long Mn anomaly. Turbidite is 5 cm long and capped with Ca and Sr increment (7000 cps and 1200 cps respectively). Fe and K are gradually decreasing through the succession where magnetic susceptibility increases drastically ranging to 10-70 u.S.I. Grain size parameters show normal grading trend on turbidite, basal part contains %45 sand fraction. There is a crack 3 cm long located 10 cm below turbidite in section 14. Foam is artificially added to prevent slipping. At the bottom part of the section there is a homogenite for another turbidite which is located on section 15 (appendix 15). Any textural aspect is seen on visual identification. However radiographic images show traces of laminations in 20 cm long sequence. Turbidite is bounded by Mn pulse at basal part reaching up to 700 cps. There are Fe anomalies present through turbidite however there is no response on magnetic susceptibility. For such a long turbidite, sand fraction is only reaching to %10-15. There is a second turbidite located on section 15 containing Mn pulse (up to ~650 cps) at basal part thus, Ca and Sr increment (4000 cps and 1000 cps respectively) at the transition between turbidite and homogenite. Turbidite thickness is 3-4 cm therefore there is no significant trace on magnetic susceptibility moreover, grainsize parameters cannot detect any grading trend on turbidite.

In section 16 (appendix 16), we encountered several cracks ranging between 1 to 5 cm due to loss of water content. Hemi pelagic sediments are dominated by muddy texture general sand fraction is around %1-2. There is a turbidite unit which has 13 cm long sequence. Turbidite is bounded by a sharp Mn pulse (up to ~1500 cps) at basal part thus, capped with Ca and Sr increment (~5000 cps and ~1200 cps respectively).

According to grain-size parameters, turbidite is inverse graded. 2 repetitive increase in sand fraction is identified (up to %20-25). At the bottom part of the section 16 FeS^{-} patches are identified correlated with anomalies on Fe value.

Section 17, muddy texture of background sediments has dark gray color. At the bottom part a few FeS^{-} nodules are present corresponding with Fe anomalies. We encountered a turbidite in section 17 showing similar tendencies such as, density increase through succession, Mn pulse at basal part (500 cps), Ca and Sr cap at transition between turbidite and homogenite, sharp decrease in Fe and K at the top of the turbidite part, magnetic susceptibility pulse at basal sandy part of succession. Grain-size parameters show inverse grading trend thus; sand fractions are reaching up to %30.

In section 18, texture is homogenous mud having dark gray color. Due to water content loss, there are large amount of cracks appears on section 18. Most of the laminated layers are actually these cracks showing lighter reflections. There is a turbidite unit identified capped with Ca and Sr (up to 4000 cps and ~1000 cps respectively). Basal margin of turbidite is correlated with strong Mn pulse reaching up to ~4000 cps. Grain-size parameters show fluctuation throughout succession (see amalgamated turbidite). Sand content is reaching up to %30-35s, therefore magnetic susceptibility values are ranging between 10-20 u.S.I.

Section 19 shows hemi pelagic mud displaying dark gray color. Again due to water loss there are cracks appeared on deeper sections therefore false laminations are appear on radiographic images. Even though general texture is dominated by muddy structure, sand content of the section is reaching up to %5-10s. there is a thick turbidite layer (15 cm long) is bounded by 15 cm long Mn enrichment sequence from basal part thus, turbidite is capped with Ca and Sr relatively poor increment (2000 cps and ~400 cps respectively). Turbidite shows fluctuations on %relative grain-size ranging between %10 and %25.

Section 20 contains hemi pelagic muddy texture. Color is dark gray through whole section. There is a turbidite unit identified which has been cut from sandy layers into 2 pieces due to water content loss. Turbidite is 4 cm long several laminations are identified with silty-sandy alternated structure. Turbidite is capped with Ca and Sr increment (up to ~5000 cps and ~1200 cps respectively). Magnetic susceptibility

shows fluctuations corresponding with sand fraction changes (ranging %10-25). Bottom part of the section 20 contains relatively higher sand content up to %15.

Section 21 includes hemi pelagic sediments and 2 thin turbidite layers. 2-3 cm long turbidite units have similar proxies that Mn enrichment at basal part (up to 1200 cps and 800 cps respectively), capped with Ca and Sr increment. Two turbidites even though they are thin show inverse grading trend. On second turbidite in section 20, we encountered magnetic susceptibility response ranging between 10-17 u.S.I.. Section 21 is the last section in CS-01 and the last radiocarbon sampling is executed below units of last turbidite unit.

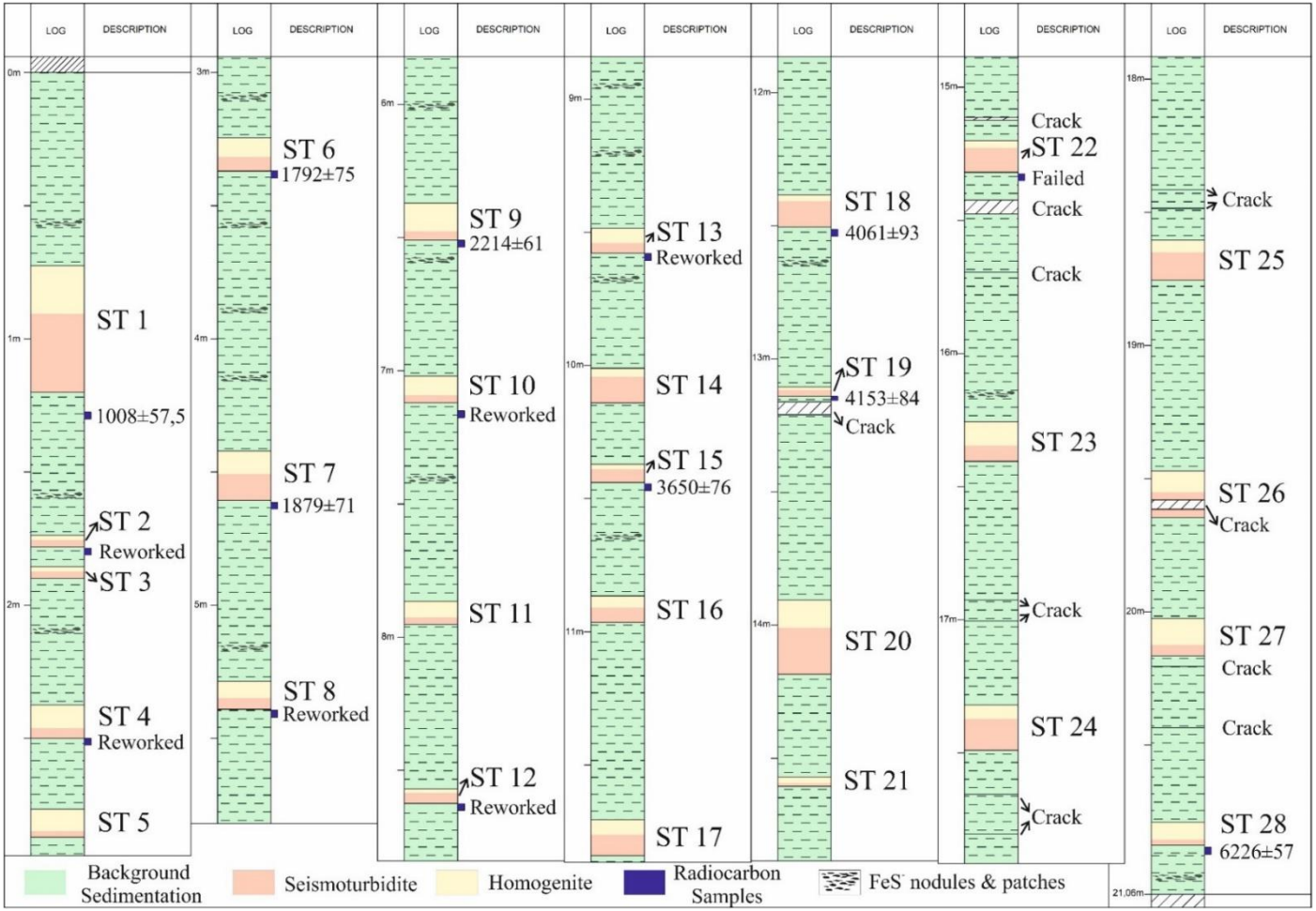

Figure 4.7: Piston Core CS-01 general lithostratigraphic units; Seismoturbidite layers (ST) contains two parts. Red color represents turbidite part; yellow color represents homogenite part of the successions. Small blue boxes indicate the C^{14} sample locations with calibrated ages. Light green color represents background sedimentation.

4.4.3. Radiocarbon Analyses

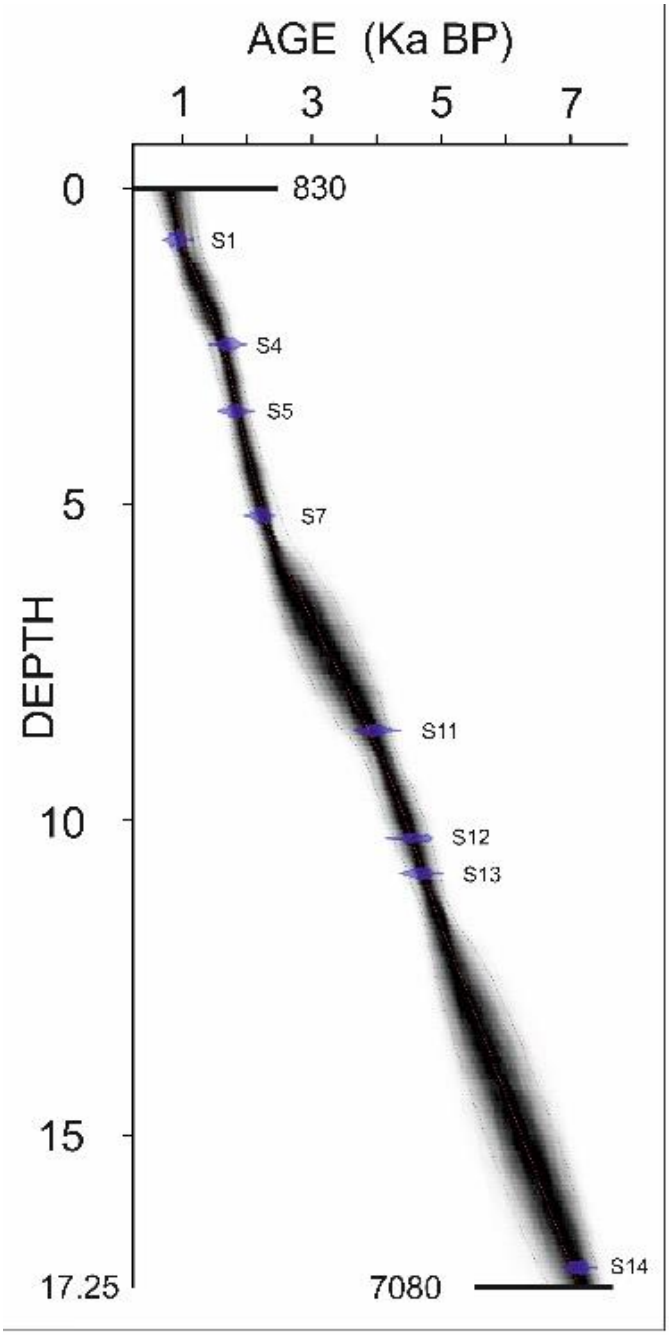

Figure 4.8: Age Model for CS-01. Eight samples are used for the model, which is executed on R-Studio, by using Bacon.r Script. Model is used 200 yr./m accumulation rate, 1.5 accumulation shape for the procreation of various iterations.

We have initiated a radiocarbon analysis to establish ages for each Seismoturbidite unit. Fourteen samples are collected and send to CEREGE Radiocarbon Laboratory in France. Initial results are shown (table 1, Bottom column, 3.raw). CALIB 7.0 software

is used for calibration. Reservoir age correction is accepted 400 years (Sinai et al 2000).

Calibrated ages (table 1, Bottom column 5. raw) are plotted at R-studio by using the script “bacon. R”, which uses Bayesian statistics to provide Bayesian accumulation histories for sedimentary units. Script created the model in %95 Gaussian confidence interval.

For CS-01, hiatuses are taken out which is turbidite-homogenite units, thus, model bases on only background sedimentation. Hiatus free sediment core has 17 m length. However, due to piston coring there is sediment loss at the top of the core. Loss is around 2 meters it is correlated with penetration length of cover (during recovering) and the estimated model. Therefore, CS-01 starts from 1249 Cal BP and in 17 m cuts the 7000 Cal BP years of units (figure 9.). We have used eight of radiocarbon results because six samples contain reworked material, which alters the model drastically. Estimated ages for Seismoturbidite horizons are plotted (table 1. Top column).

Table 4.1: List of Seismoturbidite units in core CS-01 and estimated ages from age model. Minimum and maximum age ratios are calculated by %95 Gaussian confidence interval. Mean values indicate the best fit of iteration on created age model.

depth(mm)	name	min	max	mean
725	st1	791.7	1247.7	998.1
1263	st2	946.2	1402.8	1160.2
1339	st3	965	1439.9	1190.8
1815	st4	1112.1	1613.3	1369.9
2081,5	st5	1216.6	1714.6	1472.4
2456	st6	1390.4	1803.5	1616.4
3506,5	st7	1671.6	2033.4	1854
4185,5	st8	1822.9	2199.2	2008.7
5166,5	st9	2072.9	2510.5	2259.1
5678	st10	2226.1	2733.6	2433.2
6424,5	st11	2420.2	3288.9	2802.1
7043,5	st12	2629.2	3637.2	3107.4
7905,5	st13	3037	3977.9	3539.5
8337,5	st14	3318.3	4123.6	3757.7
8567,5	st15	3458.9	4209.2	3873.6
8993,5	st16	3781.2	4334.4	4079.2
9733,5	st17	4064	4635	4352.2
10269	st18	4255.9	4811.3	4535.6
10839,5	st19	4482.4	4961.1	4725.6
11542,5	st20	4720.1	5185.5	4950.5
11927,5	st21	4806.6	5444	5094
12512,5	st22	4929	5791.4	5314.3
13396	st23	5169.5	6172.2	5643.5
14311	st24	5458.2	6521.1	5984.1
15351	st25	5811.2	6893.2	6376.5
16066	st26	6071.5	7114.9	6639.9
16446	st27	6223	7221.6	6780.2
17071	st28	6501.3	7391.7	7012.8

Table 4.2: Calibration of C^{14} Samples. List contains both uncalibrated and calibrated, ages and error intervals. Along 14 samples 8 of them used for model. 6 samples are eliminated due to containing reworked fragments. Note that reservoir ages are already included in both results.

Sample Codes	Depth (mbsf)	Uncalibrated age Reservoir Age Applied	Error Interval	2σ Calibrated Age Reservoir Age Applied	2σ Calibration Error	Status
s1	0,813	1105	±30	1008,5	±57,5	ok
s2	1,282	1715	±30	1628,5	±71,5	reworked
s3	1,829	2150	±30	2264,5	±35,5	reworked
s4	2,468	1855	±30	1792	±75	ok
s5	3,526	1825	±35	1879,5	±71,5	ok
s6	4,203	2480	±30	2576,5	±145,5	reworked
s7	5,181	2240	±35	2214,5	±61,5	ok
s8	5,721	3555	±40	3824	±107	reworked
s9	7,057	5500	±50	6330	±71	reworked
s10	7,92	3675	±35	3995,5	±95,5	reworked
s11	8,584	3415	±35	3650,5	±76,5	ok
s12	10,291	3715	±35	4061	±93	ok
s13	10,848	3760	±35	4153	±84	ok
s14	17,092	5380	±45	6226,5	±57,5	ok

4.4.4. Inverse Graded Turbidites

Turbidites are commonly normal graded depositions experiencing waning phase, which ends up gradual energy drop. There are circumstances forcing current to form inverse grading structure. In Kumburgaz basin, a bathymetric barrier located on northeastern border presents as an obstacle between basin and northeastern Canyon (figure.2.) so that, turbidity currents which is generated through Northeastern Canyon reach to the barrier eventually and start to climb the barrier. Turbidity currents are gaining speed and acceleration by moving downward through steep slopes, which makes the current more chaotic and ambivalent. Climbing up an obstacle is very opposite situation to turbidity currents thus, as a gravity flow moving against the gravitational force effects the current abruptly loosen. Therefore, instant energy drop surely causes inverse grading, which has succeeded to bypass the obstacle (figure 3.1). This behavior is seen on sand ripples which climbing material lose its energy, coarser material only carried to the top of the ripple by transporting agent. However, finer sediments are still carried down the slope of ripple. Finally, ripple shows inverse graded cross-laminated structure.

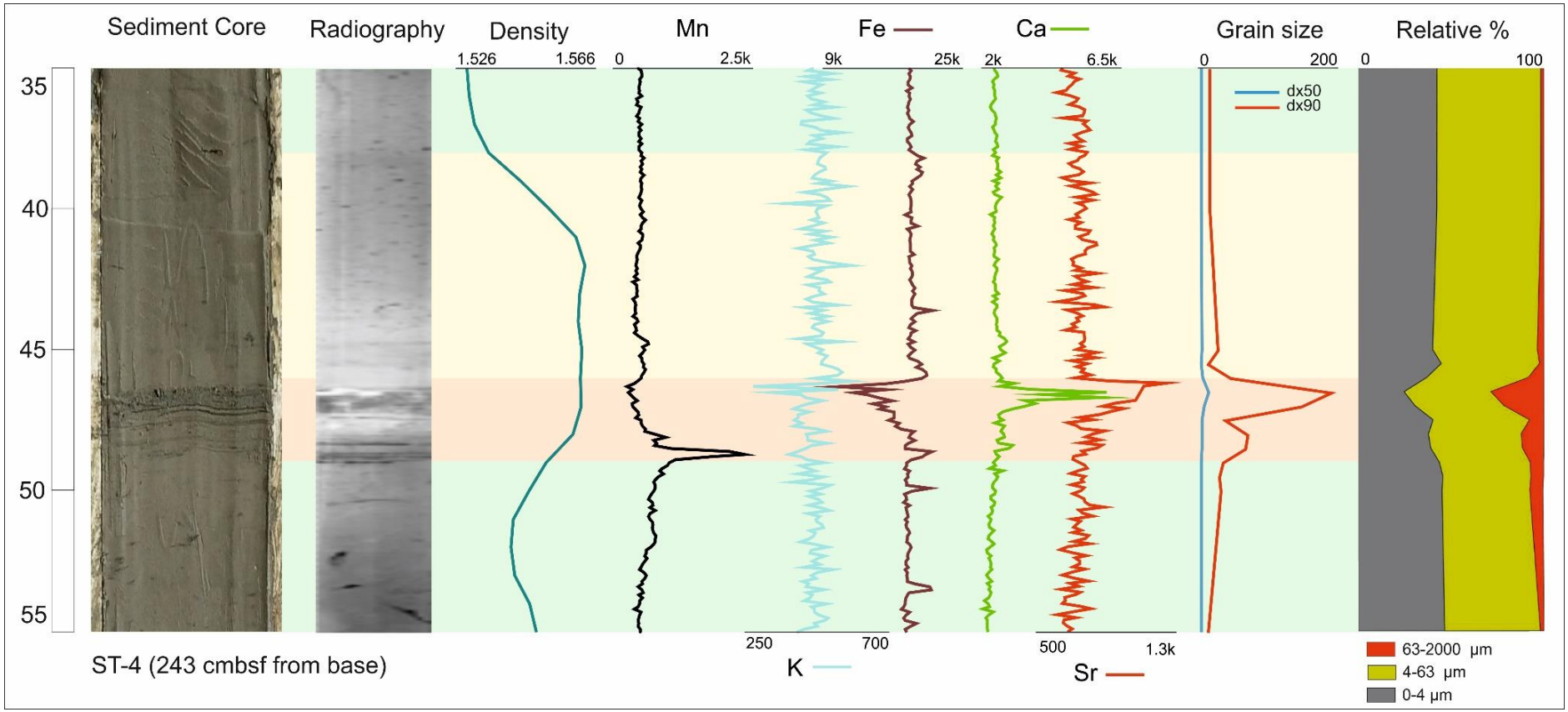

Figure 4.9: Inverse Grading Turbidite Sediment core, radiography, density, elemental proxies and grainsize parameters of a turbidite (ST-4, 243 cmbsf from base).

In Kumburgaz Basin, there are two major canyon carrying currents to the basin, which gives us the correlate, the depositions that have been carried and find the differences between them. Thus, Bathymetric barrier that makes the depositions inversely graded (figure.2) blocks Northeastern Canyon. On contrary, Turbidites, which is carried from North Canyon, displays normal graded structure, which is within the very first description of turbidites (figure x/a).

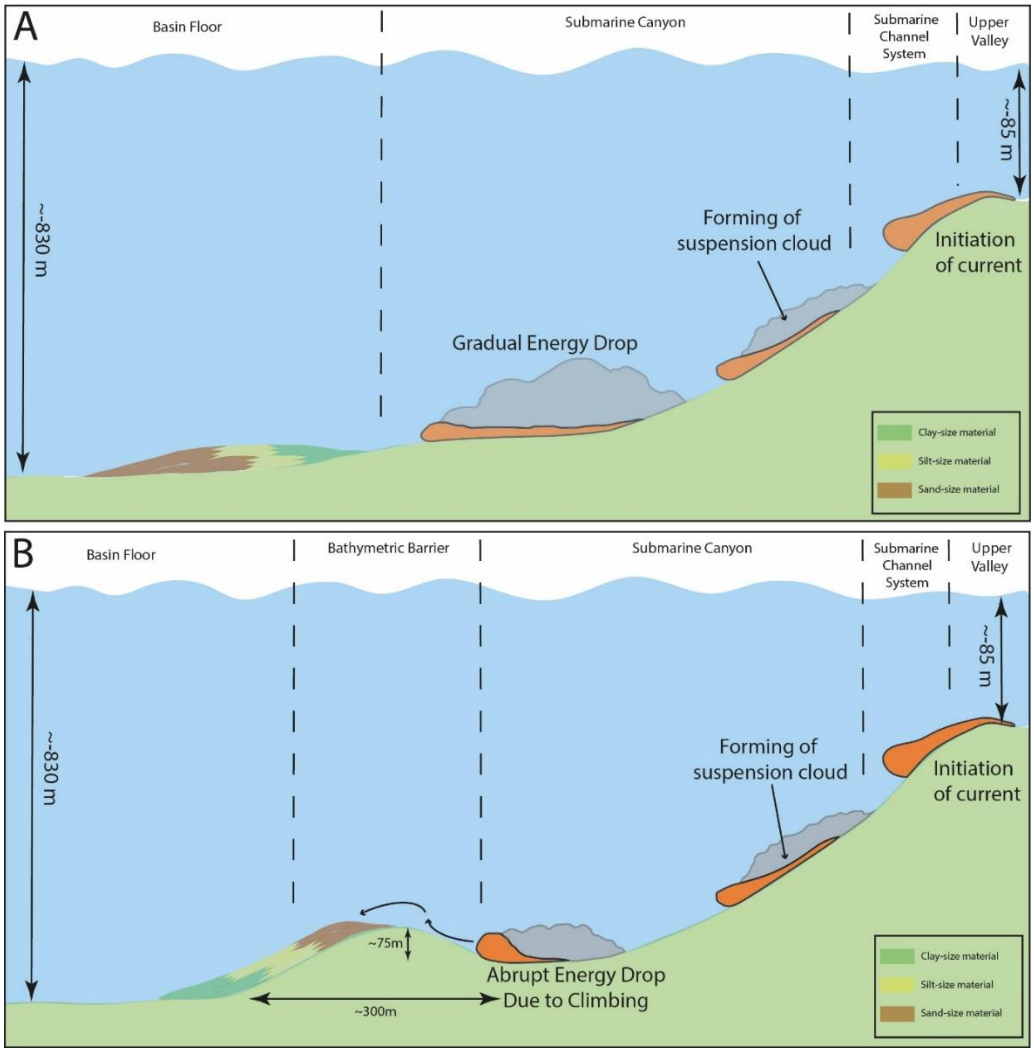

Figure 4.10: Depositional Models a) Northern Canyon Depositional Model (see Figure x/a for cross section location); Depositional processes that causes normal grading. Slope instability through an earthquake reaches its threshold starting to slide/glide. During the transportation, portion of slump/debris flow turns into turbidity flow with increasing acceleration through down the slope. Turbidity current procreates zonation regarding the density tendencies thus, formation of suspension cloud occurs alternately. As current reaches to the basin, when current is on waning phase, energy will be dropped thus, turbidite is deposited in a normal grading pattern. b) Northeastern Canyon Depositional Model (see Figure x/a for cross section location); Depositional processes that causes inverse grading; Current follows the pathway which is a single braided canyon until reaching to the barrier. Presence of Bathymetric Barrier prevents gradual energy drop, instead makes the current climb through which lead to sudden energy drop. Exceeding current behaves as the particles climbing a dune where the materials are deposited cross-laminated and inverse graded.

In our study, we have encountered 28 seismoturbidites, which is carried mostly from Northern and Northeastern Canyon. Majority of these turbidites are inverse graded showing that Northeastern Canyon is more active than Northern Canyon.

In some Seismoturbidites, it is rather complicated to see grading due to water oscillations. Even though a turbidite is affected by seiche, general trend of grading still has traces on deposition. Moreover, amalgamated structures containing multiple successions therefore, interpretations are built on each overlaying succession in order to find the grading differentiations and possible exclusive sources.

5. DISCUSSION

5.1. Encountered Distinctive Features of Seismoturbidites

5.1.1. Seiche Controlled Sedimentation

Earthquakes do not only cause slope instability, but also creates long-lasting water oscillations. When the water column is disturbed, recovery takes time, which is quite enough to generate disturbances on sediments. With every seiche period, sediment cloud is dragged with the oscillating current, which forces the sediments to form laminations (figure 5.1). Each alternating oscillation forms sand-silt size lamination, which is followed by silt-clay size overlying lamination (figure 5.1). When seiche takes place, it is not possible to see any sublayers overlaying except from homogenite.

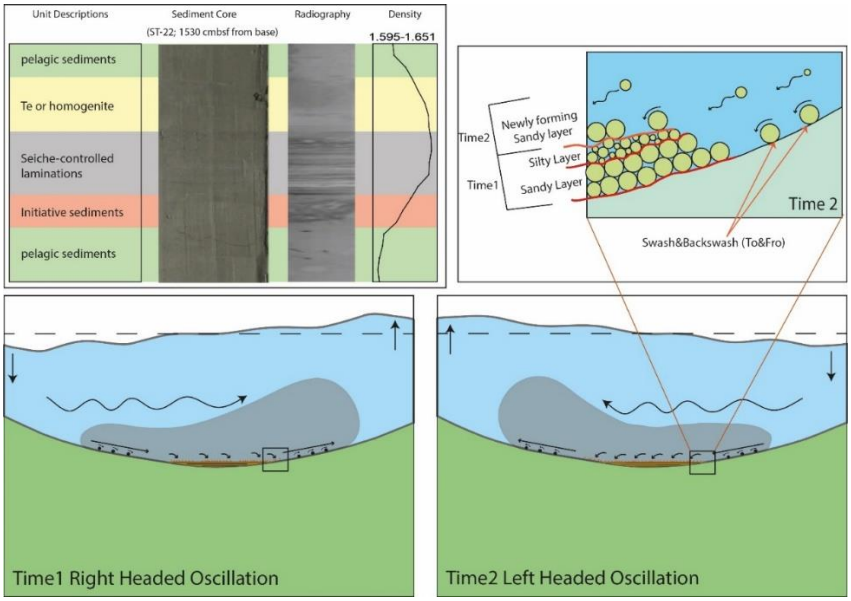

Figure 5.1 Seiche Controlled Laminations: Co-seismic shaking in the SoM could have resulted in both slope instability and the long-lasting water oscillations. As a consequence of seismic event, the long-lasting seiche effect caused the water column disturbance and concomitant to and fro bottom currents. Each alternating oscillation forms sand-silt size lamination, which is followed by silt-clay size overlaying lamination. Note that, seiche effect causes constant laminations on succession.

In Kumburgaz Basin, material dragged from slopes is rather smaller relatively to other Northern Basins in SoM (see grain size scales in figure 4.3, 5.2, 5.3). Therefore, most of the material could be under the effect of seiche controlled sedimentation. Any

deposition, which has affected by seiche, leaves traces on proxies. Grain size distributions shows repetitive pulses corresponding seiche controlled laminations (see figure 4.3, 5.2, 5.3). Radiographic images reveal presence of affected structure.

Seiche effect is the most important precursor as a distinctive feature for Seismoturbidites. Because there are not any sublayers in Ta-Td successions. Instead, initiative sediments present at the basal part with overlaying seiche controlled laminations. Homogenite deposited after the effect of water oscillations are minimized (figure 5.1).

Bathymetry (morphological aspects) and geometry (height, length) of regions alter seiche effect on sediments. Kumburgaz is the shallowest and smallest basin on the NNAF. Turbidites shows constant laminated structure of silt-clay and fine sand-silt alternations. That is because; seiche lasts for a few days which end up procreating of seiche controlled laminated structure on Seismoturbidite units. Mechanism suggests that suspension of homogenite is only possible after seiche starts to damp. Similar condition is seen at Lake Annecy in France. Lake Annecy is a much smaller basin regarding to Kumburgaz Basin. Even though, existence of currents and seiche is drastically shorter, water oscillations is delaying the suspension cloud by increasing the segregation (figure 2.10) (Beck 2009).

Moreover, Polonia et al., (2016) suggests a different model for effects of water oscillations on sediment-gravity flows. In their study, oscillations affect the Ionian Sea by creating secondary dilute turbidity currents which overlays homogenite. Furthermore, they suggest triggering of wave-induced bottom currents are caused also by seiche effect (figure 2.13).

Ionian Sea is vastly bigger in case of Lake Annecy and Kumburgaz Basin so the formation of tsunami waves is possible. Therefore, they imply that seiche can very well be a reason for secondary slope instability reasoned by tsunami waves. Seiche sequence is longer compared to Kumburgaz like conservative basins. Thus, we can assert that the depth and wideness are able to alter the influence of water oscillations by extending the seiche duration so that, deposits are shows various stratigraphic aspects accordingly.

5.1.2. Amalgamated Turbidites

In Kumburgaz Basin, various amalgamated structure depositions are present due to multiple slope failures. Earthquake-triggered currents are accumulated from one or multiple canyons and form a stack of turbidites. Stacked turbidites (Polonia et al 2016), are caused by one earthquake, which is represented by single Mn pulse of the very basal part of the stacked succession (figure 5.2).

During an earthquake, subsequent failures due to exceeding threshold multiple times through single channel are one of the possibilities for amalgamation. Hence, source is singular; it requires showing same pattern for each deposition (figure 5.2, figure 5.4). In ST7 (figure 5.2), deposition contains four turbidites overlaying each other. Each is capped with increment of Ca&Sr and shows inverse grading trend. Furthermore, radiographic images bound each succession with displaying changing shades in laminations. Therefore, ST7 is formed by four successive currents within a same event represented by single redox front.

Another possibility is the failure of multiple channels that nurtures the basin (figure 5.4). In this case, if the area is wide enough, it is possible to see the composition differences for each succession (Nakajima & Kanai 2000). However, nurturing system is limited and source is more or less similar for Kumburgaz Basin. Possibility of each scenario is also related with the amount of material that has been loaded on slope thus, intensity and duration of the earthquake directly procures such multiple failures on slopes.

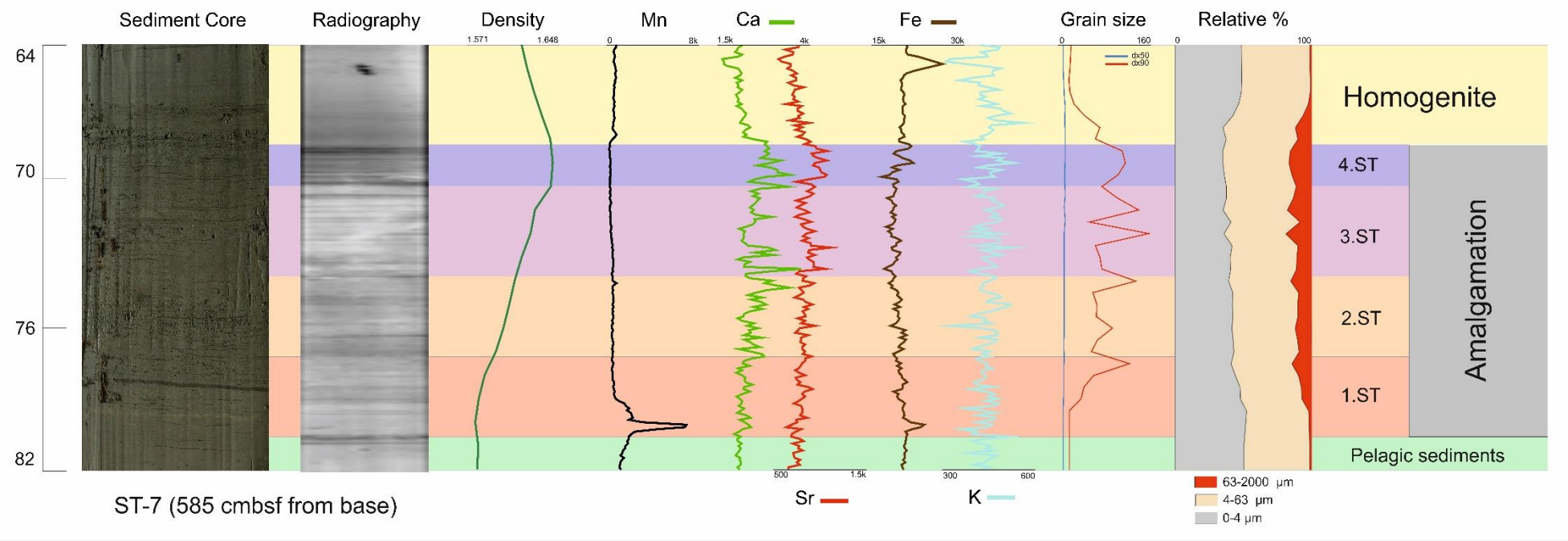

Figure 5.2 Amalgamated Turbidite. Sediment core, radiography, density, elemental proxies and grainsize parameters, corresponding descriptions of overlapping turbidites (ST-7, 585 cmbsf from base).

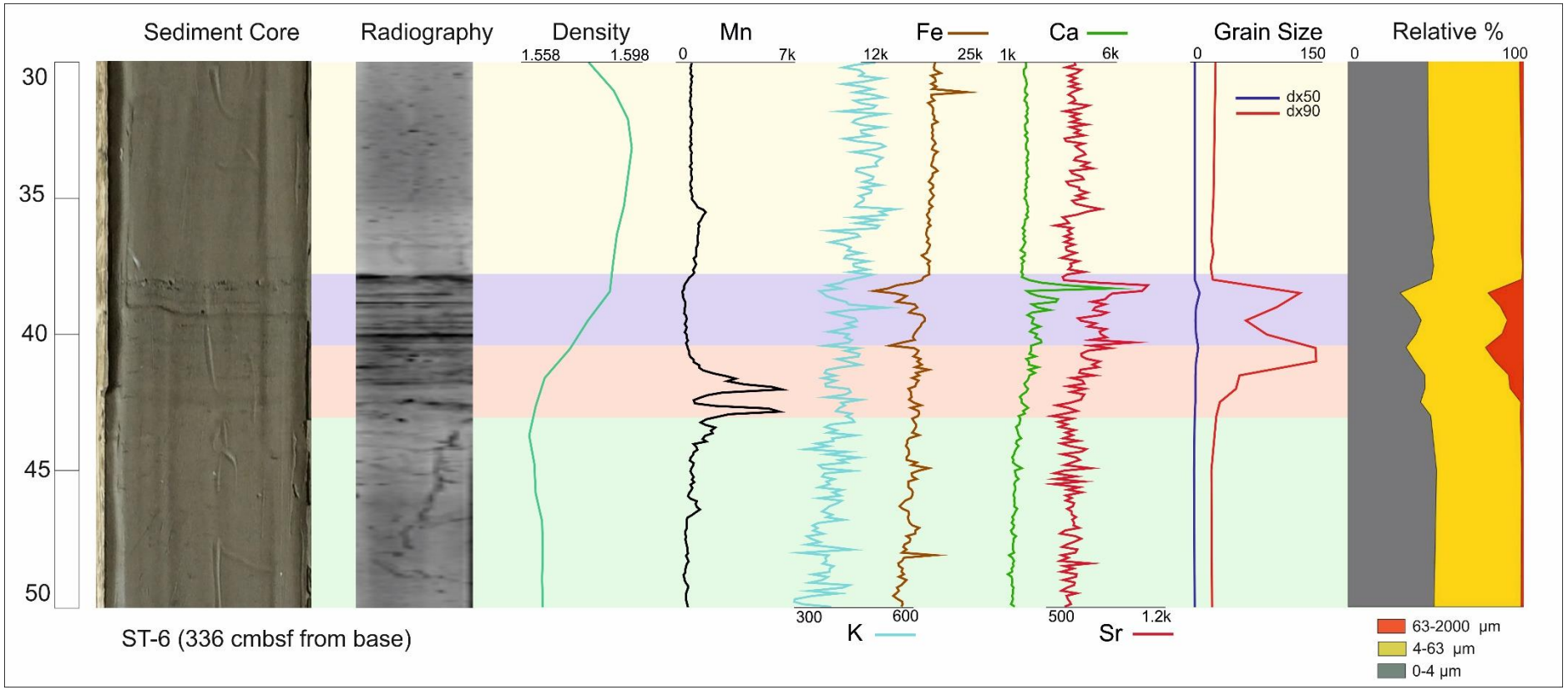

Figure 5.3 Subsequently Deposited Turbidites. Sediment core, radiography, density, elemental proxies and grainsize parameters, corresponding descriptions of subsequently deposited turbidites (ST-6, 336 cmbsf from base).

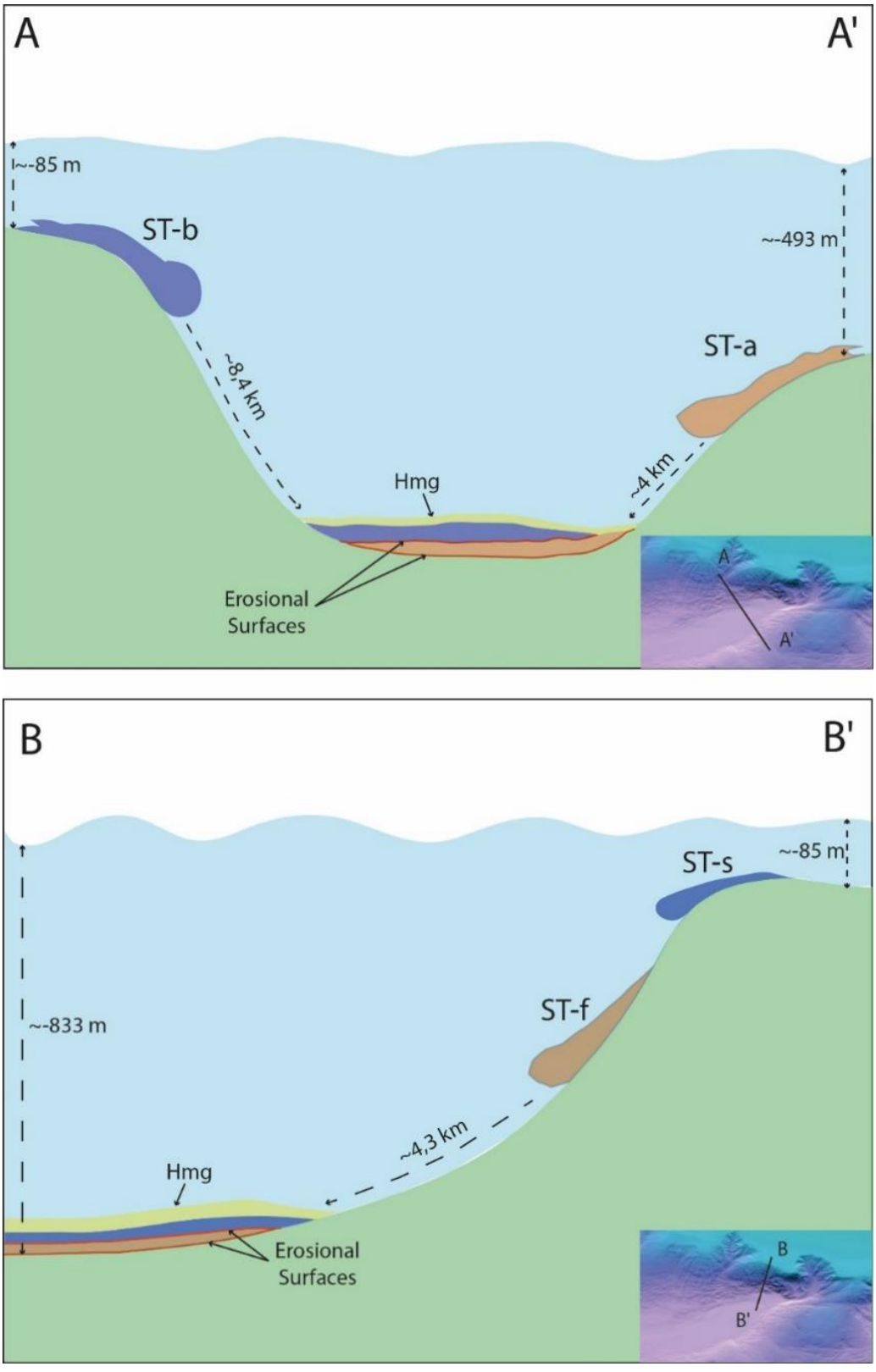

Figure 5.4 Amalgamation Processes and Depositional Scenarios Scenario 1 demonstrates reaching of multiple turbidites from different pathways. Amalgamation occurs because of the variation of distances between currents from the depositional area. Scenario 2 demonstrates reaching of multiple turbidites from the same valley. Amalgamation occurs because of the time interval between the initiations of currents.

5.1.3. Redox Front Migration

In SoM oxic-anoxic boundary is relatively shallow (20-30 cm) (ref). This peculiar situation presents a perfect usage of redox sensitive elements in order to identify sediment gravity flow deposits (Cağatay et al 2012, Polonia et al 2013). Mn used in this study for firstly to identify seismoturbidites by detecting migration of redox fronts. Furthermore, amount and thickness of Mn enrichment is a proxy to show the time intervals of sediment-gravity deposits (Cağatay et al 2004, ref). Because formation of new redox fronts is event that need time to accumulate. Therefore, number of Mn pulses in a stacked turbidite actually shows how many triggers which is deposited as a stacked succession.

Amalgamation can be formed during one event or caused by subsequent catastrophes. Mn therefore shows whether the event is singular. ST-7 (figure 5.2) is formed by four subsequent turbidites, which is transported by the submarine canyons in Kumburgaz Basin. However, ST-6 (5.3) consists of two turbidite depositions thus, each one is represented by positive Mn anomaly. Time interval between turbidites is long enough to remobilize secondary vertical Mn+2 flux through the basal part of the second turbidite. Time interval reveals that the turbidites are deposited exclusively therefore, they are not correlated with single event. Note that, there is no homogenite deposited at the top of the first turbidite (figure 5.5) because of the erosive manner of the subsequent current. However, pelagic sediments are also absent between two turbidites. It can be interpreted in two functions; each turbidite is triggered by subsequent major earthquakes or second turbidite is triggered by an aftershock so that, both supports the absence of homogenite between turbidites and the absence of pelagic sediments between turbidites (figure 5.5).

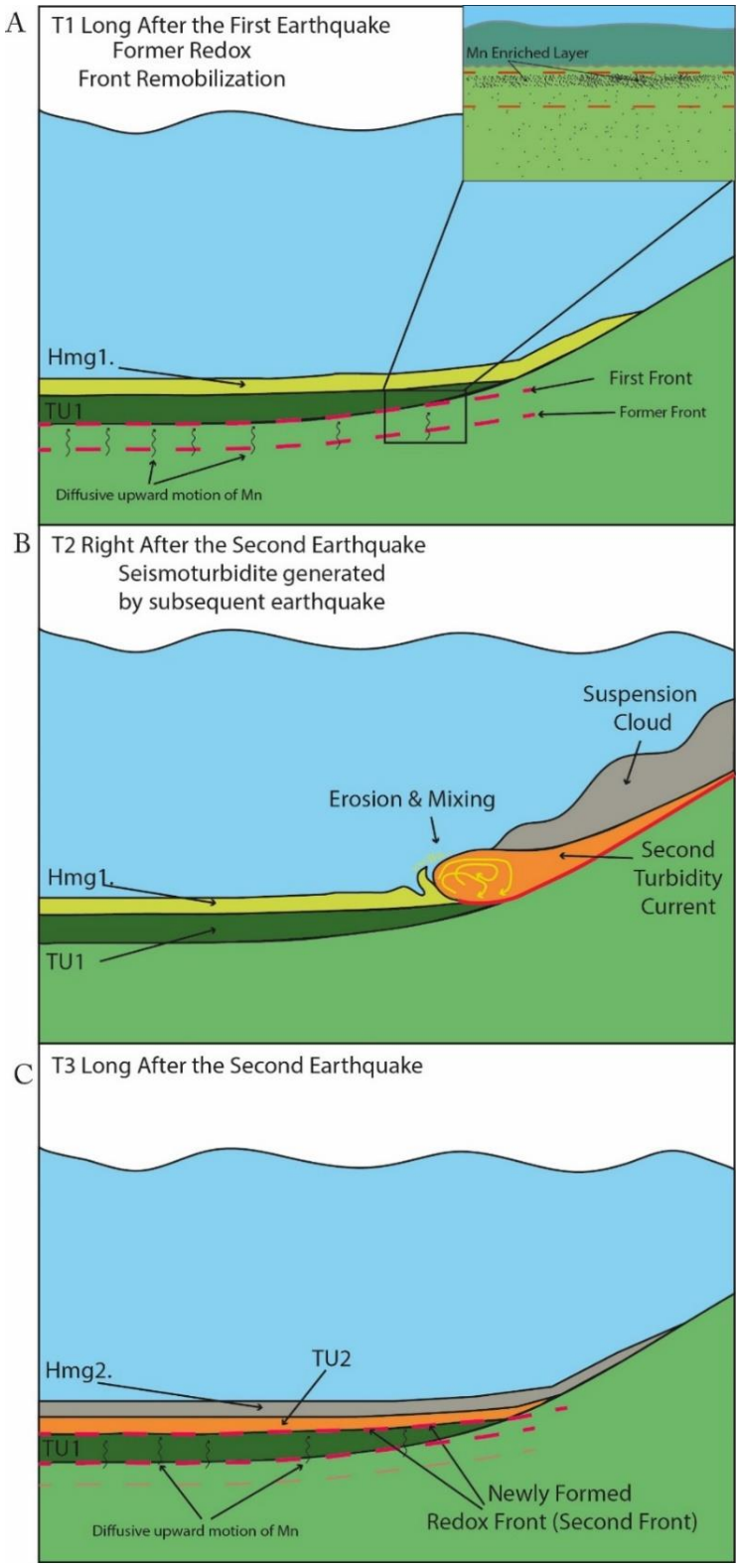

Figure 5.5: Redox Front Migration A) At T1 (time 1), turbidite-homogenite deposit (TU1-Hmg1) procreates a new redox front. Inset figure represents a close up section showing where the Mn enrichment accumulated the most. B) At T2 (time 2), figure accentuates the second current, which erodes the former TH units, accumulation to basin. Note that, current also procures material from former deposited unit (TH1-Hmg1). C) At T3 (time 3) which is after the motion stops, two turbidites (buried is mostly eroded, overlaying is successively deposited with homogenite, respectively) constrain to form most recent redox front.

5.2. Tectonic History of Kumburgaz Basin in the Last 7000 yrs.

Estimated Age model displays %95 Gaussian distribution confidence interval for the core Cs-01. We initiated a correlation between historical earthquakes and seismoturbidites in order to establish a record for earthquake history of Kumburgaz Basin. Unfortunately, around 1000 years is missing at the top during the recovery of the calypso core. Historical records extend to 2000-2500 years therefore; only top ten seismoturbidites were able to correlate. Even though age intervals often match with several earthquakes, we stuck around mean value which age model has given instead of considering whole interval.

To be sure of turbidites are generated from seismic origin, we eliminated possible trigger mechanisms in our studied area. we have explained the trigger mechanisms (see chapter, Sedimentary Records of Earthquakes: Seismoturbidites) so that, in Kumburgaz Basin, we don't see any other triggers. Shelf edge at northern slope lies at about -100 m, it is not possible storm waves can reach to that elevations. There is no volcanic activity which can be a trigger in Kumburgaz Basin. Tides can be trigger in ocean margins where water mass is extremely vast, however in case of SoM, most probable tidal range is within cm long sequences, therefore it is not possible to generate a slope failure. There is only one possible source for terrestrial input which is through Büyükçekmece lagoon, however the distance between inlet and slope edge is about 4 km which is unlikely to be a trigger for slope failure. Besides from all other possibilities, most likely turbidites are generated from earthquakes which is also correlated with historical earthquakes.

ST-1, the thickest seismoturbidite in the rest of the core, may be associated with the 989 AD Nicomedia (İzmit) earthquake. AD 989 earthquake destroyed most of the significant structures in Constantinople (İstanbul) and Nicomedia (İzmit). Prominent structures like St. Sophia church and towers of Byzantium were collapsed (Guidoboni et al., 1994).

ST-2 is correlated with the time of AD 824 earthquake. Most probably, earthquake has ruptured Ganos segment of the NNAF. Ancient city of Panion (located near current Tekirdağ City) was severely damaged. Most of the city walls were collapsed (Guidoboni et al., 1994).

ST-3 best fit of age interval includes AD 740 earthquake, which is affected mostly at Constantinople (İstanbul). Records mention at the early afternoon of 26 October earthquake has occurred and caused devastating loss. Churches, monasteries, statues like Constantine the Great and Gate of Attalus. Earthquake has affected most of the Thracian villages, Nicomedia, Praenetus and Nicea. Even it affected shorelines by creating waves which were significant enough to be recorded. Even though records suggest aftershocks are also occurred, we did not see the traces on the sediments core. They either eroded or did not procreate a deposition in Kumburgaz Basin. Given to the affected area, AD 740 earthquake should have been generated from multi-segment rupture. However, there is no specific sedimentation record regarding to multi-segment rupture, effecting southern cities of SoM cannot be ruled out to suggest a multi-segment rupture (Guidoboni et al., 1994).

AD 20 April 611 earthquake is correlated with ST-4. Although earthquake did not damage the City of Constantinople (Istanbul), it was significant enough to be recorded. It can be suggested an intermediate earthquake according to intensity can trigger slope instability (Guidoboni et al., 1994).

ST-5 could be deposited at the time of AD 526-527 earthquake. It is debated to establish a date for significant earthquake, however it is suggested that there were series of earthquakes during the years. On contrary, we did not see any traces to support the series of earthquakes. In ST-5, there is no evidence of amalgamation. Furthermore, elemental proxies do not show a trend of either for subsequent failure or amalgamated structure (Guidoboni et al., 1994).

ST-6 age interval and structure of ST-6 strongly suggest that 24 August 358 Nicomedia (İzmit) and February AD 363 Constantinople (İstanbul) earthquakes were recorded in an amalgamated structure in the sediment core. Subsequent failures with time interval is traced by exclusive Mn pulses. 5 years of interval is providing enough time to create a new redox front for the AD 363 earthquake, therefore we can identify on the ST-6 there are two events deposited (see figure 5.3) (Guidoboni et al., 1994).

ST-7 may be associated with deposition of AD 181 Nicomedia (İzmit) earthquake. Historical records imply affected region is the city of Nicomedia (İzmit) and surrounding region of Sakarya river. Distance between affected region and the studied area is wide. However, we interpret that if the earthquake has occurred due to rupture

of Izmit segment of the NNAF, it can quite provide enough instability to failure on slopes of Kumburgaz Basin (Guidoboni et al., 1994).

ST-8 may be another example of subsequent ruptures which is deposited in amalgamated structure. 24 November AD 29 Nicea (İznik) and AD 69 Constantinople (İstanbul) earthquakes are deposited subsequently with the interval of 45 years. Structure is same with the ST-6 but the interval is much wider. However, Mn pulses shows exclusive pulses corresponding each earthquake-triggered deposition and radiographic image shows sharp contact between two events. We interpret that after AD 29 seismoturbidite deposition, AD 69 earthquake-triggered turbidity current eroded at least 45 years of pelagic sedimentation and maybe some portion of the previous (AD 29's deposition) seismoturbidite (Guidoboni et al., 1994).

ST-9 is an amalgamated turbidite which might be containing BC 287 Tekirdağ-Gallipoli (Gelibolu) earthquake-triggered deposition and BC 360 Çanakkale earthquake-triggered deposition. Again the ST-9 sequence is represented by two Mn pulses each corresponding different earthquakes. Records imply that, BC 287 earthquake affected whole Thrace basin including Tekirdağ and Gallipoli (Gelibolu) region near SoM. However, BC 360 earthquake seemed to be caused by a rupture of same segment or the SNAF section (Guidoboni et al., 1994).

ST-10 may be associated with deposition during BC 427 Marmara Ereğlisi earthquake. There is only one earthquake within the age interval, therefore it is very likely BC 427 earthquake caused ST-10 to be deposited. Historical records imply earthquake affected Thracian villages thus, effect is more concentrated on Marmara Ereğlisi and surroundings. Given to the effected region, this particular earthquake must be occurred by the rupture of Central Segment of NNAF (Guidoboni et al., 1994).

Remaining 18 seismoturbidites are listed with minimum to maximum age intervals and the best fits being estimated by age model (Figure x). Despite the ST-2 and ST-3 interval of ~40 years, remaining ages of seismoturbidites have intervals changing around 100-250 years. This sequence of events is rather compatible with the reoccurrence time intervals of NAF. Lower intervals may be caused by adjacent ruptures of Central Segment which also supports the domino-like failure of NAF during sequence earthquakes (Guidoboni et al., 1994).

Another aspect is some earthquakes mentioned in historical records may have caused by multi-segment ruptured despite the limitation of effected regions. For example, 29 AD İznik earthquake and BC 360 Çanakkale earthquakes are rather far away from the Kumburgaz Basin. However, in sediment core we have encountered the seismoturbidites for each particular earthquake. It is clear that, historical records and seismoturbidite sequences are incompatible, however, we cannot ignore the fact seismoturbidite ages are colliding even with distant ruptures 29 AD, BC 360. It can be suggested these ruptures extends closer to Kumburgaz Basin than what have been implied by historical records (Guidoboni et al., 1994).

Table 5.1: Correlation between Seismoturbidites and Historical Earthquakes; Depth (mm), naming, corresponding earthquake and effected region is listed on the table. From AD 1000 to BC 450, around 1500 years of history could be matched with historical records.

Depth (mm)	Name	Correlation	Effected Region
725	st1	AD 989	İzmit
1263	st2	AD 824	Tekirdağ
1339	st3	AD 740	İstanbul
1815	st4	AD 611 April 20	İstanbul
2081,5	st5	AD 526	İstanbul
2456	st6	AD 358 August 24, subsequently AD 362	İstanbul/İzmit
3506,5	st7	AD 181	İzmit
4185,5	st8	AD 29 November 24 subsenquently AD 69	İznik/İzmit
5166,5	st9	BC 360 subsequently BC 287	Şarköy-Gelibolu/Çanakkale
5678	st10	BC 427 December	Marmara Ereğlisi

5.3 Implication on Creeping versus Locked Central Segment of NNAF

There is a current debate about the seismogenic behavior of the Central Segment of NNAF. Recent instrumental studies suggest a creeping versus locked fault segments in SoM. Ergintav et al., 2014 suggest Central High segment is not accumulating strain along the whole segment where the fault passes through Kumburgaz Basin. However, most recent studies (Schmittbuhl et al. 2015, 2016 and Sakic et al 2016) suggest fault is locked under the Kumburgaz Basin. Sakic et al. 2016, support this idea by showing there is no surface deformation on Kumburgaz basin. Their dataset displays such a situation however they also imply that; fault can be experiencing step-wise creeping which will be obtained with further studies. Schmittbuhl et al. (2015, 2016) suggests Kumburgaz may very well be locked based on interpretations and models of seismicity. They imply the locking depth is between 10 and 15 km. On the other hand, they claim that the fault passing through Central basin is experiencing creep to very shallow depth (up to ~4 km).

One of the approach of our study is to be able to see sedimentary traces of AD 1509 and 1766 earthquakes so that, we could provide solid interpretation about recent ruptures. Since the top 2 m of the core CS-01 is missing due to recovery, we were unable to analyze the most recent sediments to link with earthquakes. This study provided earthquake history between AD 1000 and BC 500, which is correlated with historical records. However, it is still unknown to correlation between seismoturbidites and segments. Even though, there are recent papers suggesting Kumburgaz basin may be creeping, however our observations from seismic reflection profiles and detailed analysis of the sediment cores show that this segment has been rupturing with earthquakes.

6. CONCLUSION

This thesis project comprises a high resolution multi-parameter study with sedimentary, physical and geochemical proxies to establish distinctive properties of earthquake-triggered turbidites aka seismoturbidites. Physical, geochemical, sedimentological methods have been performed in order to enlighten sedimentary record of Kumburgaz Basin. Morphology, tectonics and sedimentary fill of the Kumburgaz Basin is broadly covered and explained with high resolution seismic profiles, core study and multi-beam bathymetry.

Equipment such as, MSCL, XRF, Mastersizer in EMCOL facility are used during this project. All sedimentological processes are executed with mm to cm long resolution. 15 radiocarbon samples are sent to CEREGE Radiocarbon Laboratory to obtain C^{14} ages for 28 identified turbidite units in core CS-01.

Previous studies are broadly discussed to display what has been done regarding to distinguish the term seismoturbidites. We can propose that depth and the volume of water column is directly effecting the sedimentation processes. Seiche is also bounded with volume of the aqueous area.

The Kumburgaz Basin and current tectonic regime is examined with high-resolution seismic reflection profiles, multi-beam bathymetry and a piston core in this study to establish sedimentary records or effects of active faulting in the basin. Central segment of the NNAF is the main fault controlling the Kumburgaz basin with transtension where tha basin exhibit a half-graben. We have encountered that there is no southern main fault in the basin. However, minor secondary faults with dip-slip mapped in some of the CHIRP profiles may refer to the hanging-wall collapse in the basin. A secondary depocenter is mapped in the western portion of the basin which is smaller than the main depocenter in the east.

Main focus of this study was to develop a new approach to distinguish sedimentological characteristics of seismoturbidites from the general turbidity current deposits. Accordingly, stratigraphic aspects due to water oscillations forms a unique sequence mostly of a laminated structure which apparently is the most exclusive

feature for earthquake-triggered sedimentation. Geochemical and physical precursors bound basal and top part of the succession also help to constrain sublayers of turbidites (Ta-Te). Our analysis show that especially Mn exhibit a unique precursor to determine whether the sequence is instantaneous or not. Mn in this case is used to determine the time interval of alternated currents. In such effort, subsequent failures that forms amalgamated stacked turbidites become another important indicator linked with significant Mn enrichment.

This study also reveals the role of hydrodynamic and morphologic aspects of the region in order to show how sediment-gravity flow deposits can diversify due to various parameters. One thing for sure, reverse graded turbidites are only detected in Kumburgaz Basin in the northern Marmara Sea, because of a bathymetric barrier. This specific morphological feature allowed us to produce a depositional model for particular transportation dynamics.

Formation of amalgamated structures and seiche effect on sediments are directly observed from the analysis of the core CS-01. Seiche controlled sedimentation provides constant laminated structures which are vindicated by radiographic images and grain-size fluctuations. Amalgamation is shown with repetitive geochemical proxies which implies a stacked turbidite succession. Each deposition is capped with subsequent deposition with identical precursors such as Ca and Sr increment or Fe and K depletion.

Migration of redox fronts were another critical parameter to understand their relation with sediment-gravity flows deposits and helped to build the depositional models. It shows that whether the events are instantaneous or not; moreover, it provides to see the time-lapse between subsequent events.

We have established an age chronology for the latest 7000 years based on the C^{14} dating from 28 seismoturbidite sequences of CS01. Therefore, estimated age model unravels possible associations with major historical earthquakes based historical records of earthquakes. Since the top ~2 m section of the core is lost during the recovery of the piston core, we are only able to obtain ages starting from AD 1000 yrs. Therefore 10 seismoturbidites were to correlated, 18 seismoturbidites stands unmatched with historical records.

We conclude that the term seismoturbidite is studied to diversify from the general description. This thesis project aims to make an important contribution on unraveling the characteristics of “seismoturbidites”. We have broadly explained how hydrodynamic conditions and morphological structures are counted for as a parameter in depositional processes. Former proxies which has been used, are combined with sedimentological processes to vindicate the differences of earthquake-triggered sediment-gravity flows. Our analysis in this project suggest that sedimentological and geochemical proxies are very important precursors to distinguish sediment-gravity flow deposits. However, more multi-disciplinary studies are needed to better analyze the seismoturbidites worldwide.

REFERENCES

Ambraseys, N.N., (2002). The seismic activity of the Marmara Sea region over the last 2000 years. Bulletin of the Seismological Society of America 92, 1–18.

Ambraseys, N.N., (2009). Earthquakes in the Mediterranean and Middle East: A Multidisciplinary Study of Seismicity up to 1900. Cambridge University Press, Cambridge, U. K. (947 pp.).

Ambraseys, N.N., Finkel, C.F., (1991). Long term seismicity of the Istanbul and of the Marmara Sea region. Terra Nova 3, 527–539.

Ambraseys, N.N., Finkel, C.F., (1995). The Seismicity of Turkey and Adjacent Areas-A Historical Review. Eren Yayıncılık, Istanbul, pp. 1500–1800. 240 pp.

Ambraseys, N.N., Jackson, J.A., (2000). Seismicity of Sea of Marmara (Turkey) since 1500. Geophysics Journal International 141, F1–F6.

Arai, K., Naruse, H., Miura, R., Kawamura, K., Hino, R., Ito, Y., Inazu, D., Yokokawa, M.,Izumi, N., Murayama, M., Kasaya, T., (2013). Tsunami-generated turbidity current of the 2011 Tohoku-Oki earthquake. Geology 41, 1195–1198.

Armijo, R., Meyer, B., Navarro, S., King, G., Barka, A., (2002). Asymmetric slip partitioning in the Sea of Marmara pull-apart: a clue to propagation processes of the North Anatolian Fault. Terra Nova 14 (2), 80–86.

Armijo, R., Pondard,N., Meyer, B.,Mercier de Lapinay, B.,Ucarkus,G., theMARMARASCARPS Cruise Party, (2005). Submarine fault scarps in the Sea of Marmara pull-apart (North Anatolian Fault): implications for

seismic hazard in Istanbul. Geochemistry, Geophysics, Geosystems 6, 1–29.

Arnaud, F., Lignier, V., Revel, M., Desmet, M., Beck, C., Pourchet, M., Charlet, F., Trentesaux, A., Tribovillard, N., (2002). Flood and earthquake disturbance of 210Pb geochronology (Lake Anterne, NW Alps). Terra Nova 14, 225–232.

Barka, A., Akyuz, H.S., Altunel, E., Sunal, G., Cakir, Z., Dikbas, A., Yerli, B., Armijo, R., Meyer, B., de Chabalier, J.B., Rockwell, T., Dolan, J.R., Hartleb, R., Dawson, T., Christofferson, S., Tucker, A., Fumal, T., Langridge, R., Stenner, H., Lettis, W., Bachhuber, J., Page, W., (2002). The surface rupture and slip distribution of the 17 August 1999 Izmit earthquake (M 7.4), North Anatolian Fault. Bulletin of the Seismological Society of America 92, 43–60.

Barka, A.A., Kadinsky-Cade, K., (1988). Strike slip fault geometry in Turkey and its influence on earthquake activity. Tectonics 7, 663–684.

Beck, C., (2009). Late Quaternary lacustrine paleo-seismic archives in north-western Alps: examples of earthquake-origin assessment of sedimentary disturbances. Earth Sci. Rev. 96, 327–344.

Beck, C., Manalt, F., Chapron, E., Van Rensbergen, P., De Batist, M., (1996). Enhanced seismicity in the early post-glacial period: evidence from the post-würm sediments of Lake Annecy, Northwestern Alps. Journal of Geodynamics 22, 155–171.

Beck, C., Mercier de Lapinay, B., Schneider, J.L., Cremer, M., Cagatay, N., Wendenbaum, E., Boutareaoud, S., Menot, G., Schmidt, S., Webe, O., Eris, K., Armijo, R., Meyer, B., Pondard, N., Gutcher, M.A., Turon, J.L., Labeyrie, L., Cortijo, E., Gallet, Y., Bouquerel, H., Gorur, N., Geravis, A., Castera, M.H., Londeix, L., de Resseguier, A., Jaouen, A., (2007). Late Quaternary co-seismic sedimentation in the Sea of Marmara's deep basins. Sedimentary Geology 199, 65–89.

Bertrand, S., Doner, L., Akçer, S., Sancar, Ü., Schudack, U., Mischke, S., Çağatay, M.N., Leroy, S.A., (2011). Sedimentary record of coseismic subsidence in Hersek coastal lagoon (Izmit Bay, Turkey) and the late Holocene activity of the North Anatolian Fault. Geochemistry, Geophysics, Geosystems 12 (6), Q06002. http://dx.doi.org/10.1029/2011GC003511.

Bouma AH (1964) Turbidites. In: Bouma AH, Brouwer A (eds) Turbidites. Developments in sedimentology, vol 3. Elsevier, Amsterdam, pp 247–256. doi:10.1016/S0070-4571(08)70967-1

Calvert, S.E., Pederson, T.F., (1993). Geochemistry of recent oxic and anoxic marine sediments: implications for the geological record. Marine Geology 113, 67–88.

Carrillo, E., Beck, C., Audemard, F.A., Moreno, E., Ollarves, R., 2008. Disentangling Late Quaternary climatic and seismo-tectonic controls on Lake Mucubaji sedimentation (Merida Andes, Venezuela). Palaeogeography Palaeoclimatology Palaeoecology 259, 284–300.

Chapron, E., Beck, C., Pouchet, M., Deconninck, J.F., (1999). 1822 earthquake-triggered homogenite in Lake Le Bouget (NW Alps). Terra Nova 11, 86–92.

Cita, M.B., Aloisi, G., (2000). Deep-sea tsunami deposits triggered by the explosion of Santorini (3500 a BP), Eastern Mediterranean. Sedimentary Geology 135, 181–203.

Cita, M.B., Beghi, C., Camerlenghi, A., Kastens, K.A., McKoy, F.W., Nosetto, A., Parisi, E., Scolari, F., Tomadin, L., (1984). Turbidites and megaturbidites from the Herodotus Abyssal Plain (Eastern Mediterranean) unrelated to seismic events. Marine Geology 55, 79–101.

Cita, M.B., Bossio, A., Colombio, A., Gnaccolini, M., Salvatorini, G., Broglia, C., Camerlenghi, A., Catrullo, D., Clauzon, G., Croce, M., Giambastiani, M., Kastens, K.A., Malinverno, A., McKoy, F.W., Parisi, E., (1982).

Sedimentation in the Mediterranean Ridge Cleft (DSDP Site 126). Member of Society of Geology, Italy 24, 427–442.

Cita, M.B., Carmerlenghi, A., Rimoldi, B., (1996). Deep-sea tsunami deposits in the eastern Mediterranean: new evidence and depositional models. Sedimentary Geology 104, 155–173.

Çagatay, M.N., Erel, L., Bellucci, L.G., Polonia, A., Gasperini, L., Eris, K., Sancar, Ü., Biltekin, D., Uçarkus, G., Ülgen, U.B., Damci, E., (2012). Sedimentary earthquake records in the Izmit Gulf, Sea of Marmara, Turkey. Sediment. Geol. 282, 347–359. http://dx.doi.org/10.1016/j.sedgeo.2012.10.001.

Çağatay, M.N., Özcan, M., Güngör, E., (2004). Pore water and sediment geochemistry in the Marmara Sea (Turkey): early diagenesis and diffusive fluxes. Geochemistry: Exploration, Environment, Analysis 4, 213–225.

Dott Jr, R. H. (1963). Dynamics of subaqueous gravity depositional processes. AAPG Bulletin, 47(1), 104-128.

Drab, L., Hubert-Ferrari, A., Schmidt, S., Martinez, P., (2012). The earthquake record in the western part of the Sea of Marmara, Turkey. In: Pantosi, D. (Ed.), Natural Hazards and Earth System Sciences, Special Issue "Subaqueous Paleoseismology", pp. 1235–1254. http://dx.doi.org/10.5194/nhess-12-2012.

Ergin, M., (1994). Possible sources and mechanisms of manganese enrichment in the deep-sea sediments of the Marmara Trough depressions (NE-Mediterranean, Turkey). Oceanologica Acta 17 (5), 535–546.

Eris, K.K., Çağatay, N., Beck, C., Mercier de Lepinay, B., Campos, C., (2012). Late-Pleistocene to Holocene sedimentary fills of the Cinarcik Basin of the Sea of Marmara. Sedimentary Geology 281, 151–165.

Gasperini, L., Polonia, A., Çağatay, M.N., Bortoluzzi, G., Ferrante, V., (2011). Geological slip rates along the North Anatolian Fault in the Marmara Sea. Tectonics 30, TC6001.

Géli, L., Henry, P., Zitter, T., Dupré, S., Tryon, M., Çağatay, M.N., de Lépinay, B., Mercier, Le Pichon, X., Sengör, A.M.C., Görür, N., Natalin, B., Uçarkus, G., Özeren, S., Volker, D., Gasperini, L., Burnard, P., Bourlange, S., the Marnaut Scientific, Party, (2008). Gas emissions and active tectonics within the submerged section of the North Anatolian Fault zone in the Sea of Marmara. Earth and Planetary Science Letters 274 (1–2), 34–39.

Goldfinger, C., (2011). Submarine paleoseismology based on turbidite records. Annual Review of Marine Science 3, 35–66.

Goldfinger, C., Grijalva, K., Burgmann, K., Morey, A., Johnson, J.E., Nelson, C.H., Gutiérrez- Pastor, J., Karabanov, E., Patton, J., Gracia, E., (2008). Late Holocene rupture of the northern San Andreas Fault and possible stress linkage to the Cascadia Subduction Zone. Seismological Society of America, Bulletin 98, 861–899.

Goldfinger, C., Morey, A.E., Nelson, C.H., Gutierrez-Pastor, J., Johnson, J.E., et al., (2007). Rupture lengths and temporal history of significant earthquakes on the offshore and north coast segments of the northern San Andreas Fault based on turbidite stratigraphy. Earth Planet. Sci. Lett. 254, 9–27.

Goldfinger, C., Nelson, C.H., Johnson, J.E., (2003). Holocene earthquake records from the Cascadia subduction zone and northern San Andreas fault based on precise dating of offshore turbidites. Annual Review of Earth and Planetary Sciences 31, 555–577.

Goldfinger, C., Nelson, C.H., Johnson, J.E., (2003a). Deep-water turbidites as Holocene earthquake proxies: The Cascadia Subduction Zone and northern San Andreas Fault systems. Ann. Geophys. 46 (5), 1169–1194.

Goldfinger, C., Nelson, C.H., Morey, A., Johnson, J.E., Gutierrez-Pastor, J., Eriksson, A.T., Karabanov, E., Patton, J., Gracia, E., Enkin, R., Dallimore, A., Dunhill, G., Vallier, T., (2012). Turbidite event history—methods and implications for Holocene paleoseismicity of the Cascadia subduction zone. U.S. Geological Survey Professional Paper 1661-F, p. 170 (available at http://pubs.usgs.gov/pp/pp1661f/, March 2016).

Goldfinger, C., Patton, J.R., Van Daele, M., Moernaut, J., Nelson, C.H., de Batist, M., Morey, A., (2014). Can turbidites be used to reconstruct a paleo earthquake record for the central Sumatran margin: comment. Geology Society of America 42, e344. http://dx.doi.org/10.1130/G35510C.1.

Gorsline, D.S., Diego, T.D., Nava-Sanchez, E.H., (2000). Seismically triggered turbidities in small margin basins: Alfonso Basin, Western Gulf of California and Santa Monica Basin, California Borderland. Sedimentary Geology 135, 342–352.

Gracia, E., Vizcaino, A., Escutia, C., Asioi, A., Rodes, A., Pallas, R., Garcia-Orellana, J., Lebreiro, S., Goldfinger, C., (2010). Holocene earthquake records offshore Portugal (SW Iberia): testing turbidite paleoseismology in a slow-convergence margin. Quaternary Science Reviews 29, 1156–1172.

Grall, C., Herny, P., Thomas, Y., Westbrook, G.K., Çağatay, M.N., Marsset, B., Saritas, H., Çifici, G., Geli, L., (2013). Slip rate estimations along the western segment of the Main Marmara Fault over the last 405–490 ka by correlating mas transport deposits. Tectonics 32, 1–15.

Guidoboni, E., Comastri, A., (2005). Catalogue of Earthquakes and Tsunamis in the Mediterranean Area from 11th to the 15th Century. INGV-SGA, Bologna. 1057 pp.

Guidoboni, E., Comastri, A., Traina, G., (1994). Catalogue of Ancient Earthquakes in the Mediterranean Area up to 10th Century. INGV-SGA, Bologna. 504 pp.

Gutiérrez-Pastor, J., Nelson, C.J., Goldfinger, C., Escutia, C., (2013). Sedimentology of seismoturbidites off the Cascadia and northern California active tectonic continental margins, northwest Pacific Ocean. Mar. Geol. 336, 99–119. http://dx.doi.org/10.1016/j. margeo.2012.11.010.

Houghton, P.D.V., (1994). Deposits of deflected or ponded turbidity currents, Sorbas Basin, southeast Spain. Journal of Sedimentary Research A64, 233–246.

Inouchi, Y., Kinugasa, Y., Kumon, F., Nakano, S., Yasumatsu, S., Shiki, T., (1996). Turbidites as records of intense palaeoearthquakes in Lake Biwa, Japan. Sedimentary Geology 104, 117–125.

Johnson. D. (1938) The origin of submarine canyons. Journal of Geo. Morphology. 1, 111-340.

Kastens, K., Cita, M.B., (1981). Tsunami-induced sediment transport in the abyssal Mediterranean Sea. Geological Society of America Bulletin 119, 151–165.

Kastens, K.A., (1984). Earthquakes as a triggering mechanism for debris flows and turbidites on the Calabrian Ridge. Mar. Geol. 55, 13–33.

Kuenen, P. H. (1957). Sole markings of graded graywacke beds. The Journal of Geology, 231-258.

Kuenen, P. H. (1958). Problems concerning source and transportation of flysch sediments. Geol. Mijnbouw, 20, 329-339.

Kuenen, P. H., & Migliorini, C. I. (1950). Turbidity currents as a cause of graded bedding. The Journal of Geology, 91-127.

Kuşcu, İ., Okamura, M., Matsuoka, H., Gökaşan, E., Awata, Y., Tur, H., Şimşek, M., Keçer, M., (2005). Seafloor gas seeps and sediment failures triggered by the August 17, 1999 earthquake in the eastern part of the Gulf of Izmit, Sea of Marmara, NW Turkey. Marine Geology 215, 193–214.

Le Pichon, X., Şengör, A.M.C., Demirbağ, E., Rangin, C., Imren, C., Armijo, R., Görür, N., Çağatay, N., de Lepinay, B.M., Meyer, B., Saatçılar, R.,

Tok, B., (2001). The active main Marmara fault: comparative anatomy of a continental transform fault in a marine setting. Earth and Planetary Science Letters 192, 595–616.

Lowe, D. R. (1979). Sediment gravity flows: their classification and some problems of application to natural flows and deposits.

Masson, D.G., Arzola, R.G.,Wynn, R.B., Hunt, J.E.,Weaver, P.P.E., (2011). Seismic triggering of landslides and turbidity currents offshore Portugal. Geochemistry, Geophysics, Geosystems 12, 1–19. http://dx.doi.org/10.1029/2011GC003839.

McClusky, S., Bassalanian, S., Barka, A., Demir, C., Ergintav, S., Georgiev, I., Gurkan, Hamburger, O.M., Hurst, K., Hans-Gert, H.-G., Karstens, K., Kekelidze, G., King, R., Kotzev, V., Lenk, O., Mahmoud, S., Mishin, A., Nadariya, M., Ouzounis, A., Paradissis, D., Peter, Y., Prilepin, M., Relinger, R., Sanli, I., Seeger, H., Tealeb, A., Toksoz, M.N., Veis, G., (2000). Global Positioning System constraints on plate kinematics and dynamics in the eastern Mediterranean and Caucasus. Journal of Geophysical Research 105 (B3), 5695–5719.

McHugh, C.M., Seeber, L., Braudy, N., Cormier, M.-H., Davis, M.B., Diebold, J.B., Dieudonne, N., Douilly, R., Gulick, S.P.S., Hornbach, M.J., Johnson III, H.E., Ryan, K.M., Sorlien, C.C., Steckler,M.S., Symithe, S.J., Templeton, J., (2011). Offshore sedimentary effects of the 12 January 2010 Haiti earthquake. Geology 39, 723–726.

McHugh, C.M.G., Seeber, L., Cormier, M.-H., Dutton, J., Çağatay, N., Polonia, A., Ryan, W.B.F., Görür, N., (2006). Submarine earthquake geology along the North Anatolia Fault in the Marmara Sea, Turkey: a model for transform basin sedimentation. Earth and Planetary Science Letters 248, 661–684.

McKenzie, D.P., (1972). Active tectonics of the Mediterranean region. Geophysical Journal of the Royal Astronomical Society 30, 109–185.

Middleton, G. V., & Hampton, M. A. (1973). Part I. Sediment gravity flows: mechanics of flow and deposition.

Migowski, C., Agnon, A., Bookman, R., Negendank, J.F.W., Stein, M., (2004). Recurrence pattern of Holocene earthquakes along the Dead Sea transform revealed by varvecounting and radiocarbon dating of lacustrine sediments. Earth and Planetary Science Letters 222, 301–314.

Mulder, T., Alexander, J., 2001. The physical character of subaqueous sedimentary density currents and their deposits. Sedimentology 48, 269–299.

Mulder, T., Syvitski, J.P.M., 1995. Turbidity currents generated at river mouths during exceptional discharges to the world oceans. Journal of Geology 103, 285–299.

Mulder, T., Syvitski, J.P.M., Migeon, S., Faugères, J.C., Savoye, B., 2003. Marine hyperpycnal flows: initiation, behavior and related deposits. A review.Mar. Pet. Geol. 20, 861–882.http://dx.doi.org/10.1016/j.marpetgeo.2003.01.003.

Mutti, E. (1985). Turbidite systems and their relations to depositional sequences. In Provenance of arenites (pp. 65-93). Springer Netherlands.

Mutti, E. Ricci Lucchi F. (1975) Turbidite facies and facies associations In: Examples of turbidite facies and facies associations from selected formations of the northern Apennines Field Trip Guide International Sedimentologic Congress IX, Nice 21-36.

Mutti, E., Ricci Lucchi, F., Seguret, M., Zanzucchi, G., (1984). Seismoturbidites: a new group of resedimented deposits. Mar. Geol. 55, 103–116.

Nakajima, T., Kanai, Y., (2000). Sedimentary features of seismoturbidites triggered by the 1983 and older historical earthquakes in the eastern margin of the Japan Sea. Sedimentary Geology 135, 1–19.

Nelson, C.H., Escutia, C., Damuth, J.E., Twichell, D.C., (2009). Different active tectonic and passive continental margin settings: external and local controlling factors. Mass Transport Deposits in Deep Water Settings, SEPM Special Publication No. 95, SEPM. Society for Sedimentary Geology. ISBN: 978-1-56576-287-9. 28 p.

Nomade, J., Chapron, E., Desmet, M., Reyss, J.L., Arnaud, F., Lignier, V., (2005). Reconstructing historical seismicity from lake sediments (Lake Laffrey, Western Alps, France). Terra Nova 17, 350–357.

Parsons, T., (2004). Recalculated probability of M>7 earthquakes beneath the Sea of Marmara. Journal of Geophysical Research 109. http://dx.doi.org/10.1029/ 2003JB002667.

Parsons, T.S., Toda, T.S., Stein, R.S., Barka, A., Dietrich, J.H., (2000). Heightened odds of large earthquakes near Istanbul, an interaction-based probability calculation. Science 288, 661–665.

Pickering, K.T., Hiscott, R.N., (1985). Contained (reflected) turbidity currents in the Middle Ordovician Cloridorme Formation, Quebec, Canada: an alternative to the antidune hypothesis. Sedimentology 32, 373–394.

Piper, D. W. (1978). Turbidite muds and silts on deep sea fans and abyssal plains. Sedimentation in submarine canyons, fans, and trenches.

Polonia, A., et al., (2016). A depositional model for seismo-turbidites in confined basins based on Ionian Sea deposits, Marine Geology.

Polonia, A., Gasperini, L., Amorosi, A., Bonatti, E., Çağatay, N., Capotondi, L., Cormier,M.-H., Görür, N.,McHugh, C., Seeber, L., (2004). Holocene slip rate of the North Anatolian Fault beneath the Sea of Marmara. Earth and Planetary Science Letters 227, 411–426.

Postma, G., Babic, L., Zupanic, J., Roe, S.L., (1988). Delta-front failure and associated bottomset deformation in a marine, gravelly Gilbert-type delta.

In: Nemec, N., Steel, R.J. (Eds.), Fan Deltas: Sedimentology and Tectonic Settings. Blackie, Glasgow & London, pp. 91–102.

Pouderoux, H., Lamarche, G., Proust, J.-N., (2012). Building a 18,000 year-long paleoearthquake record from detailed deep-sea turbidite characterization in Poverty Bay, New Zealand. Natural Hazards and Earth System Sciences 12, 2077–2101.

Prior, D.B., Suhayda, J.N., Lu, N.Z., Bornhold, B.D., Keller, G.H., Wiseman, W.J., Wright, L.D., Yang, Z.S., (1989). Storm wave reactivation of a submarine landslide. Nature 341, 47–50.

Sarı, E., Çağatay, M.N., (2006). Turbidities and their association with past earthquakes in the deep Çınarcık Basin of the Marmara Sea. Geo-Marine Letters 26, 69–76.

Schmittbuhl, J., H. Karabulut, O. Lengline, and M. Bouchon (2015), Seismicity distribution and locking depth along the Main Marmara Fault, Turkey, Geochem. Geophys. Geosyst., 17, 954–965, doi:10.1002/2015GC006120.

Schmittbuhl, J., H. Karabulut, O. Lengliné, and M. Bouchon (2016), Long-lasting seismic repeaters in the Central Basin of the Main Marmara Fault, Geophys. Res. Lett., 43, 9527–9534, doi:10.1002/2016GL070505.

Schnellmann, M., Flavio, S.A., Domenico, G., Judith, A.M., (2005). Mass movementinduced fold-and-thrust belt structures in unconsolidated sediments in Lake Lucerne (Switzerland). Sedimentology 52, 271–289.

Shanmugam, G., (2000). 50 years of the turbidite Paradigm(1950s-1990s): deep-water processes and facies models-a critical perspective. Mar. Pet. Geol. 17, 285e342.

Sheldon P.G. (1928) Some sedimentation conditions in Middle Port-age rocks. American Journal of Science, 15 243-252.

Shepard, F. P. (1951). Mass movements in submarine canyon heads. Eos, Transactions American Geophysical Union, 32(3), 405-418.

Shiki, T., Kumon, F., Inouchi, Y., Kontani, Y., Sakamoto, T., Tateishi, M., Matsubara, H., Fukuyama, K., (2000). Sedimentary features of the seismo-turbidites, Lake Biwa, Japan. Sedimentary Geology 135, 37–50.

Siani, G., Paterne, M., Arnold, M., Bard, E., Metivier, B., Tisnerat, N., Bassinot, F., (2000). Radiocarbon reservoir ages in the Mediterranean Sea and Black Sea. Radiocarbon 42, 271–280.

Signorini, R. (1936) Determinazione del senso di sedimentazione degli strati nelle formazione arenacea dell' Appennino settentrionale. Boll.Soc.Geol.Ital 44. 148-156.

Stein, R.S., Barka, A.A., Dieterich, J.H., (1997). Progressive failure of the North Anatolia Fault since 1939 by earthquake stress triggering. Geophysical Journal International 128, 594–604.

Stow, D. A. (1979). Distinguishing between fine-grained turbidites and contourites on the Nova Scotian deep water margin. Sedimentology, 26(3), 371-387.

Şengör, A.M.C., Tüysüz, O., İmren, C., Sakınç, M., Eyidoğan, H., Görür, N. Le, Pichon, X., Rangin, C., (2005). The North Anatolian Fault: a new look. Annual Review of Earth and Planetary Sciences 33, 37–112.

Thunell, R., Tappa, E., Varela, R., Llano, M., Astor, Y., Muller-Karger, F., Bohrer, R., (1999). Increased marine sediment suspension and fluxes following an earthquake. Nature 398, 233–236.

Uçarkuş, G., Çakır, Z., Armijo, R., (2011). Western termination of the Mw 7.4, 1999 Izmit earthquake rupture: implications for the expected large earthquake in the Sea of Marmara. Turkish Journal of Earth Sciences. http://dx.doi.org/10.3906/yer-0911-72.

Walton, E. K. (1967). The sequence of internal structures in turbidites. Scottish Journal of Geology, 3(2), 306-317.

Yılmaz, Y., Gökaşan, E., Erbay, A.Y., (2009). Morphotectonic development of the Marmara region. Tectonophysics 488, 51–70.

APPENDICES

Appendix 1: Section 1 of CS-01, physical, elemental, textural proxies.

Appendix 2: Section 2 of CS-01, physical, elemental, textural proxies.

Appendix 3: Section 3 of CS-01, physical, elemental, textural proxies.

Appendix 4: Section 4 of CS-01, physical, elemental, textural proxies.

Appendix 5: Section 5 of CS-01, physical, elemental, textural proxies.

Appendix 6: Section 6 of CS-01, physical, elemental, textural proxies.

Appendix 7: Section 7 of CS-01, physical, elemental, textural proxies.

Appendix 8: Section 8 of CS-01, physical, elemental, textural proxies.

Appendix 9: Section 9 of CS-01, physical, elemental, textural proxies.

Appendix 10: Section 10 of CS-01, physical, elemental, textural proxies.

Appendix 11: Section 11 of CS-01, physical, elemental, textural proxies.

Appendix 12: Section 12 of CS-01, physical, elemental, textural proxies.

Appendix 13: Section 13 of CS-01, physical, elemental, textural proxies.

Appendix 14: Section 14 of CS-01, physical, elemental, textural proxies.

Appendix 15: Section 15 of CS-01, physical, elemental, textural proxies.

Appendix 16: Section 16 of CS-01, physical, elemental, textural proxies.

Appendix 17: Section 17 of CS-01, physical, elemental, textural proxies.

Appendix 18: Section 18 of CS-01, physical, elemental, textural proxies.

Appendix 19: Section 19 of CS-01, physical, elemental, textural proxies.

Appendix 20: Section 20 of CS-01, physical, elemental, textural proxies.

Appendix 21: Section 21 of CS-01, physical, elemental, textural proxies.

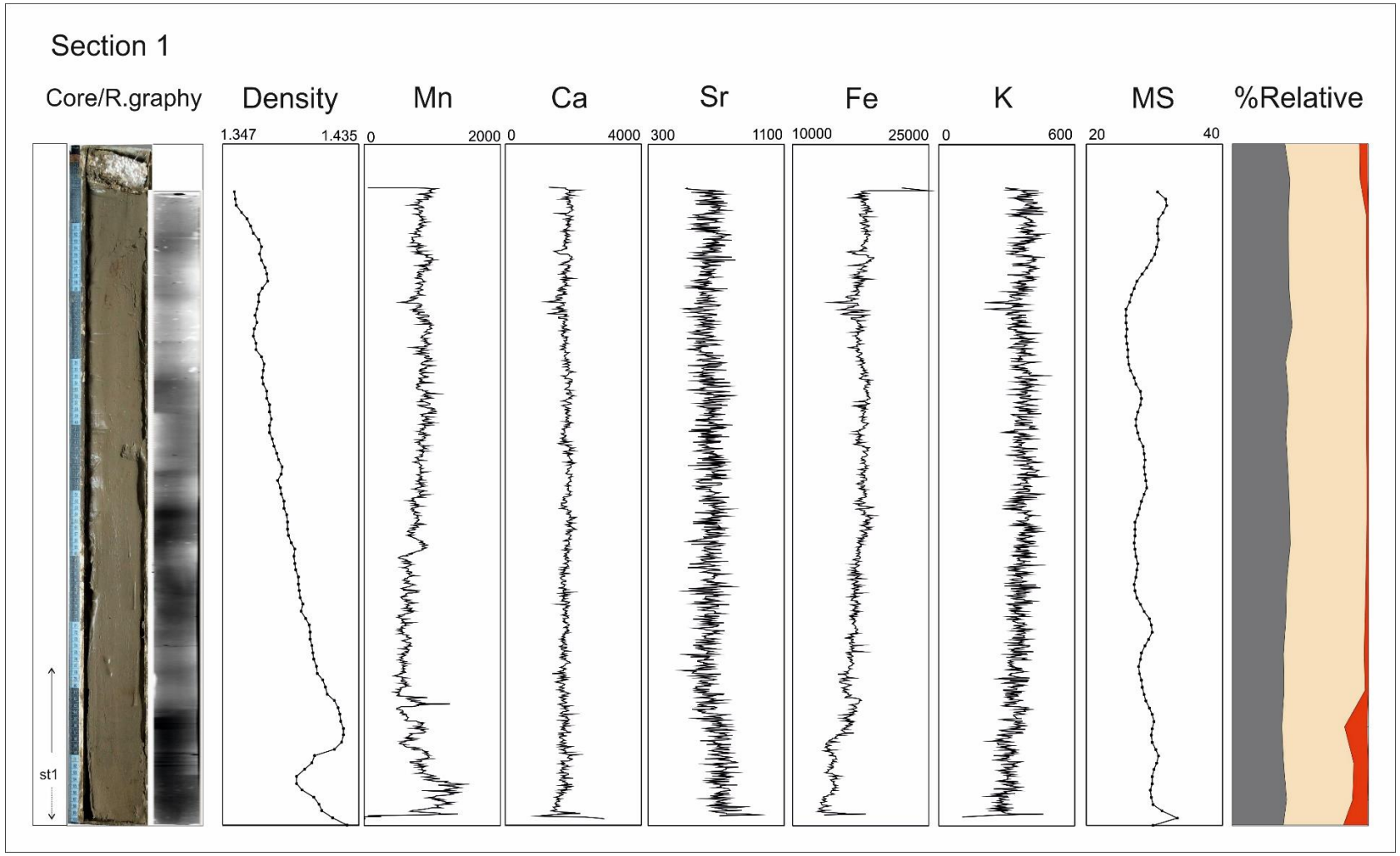

Appendix 1: Section 1 of CS-01, physical, elemental, textural proxies.

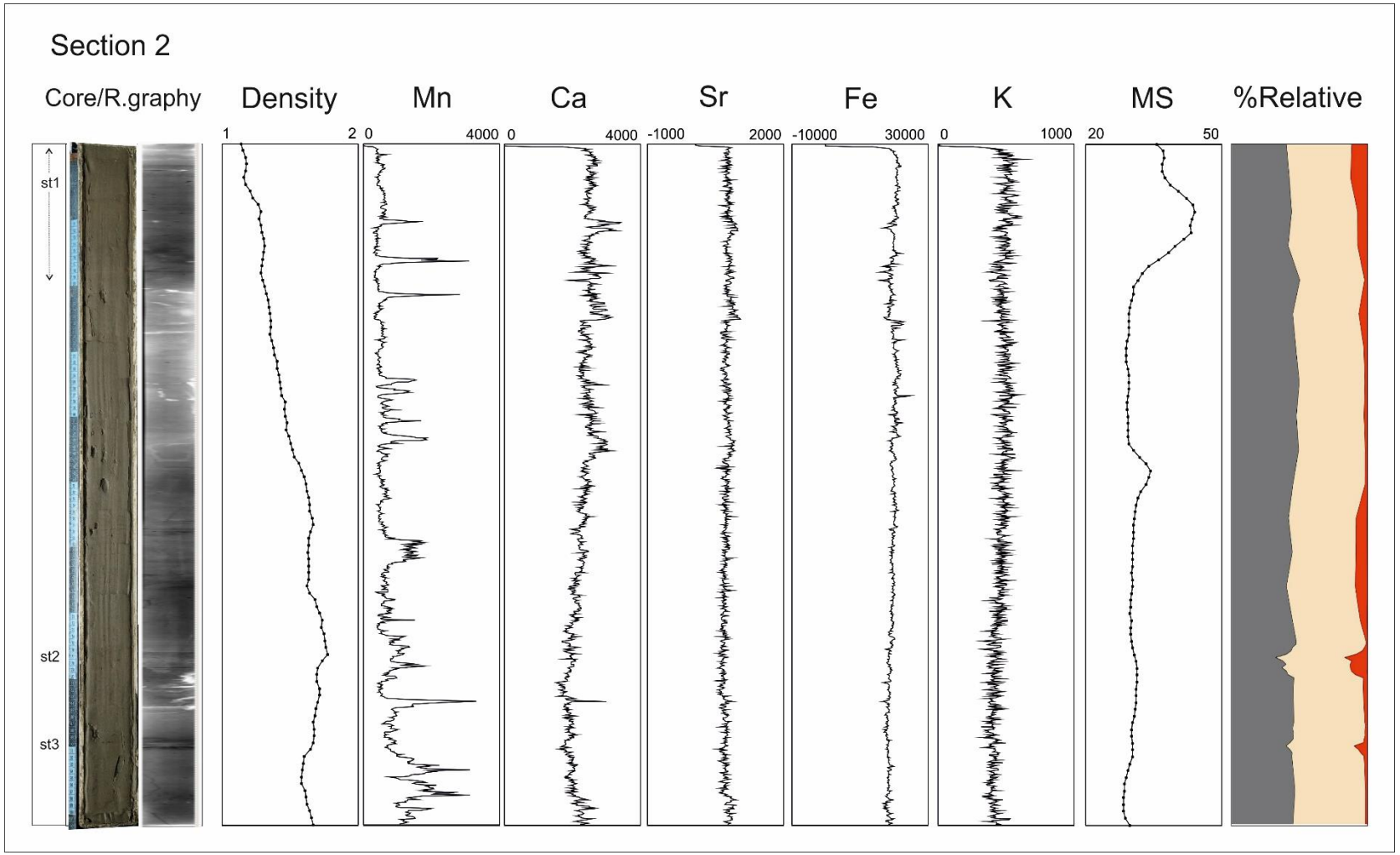

Appendix 2: Section 2 of CS-01, physical, elemental, textural proxies.

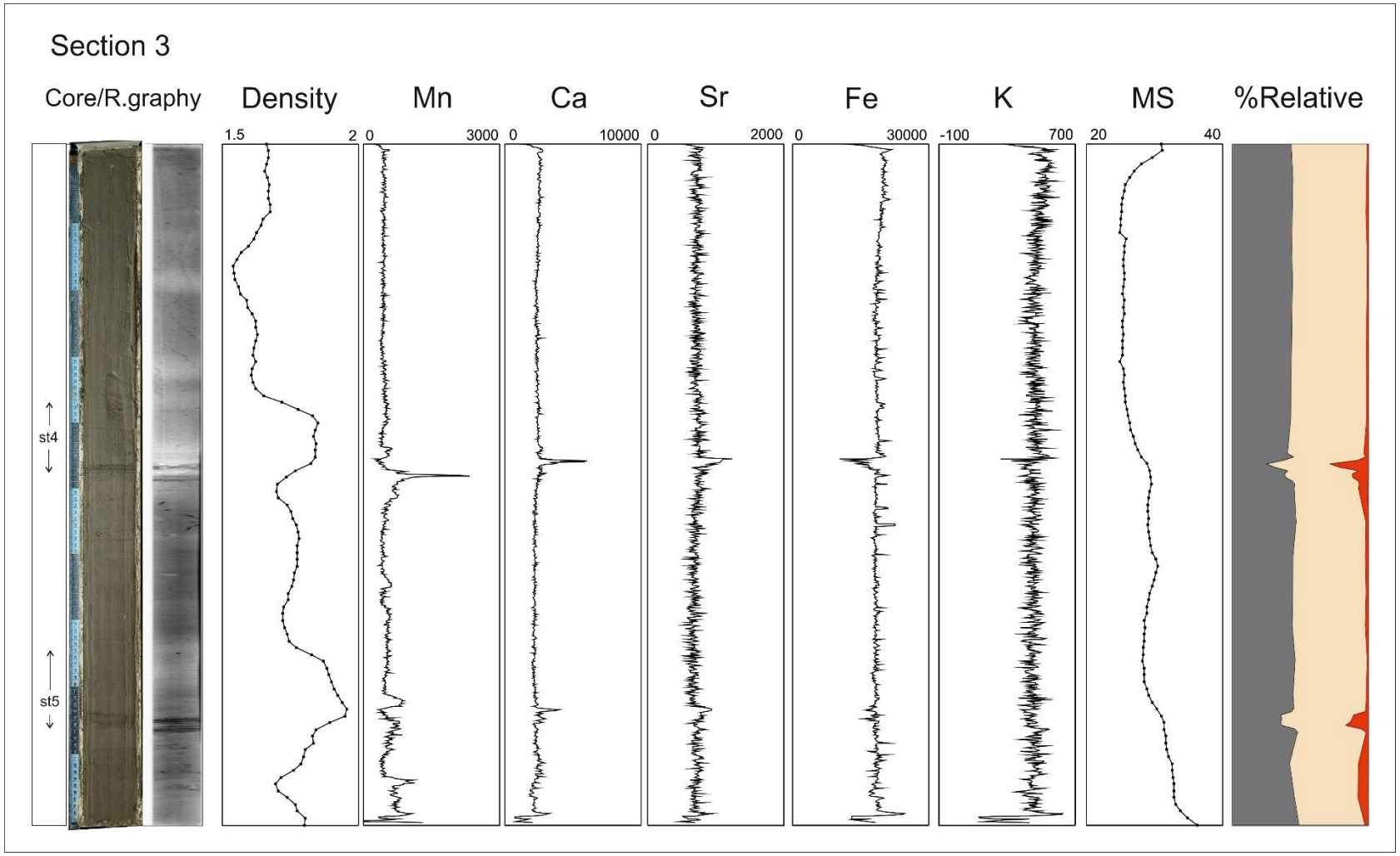

Appendix 3: Section 3 of CS-01, physical, elemental, textural proxies.

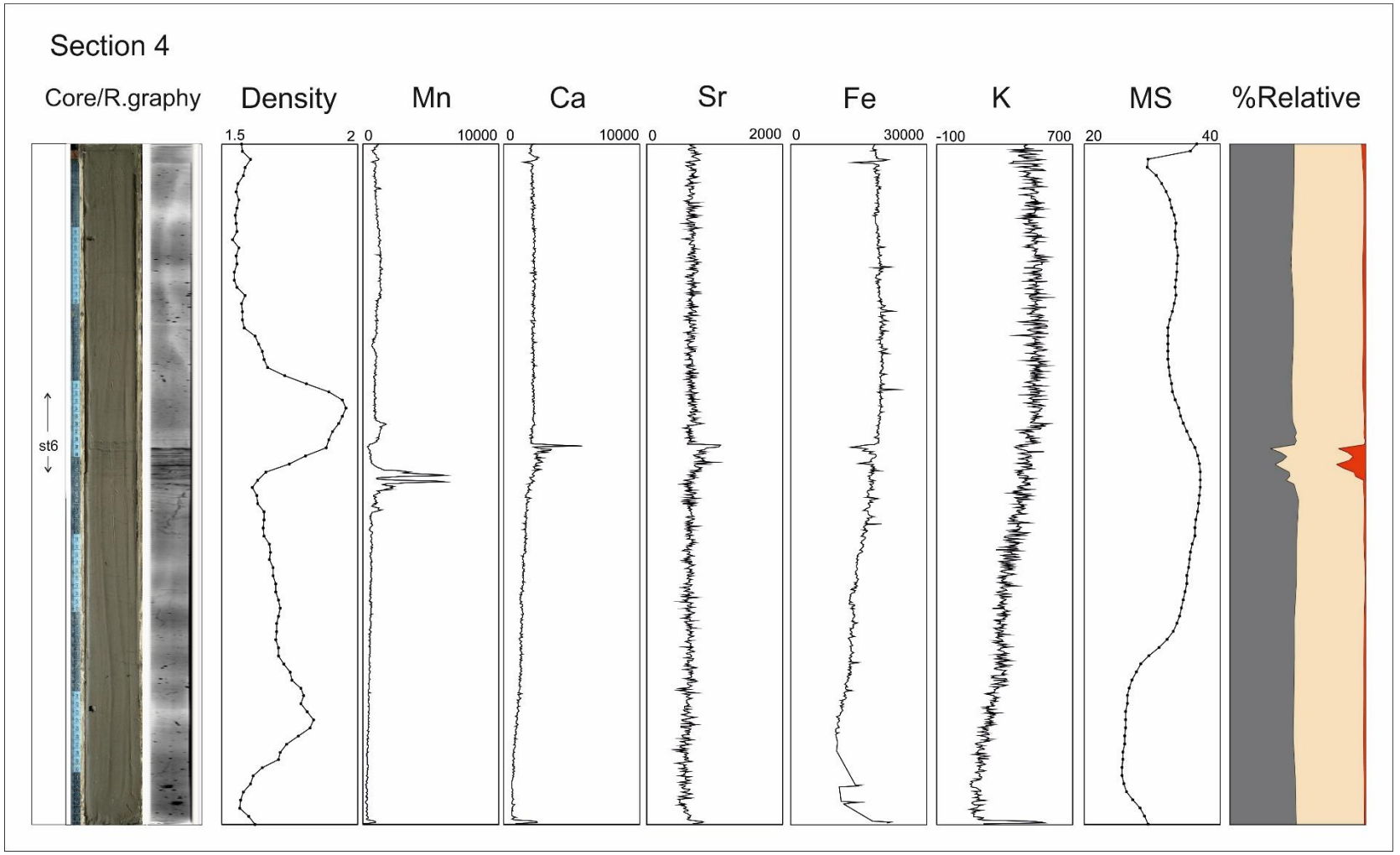

Appendix 4: Section 4 of CS-01, physical, elemental, textural proxies.

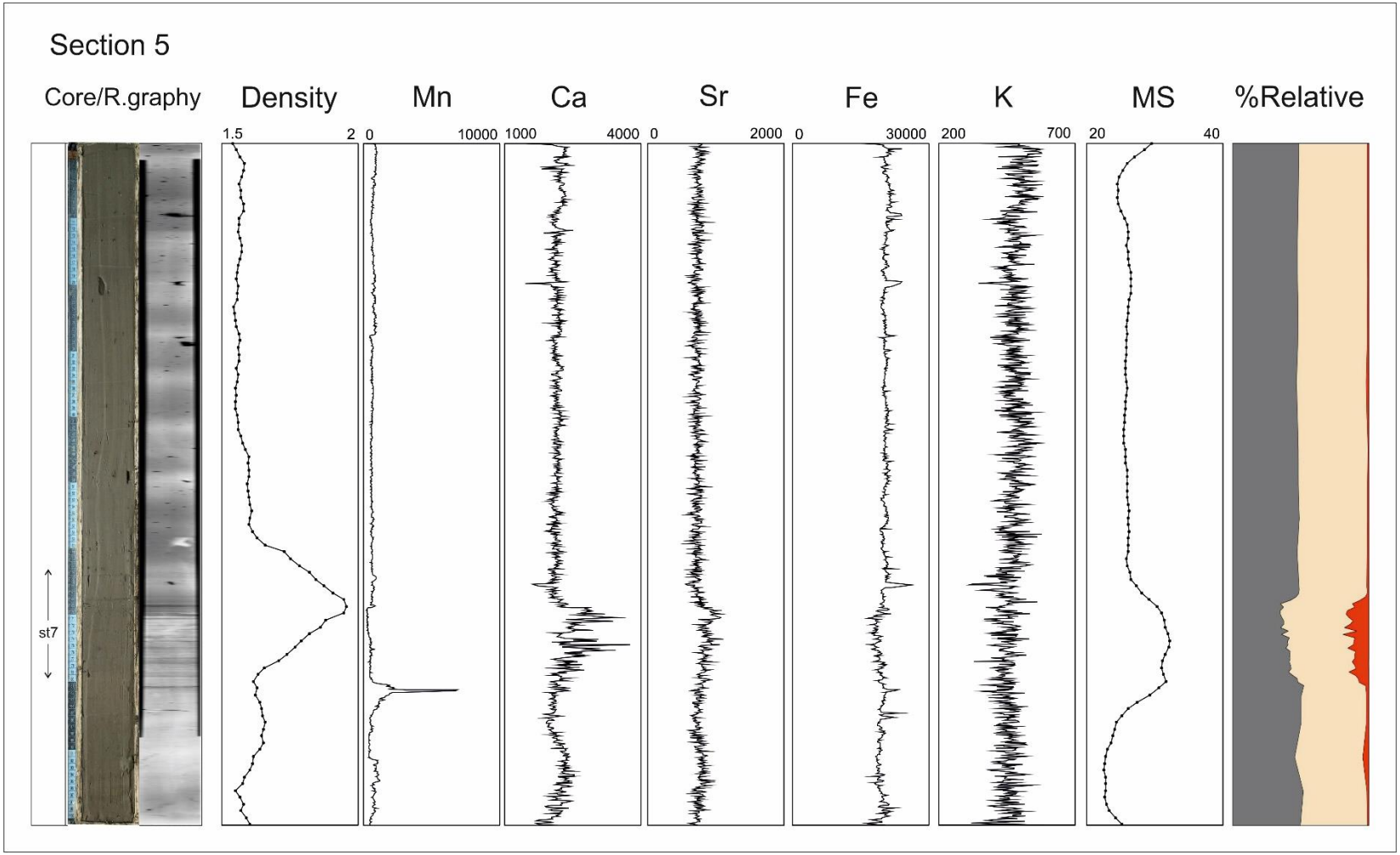

Appendix 5: Section 5 of CS-01, physical, elemental, textural proxies.

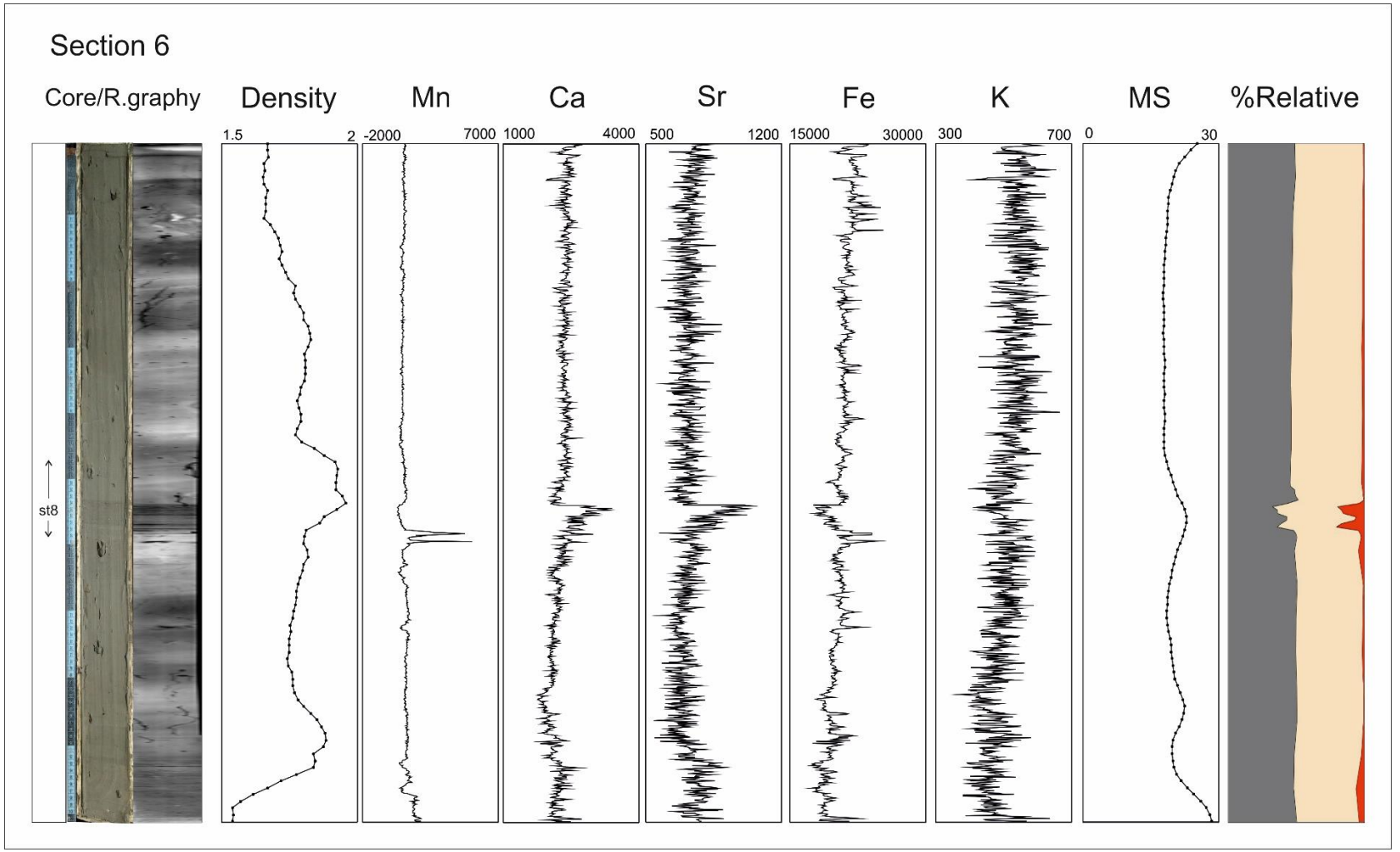

Appendix 6: Section 6 of CS-01, physical, elemental, textural proxies.

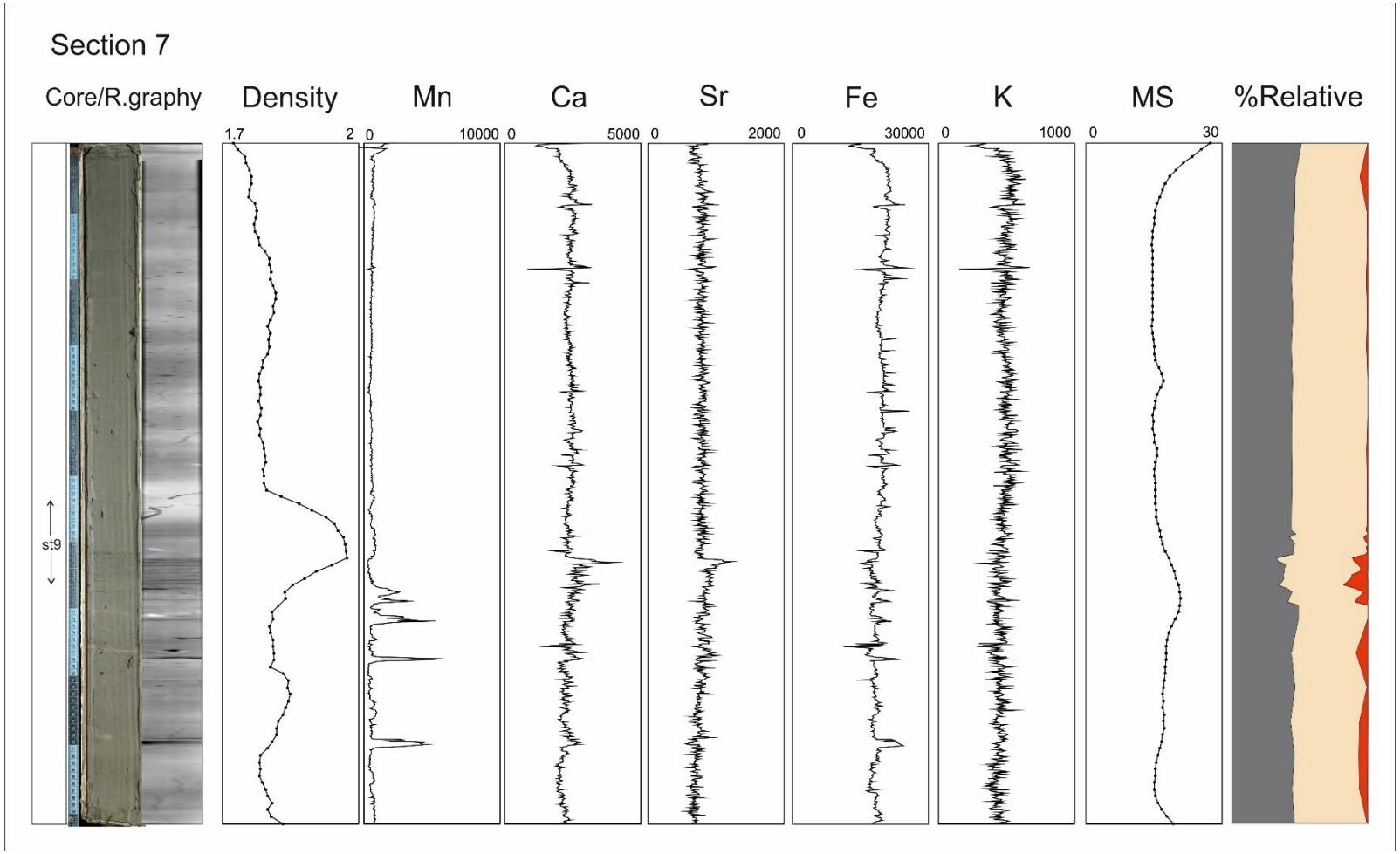

Appendix 7: Section 7 of CS-01, physical, elemental, textural proxies.

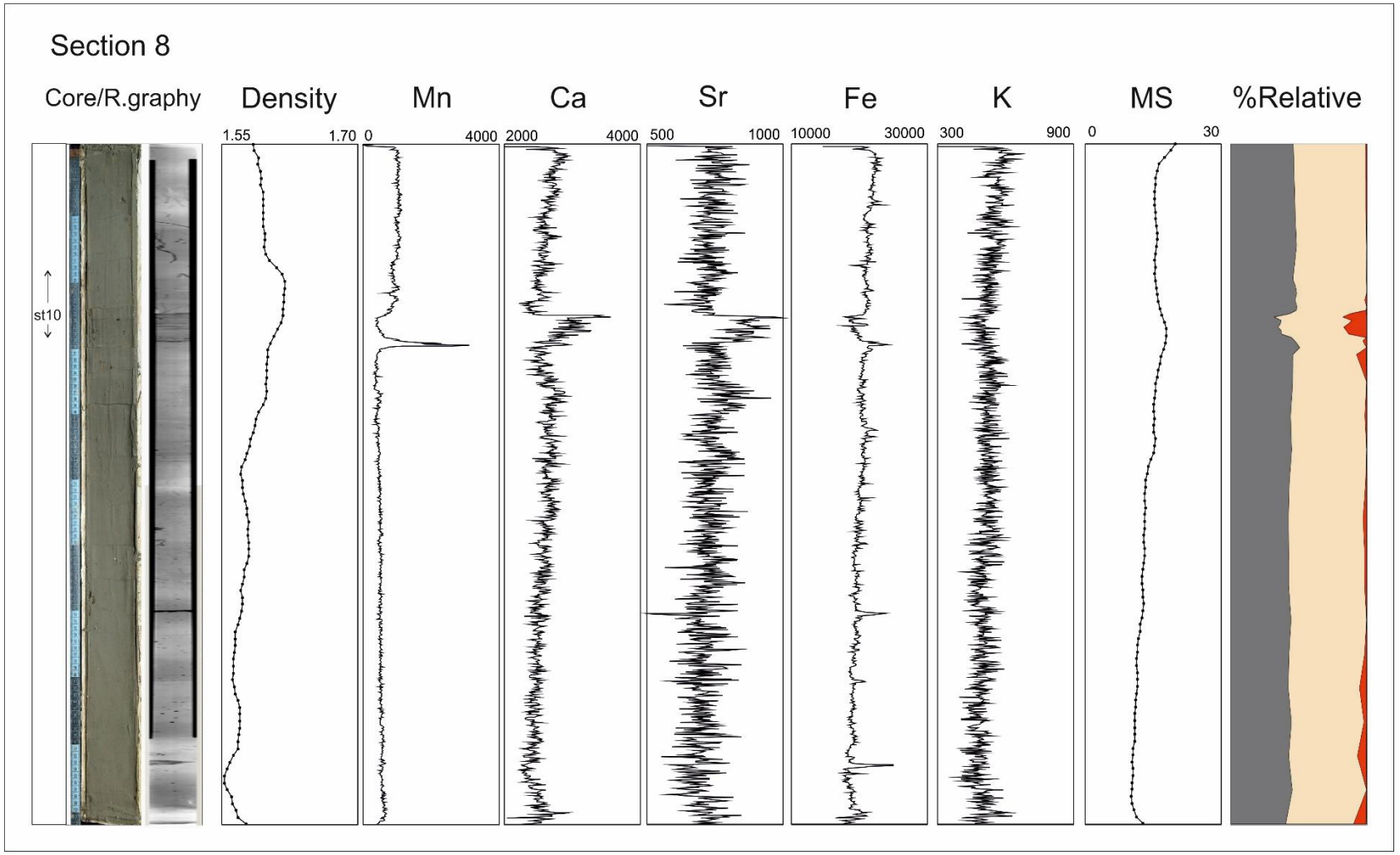

Appendix 8: Section 8 of CS-01, physical, elemental, textural proxies.

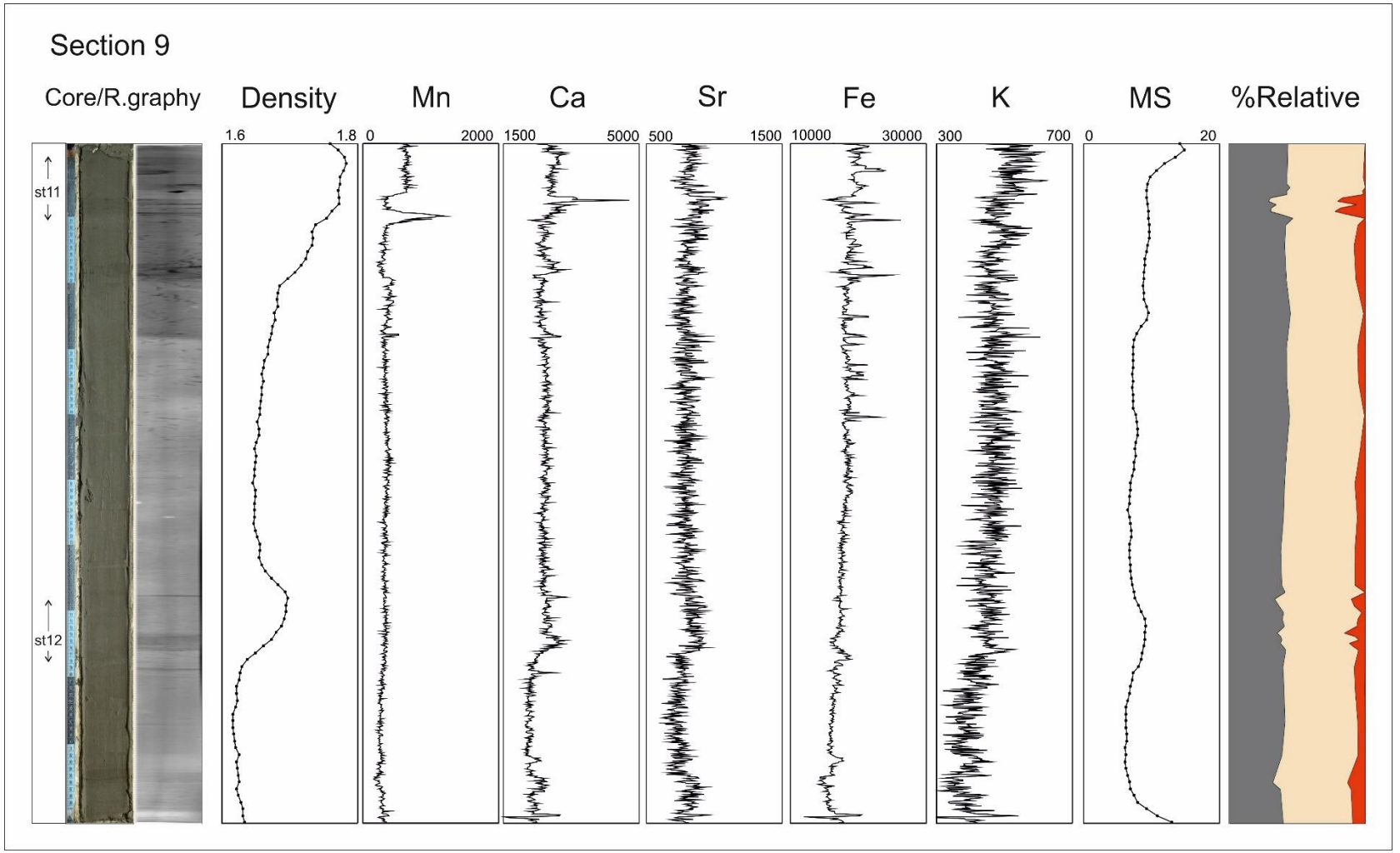

Appendix 9: Section 9 of CS-01, physical, elemental, textural proxies.

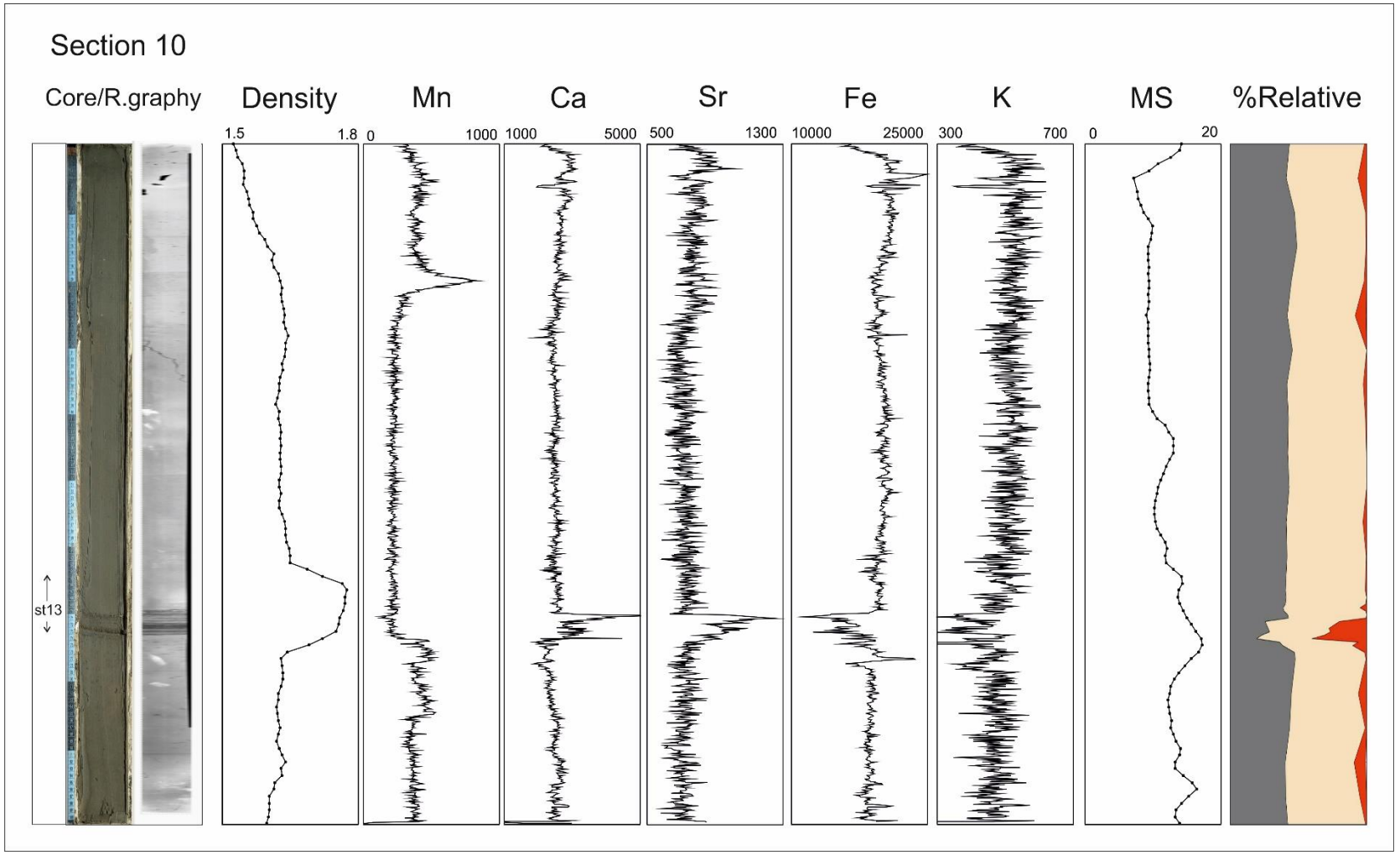

Appendix 10: Section 10 of CS-01, physical, elemental, textural proxies.

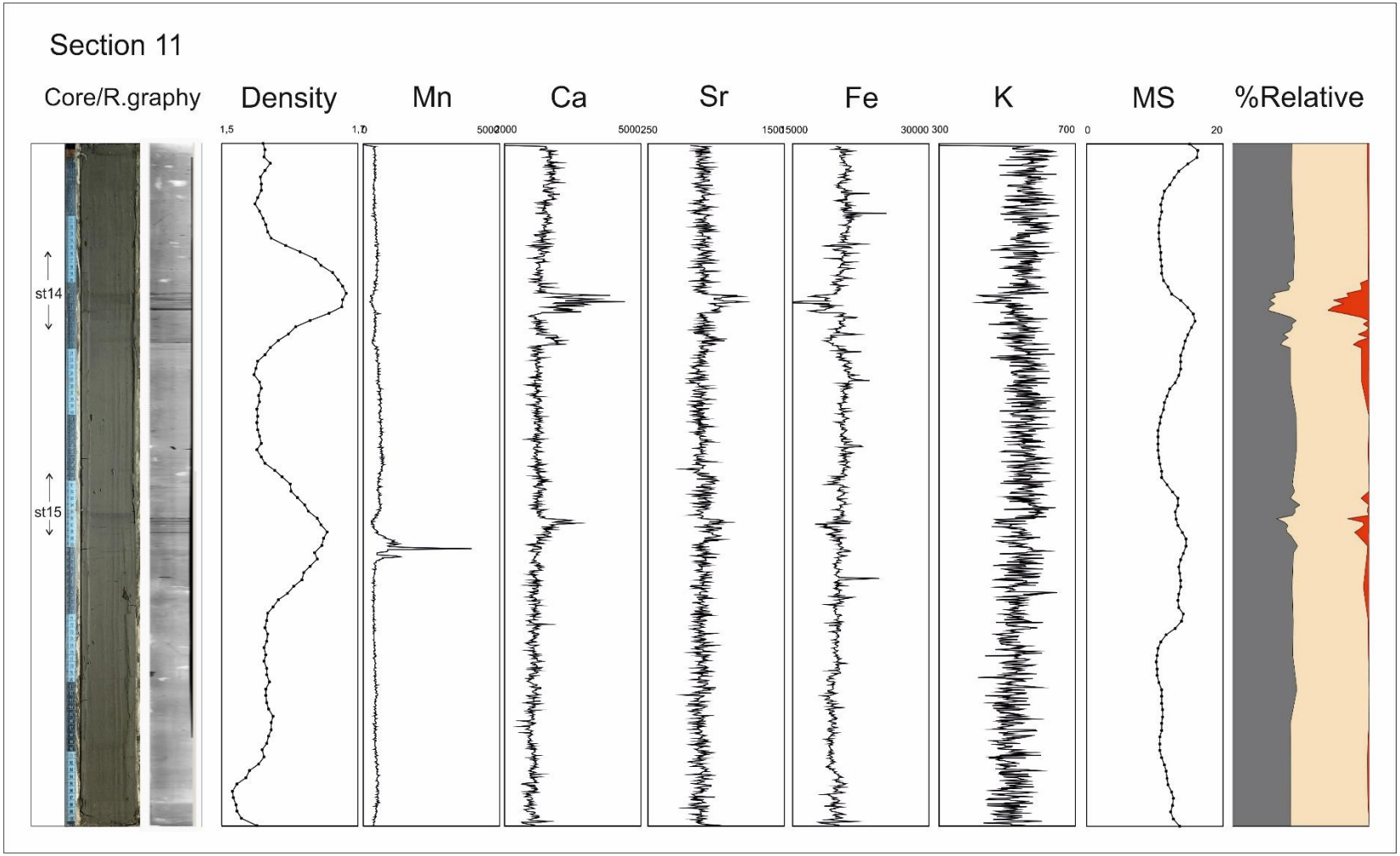

Appendix 11: Section 11 of CS-01, physical, elemental, textural proxies.

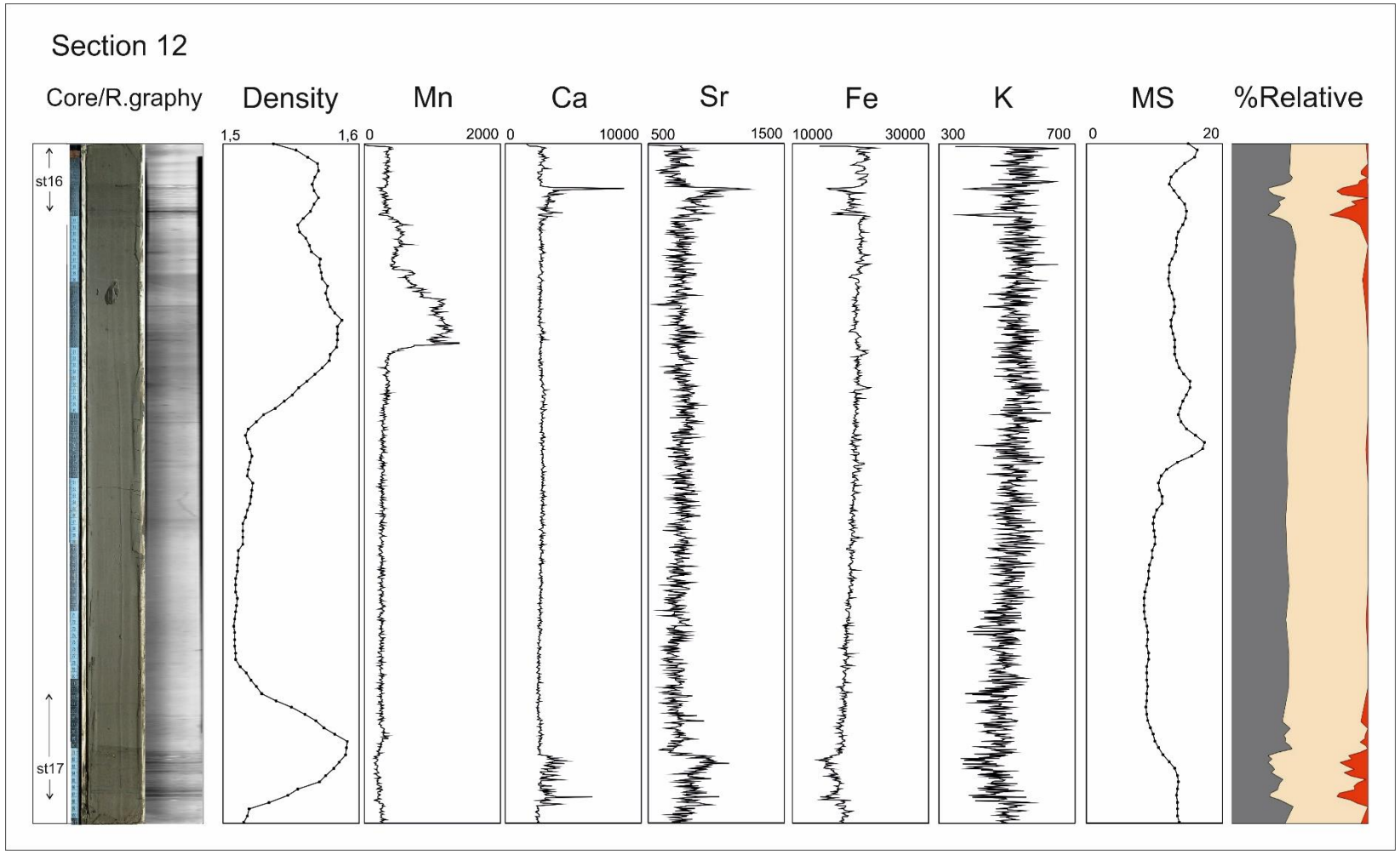

Appendix 12: Section 12 of CS-01, physical, elemental, textural proxies.

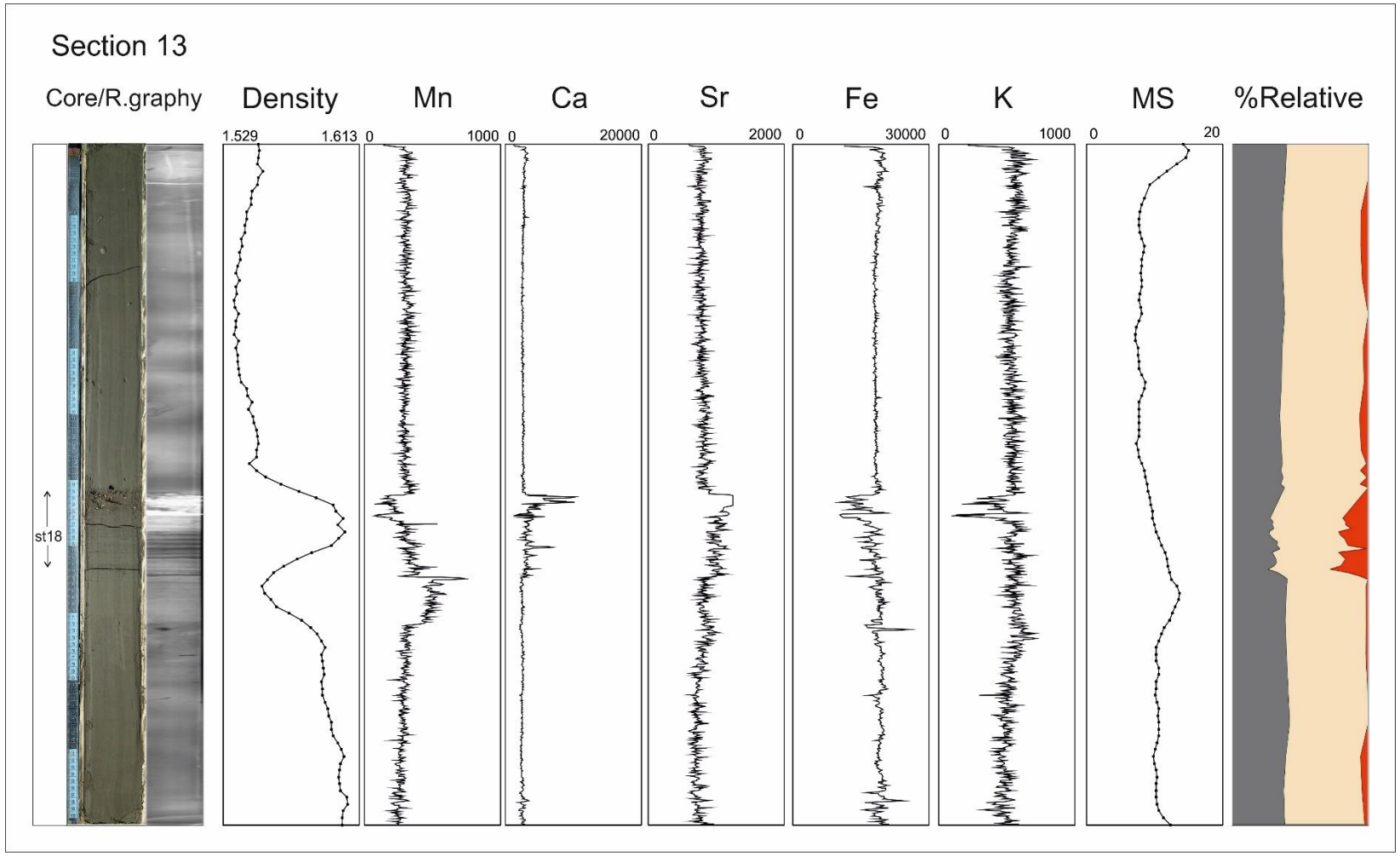

Appendix 13: Section 13 of CS-01, physical, elemental, textural proxies.

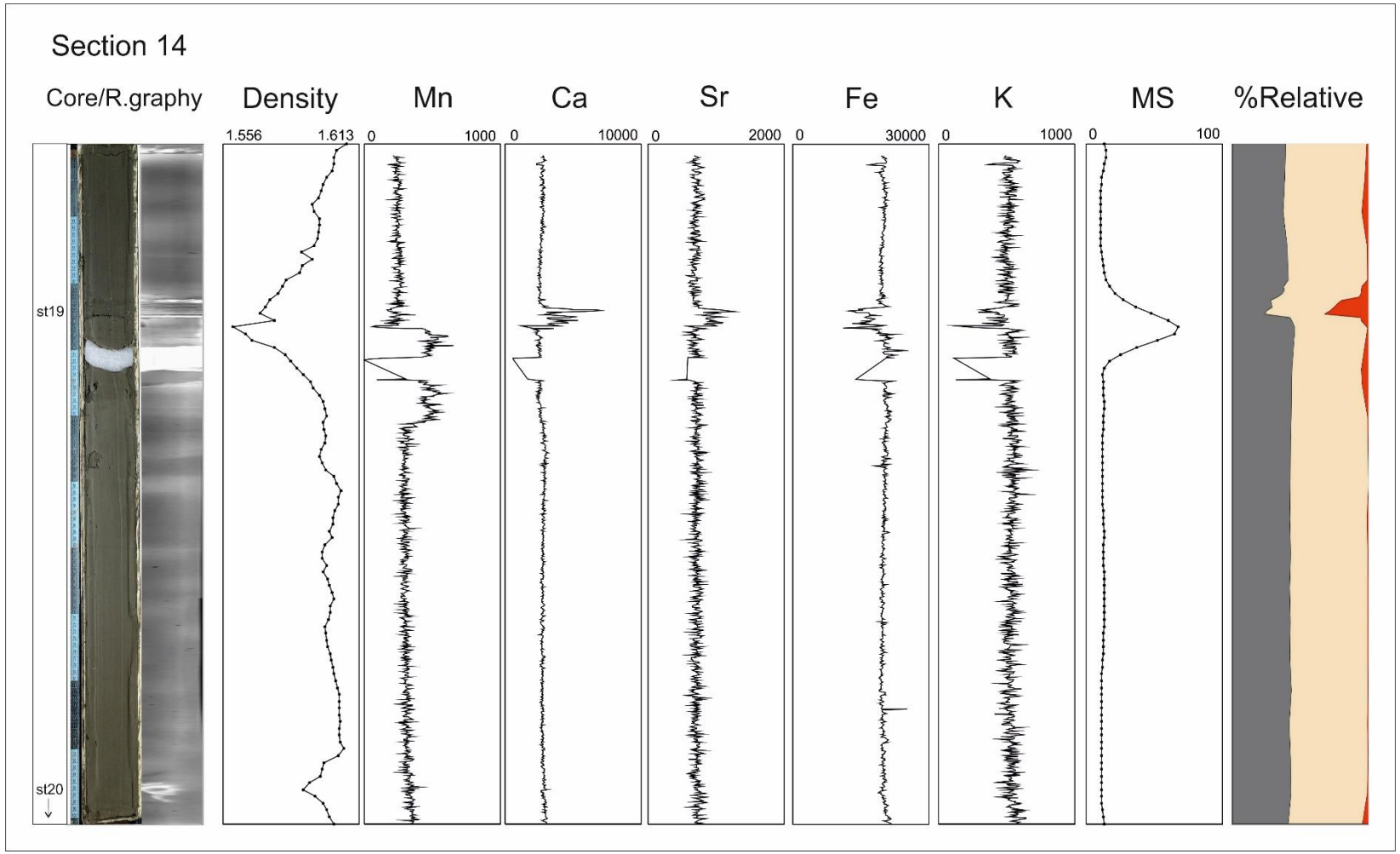

Appendix 14: Section 14 of CS-01, physical, elemental, textural proxies.

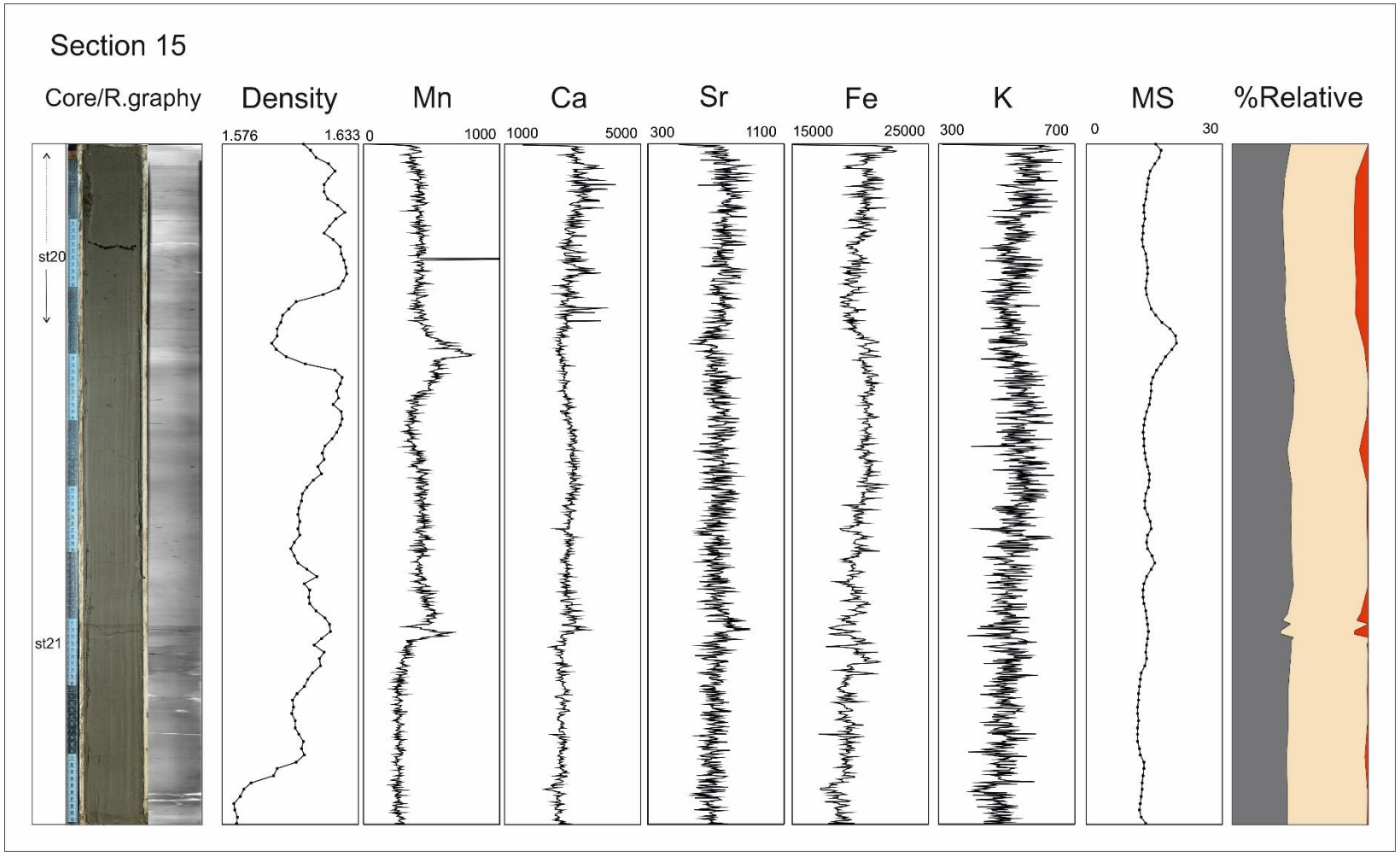

Appendix 15: Section 16 of CS-01, physical, elemental, textural proxies.

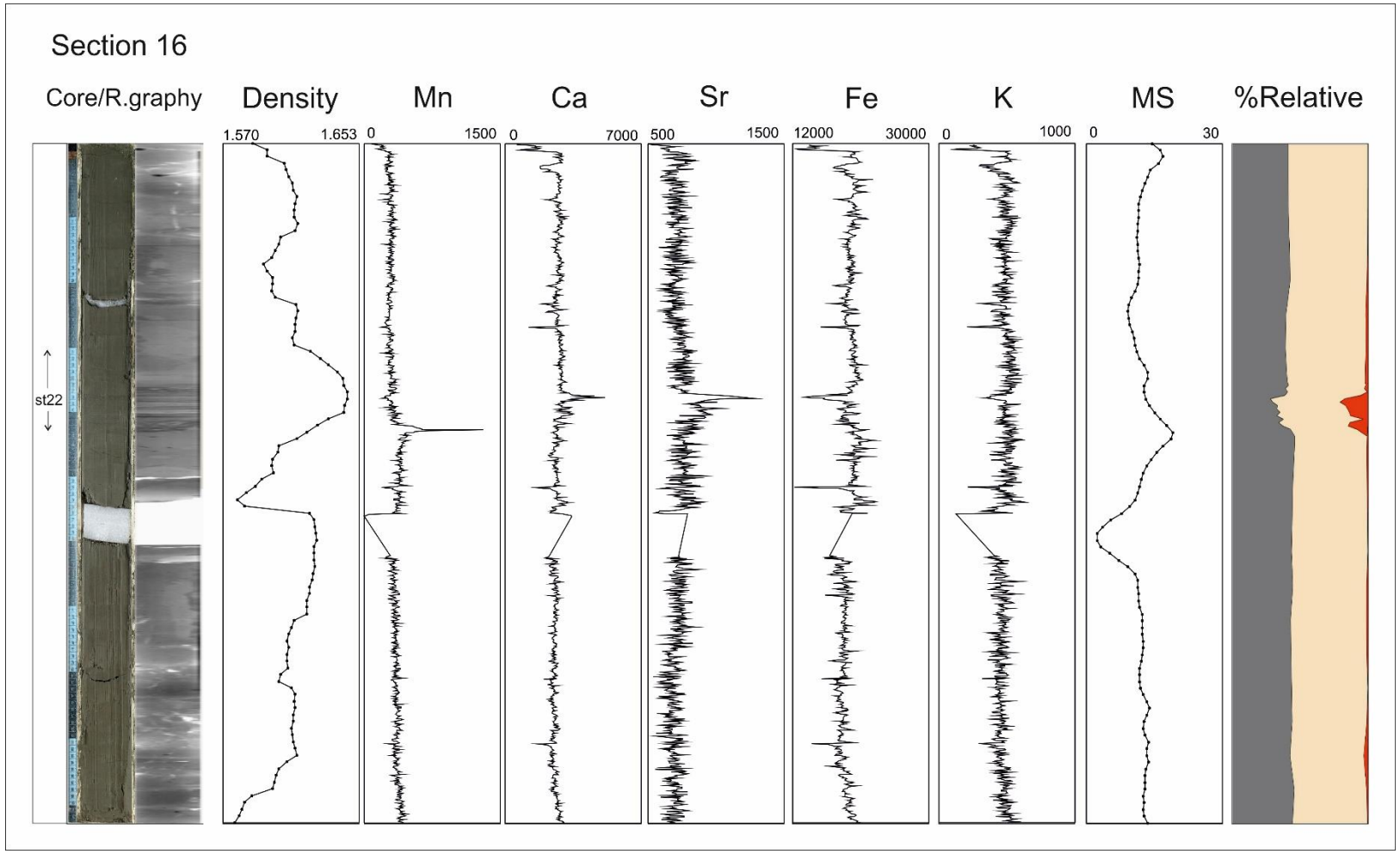

Appendix 16: Section 16 of CS-01, physical, elemental, textural proxies.

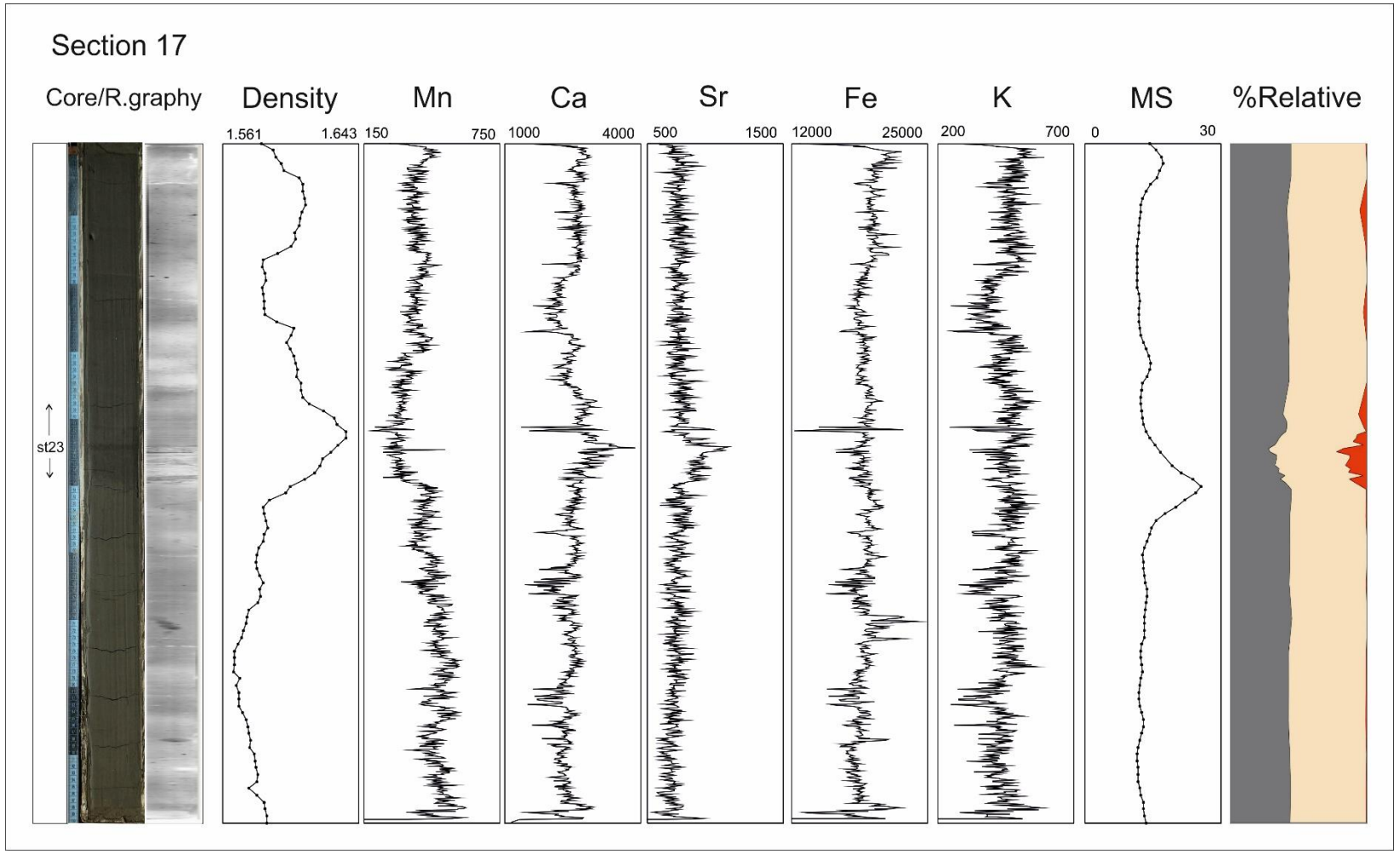

Appendix 17: Section17 of CS-01, physical, elemental, textural proxies.

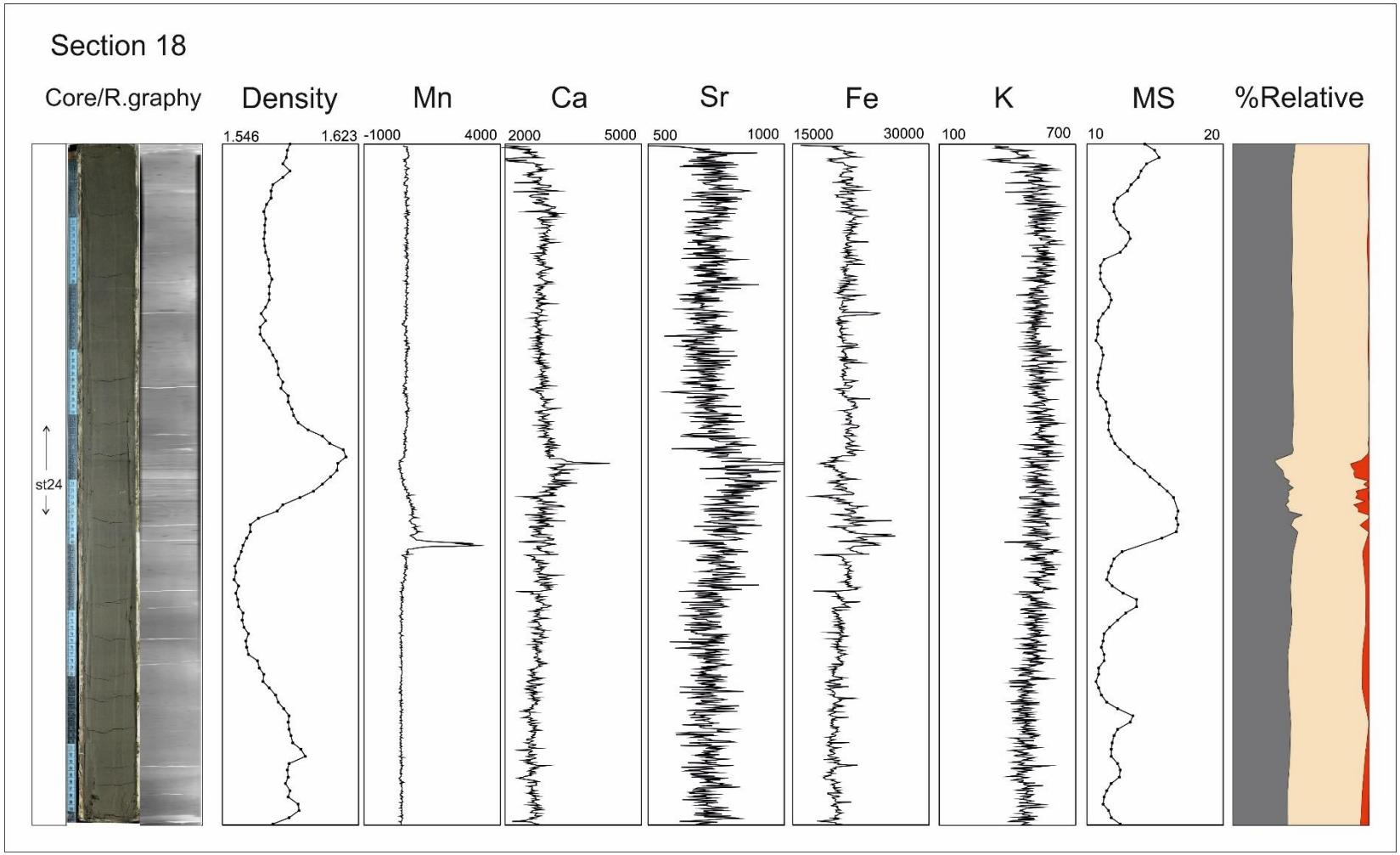

Appendix 18: Section 18 of CS-01, physical, elemental, textural proxies.

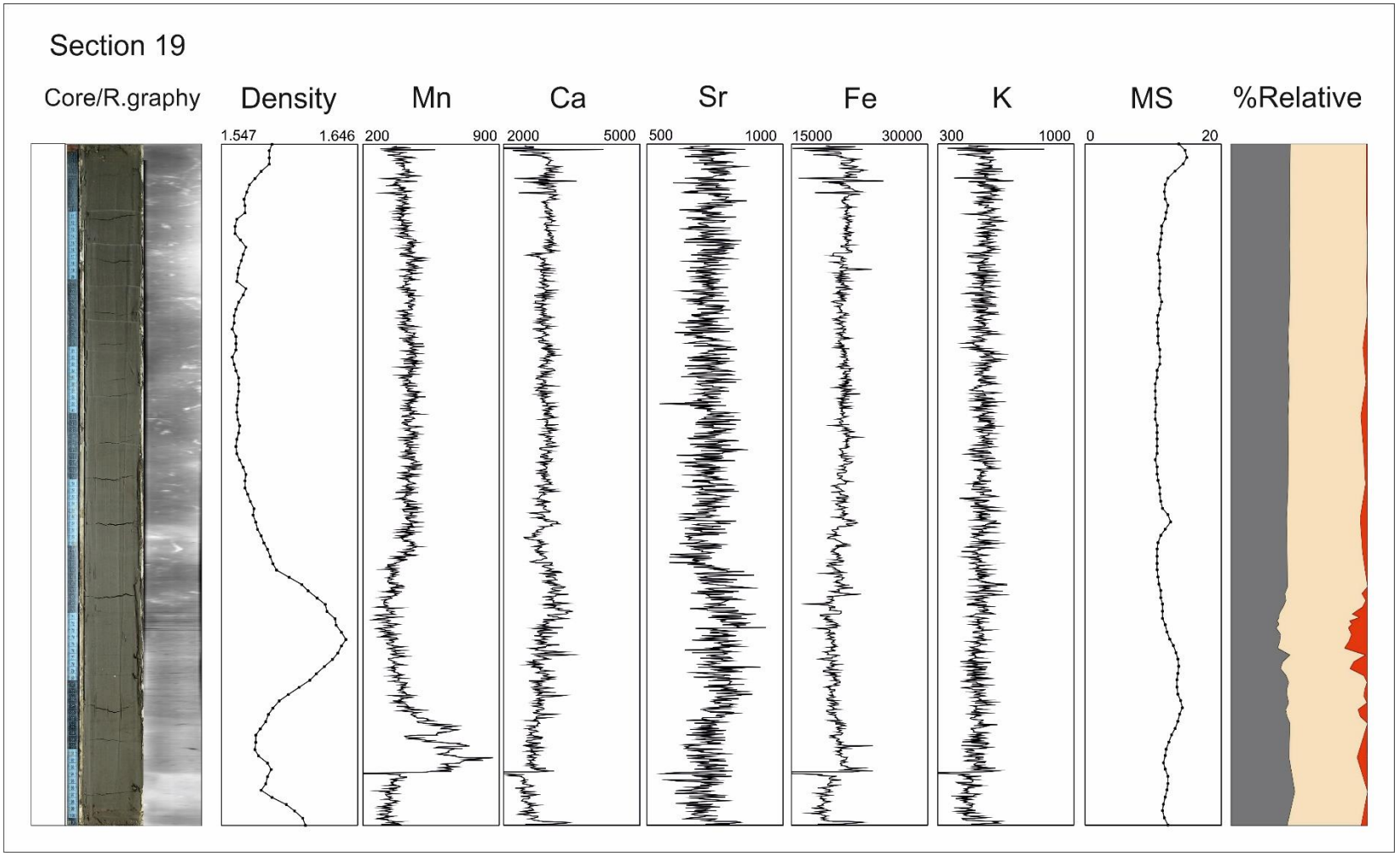

Appendix 19: Section 19 of CS-01, physical, elemental, textural proxies.

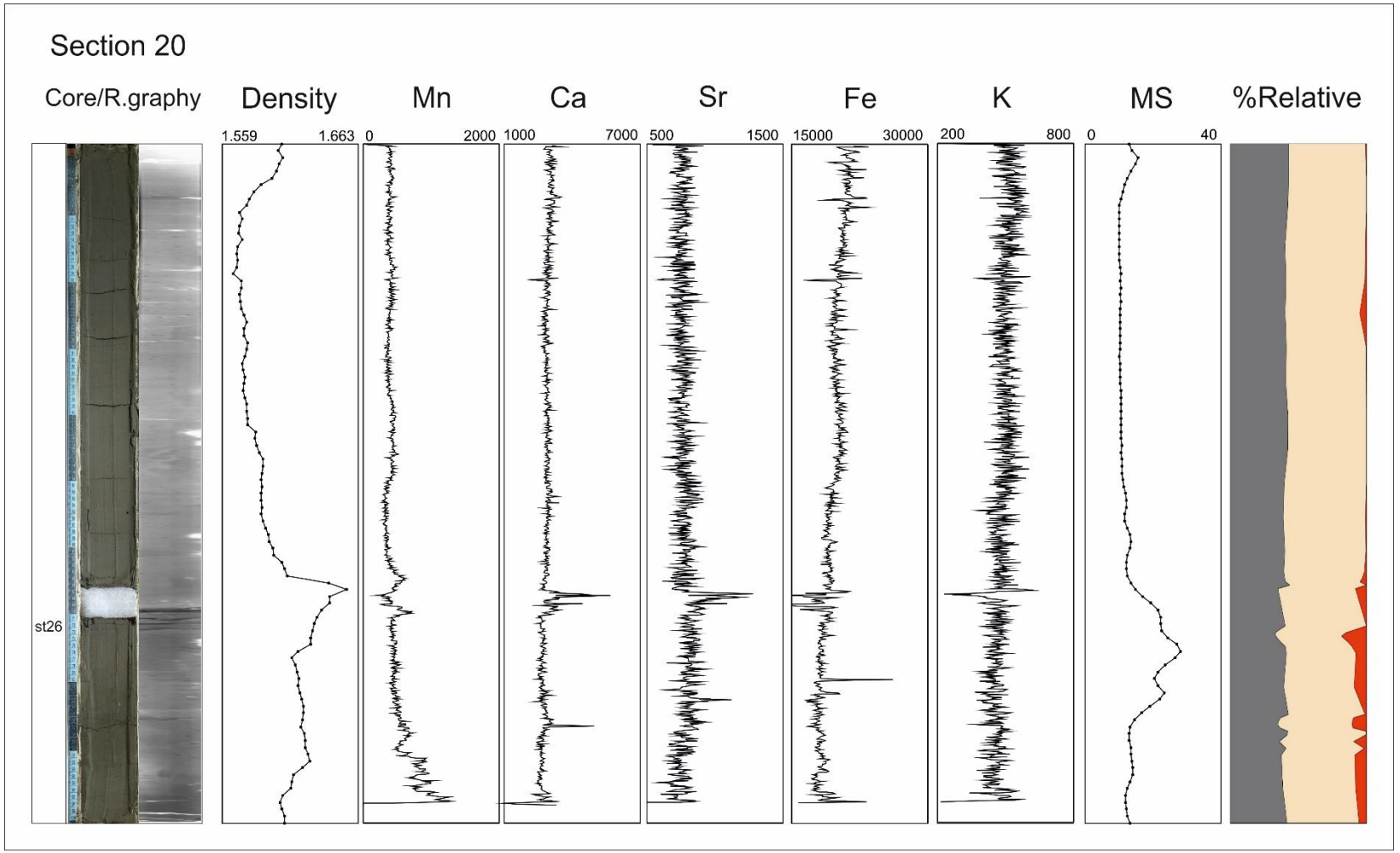

Appendix 20: Section 20 of CS-01, physical, elemental, textural proxies.

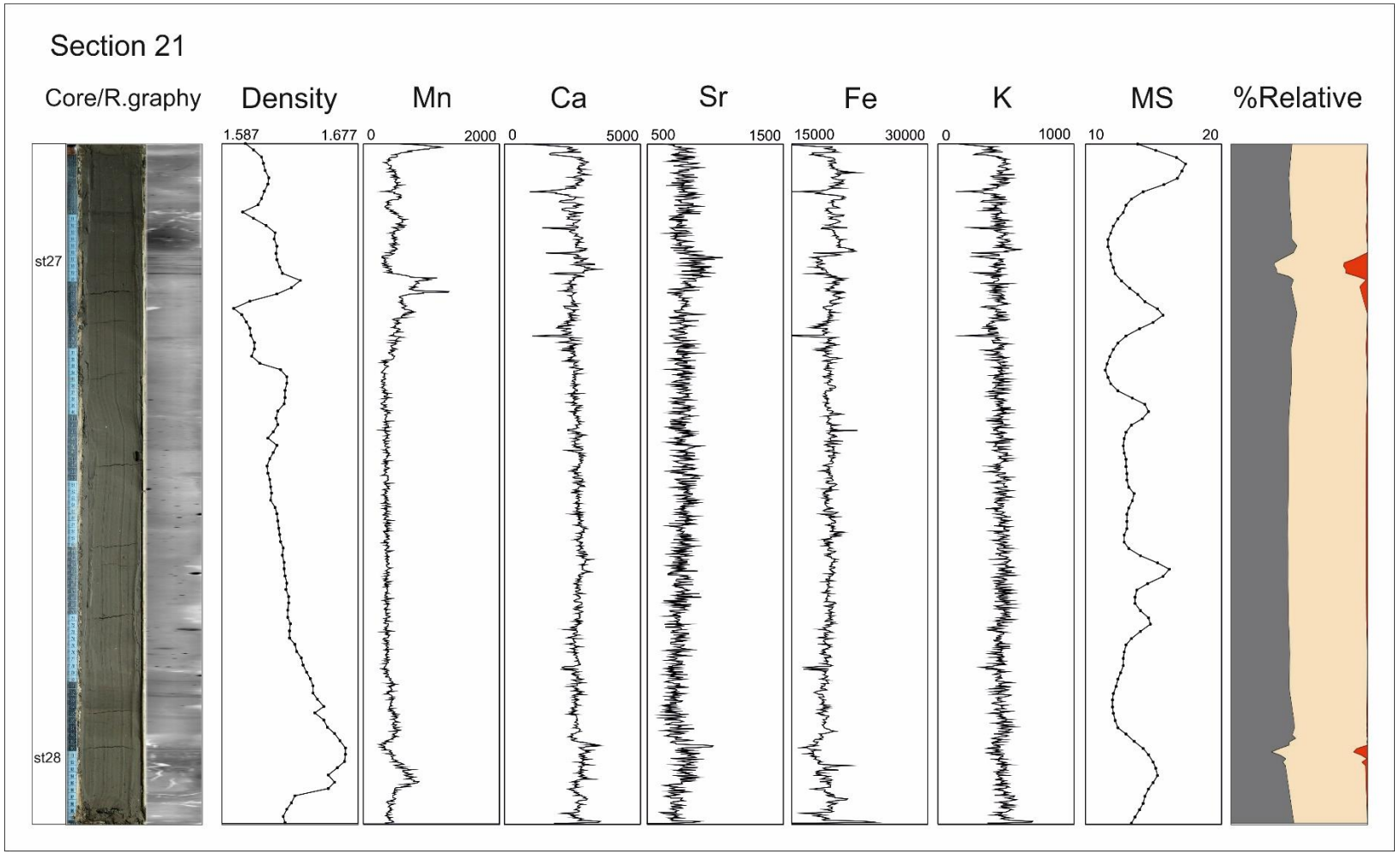

Appendix 7: Section 7 of CS-01, physical, elemental, textural proxies.

CURRICULUM VITAE

Name-Surname	**:** Nurettin Yakupoğlu
Birthday and birthplace	**:** 22/11/1988 Seyhan/ADANA
E-mail	**:** yakupoglu@itu.edu.tr

EDUCATION:

- **B.Sc :** 2014-2015, Istanbul Technical University, Faculty of Mining, Geology Engineering

PROFESSIONAL EXPERIENCE AND REWARDS:

- ITU EMCOL member as a researcher (2014-current)
- MARsite Project participant (2014-current)

PUBLICATIONS, PRESENTATIONS AND PATENTS ON THE THESIS:

- Yakupoglu, N., Uçarkus, G., Eris, K. K., Çagatay, M. N., Henry, P., Yalamaz, B., ... & Acar, D. (2016, April). Multi-parameter analysis of seismoturbidites in the Kumburgaz Basin of Sea of Marmara: Implications for creeping versus locked Central High segment of the North Anatolian Fault. In EGU General Assembly Conference Abstracts (Vol. 18, p. 644).